Factors Affecting Piston Ring Friction

by

Kai Liao

B.E. in Jet Propulsion
Beijing University of Aeronautics and Astronautics (2007)

S.M. in Aeronautics and Astronautics
Massachusetts Institute of Technology (2009)

Submitted to the Department of Aeronautics and Astronautics in Partial Fulfillment of the Requirements of the Degree of

Doctor of Philosophy in Aeronautics and Astronautics

at the

Massachusetts Institute of Technology

June 2013

Author: _____
Department of Aeronautics and Astronautics
May 9, 2013

Certified by: _____
Tian Tian
Principle Research Engineer, Department of Mechanical Engineering
Thesis Supervisor

Certified by: _____
Mark Drela
Professor of Aeronautics and Astronautics
Chairman, Thesis Committee

Certified by: _____
Wai K. Cheng
Professor of Mechanical Engineering
Thesis Committee

Certified by: _____
Oyelayo O. Ajayi
Scientist, Argonne National Laboratory
Thesis Committee

Accepted by: _____
Eytan H. Modiano
Professor of Aeronautics and Astronautics
Chair, Graduate Program Committee

Factors Affecting Piston Ring Friction

by

Kai Liao

Submitted to the Department of Aeronautics and Astronautics in Partial Fulfillment of the Requirements of the Degree of

Doctor of Philosophy in Aeronautics and Astronautics

Abstract

The piston ring pack friction is a major contributor to the internal combustion engine mechanical friction loss. The oil control ring decides the oil supply to the top two rings in addition to being the major friction contributor in the ring pack. This work concentrated on the oil control ring friction. A large range of ring land widths and tensions, liner finish, and oil viscosity were investigated both experimentally and numerically to reveal how different factors affect the piston ring friction.

A floating liner engine (FLE) was modified for motoring tests. The engine system repeatability and self-consistency were demonstrated. The thesis then discussed proper methods to select and measure the rings, liners and oil, which were important to generating meaningful results from the experiment. The ranges of engine speeds and liner temperatures were designed to ensure that all the lubrication modes, namely, boundary, mixed and hydrodynamic, can become dominant in both the instantaneous friction over a cycle and the FMEP over the engine speed range for any combination of rings, liners and lubricants.

A parallel modeling effort was made to the experiments. The work showed that with careful preparation of adequate information on rings, liners and lubricants, the model can match the friction trends observed in the experiment over a large range of operating parameters and designs on the ring, liner finish and lubricant viscosity.

The ring friction change over the liner break-in was studied using liners covering a wide range of surface roughness. The hydrodynamic pressure generation ability of the liner appears to be decided by the large surface structure. Therefore, the break-in process, which removes individual asperities from the plateau, does not affect pure hydrodynamic lubrication, and only the mixed lubrication is affected by the plateau roughness change. By keeping the same hydrodynamic pressure - ring/liner clearance (P-h) correlation and changing the plateau roughness, the model can predict the ring friction change over different lubrication regimes during the break-in.

Compared to the current industry norm, a new engine power cylinder system design using a smaller land width twin land oil control ring with a lower ring tension and accompanied by a smoother liner surface gives lower friction and better oil control at the same time.

Thesis Supervisor:

Dr. Tian Tian, Department of Mechanical Engineering

Thesis Committee:

Professor Mark Drela (Committee Chairman), Department of Aeronautics and Astronautics
Professor Wai Cheng, Department of Mechanical Engineering
Dr. Layo Ajayi, Argonne National Laboratory

Acknowledgement

There are many people I should thank without whom my PhD research experience at MIT wouldn't be so unforgettable.

First and foremost, I want to thank my thesis advisor, Dr. Tian Tian, and other committee members, committee chair, Professor Mark Drela, Professor Wai Cheng and Dr. Layo Ajayi, who gave me extensive academic guidance and intellectual motivation. I always gain more insight into my research field when talking to them. I want to thank my academic advisor, Professor Edward Greitzer who guided me through the academic milestones I should achieve at MIT. They all have helped me develop in both academic and professional aspects.

I would also like to thank my peers who worked with me together through my research. I would like to thank Shuma Aoki who helped me install the floating liner engine and taught me how to operate the engine. I would like to thank Dallwoo Kim who devoted lots of time in lab experiments. He has helped me take many measurements whose results are used in this work. I would like to thank Haijie Chen and Yang Liu who helped me prepare model inputs using deterministic calculation. I absorbed new knowledge and generated new ideas through the inspiring discussions with them.

In addition, I would like to thank the sponsors who provided financial support for my research. My work was sponsored by the consortium on lubrication in IC engines at MIT and the Argonne National Laboratory. The current consortium members are Daimler, Mahle, PSA, Renault, Shell, Toyota, Volkswagen, and Volvo. Especially, I would like to thank the representatives from the companies who regularly attended the consortium meeting and gave me valuable suggestions: Hans-Jurgen Fuesser, Matthias Martin, Rolf-Gerhard Fiedler, Remi Rabute, Bengt Olson, Gabriel Cavallaro, Bernard laeer, Paulo Urzua Torres, Tom Shieh, Yeongching Lin, Guilleaume Mermaz-Rollet, Shohei Nomura, Erich Rabassa, Fredrick Stromstedt, George Fenske, Steve Przesmitzki, Brian Papke, Scott Rappaport and others. I would like to specifically thank Emmanuel Oliviera and Remi Rabute at Mahle for procuring the ring parts and conducting ring measurements for my research; thank Hans-Juergen Fuesser and Paulo Urzuz Torres for providing the liner sleeves and roughness measurement used in this study. Without their contributions my research would be impossible.

I would also like to thank the members from the Sloan Automotive Laboratory for their support. Janet Maslow gave us great administrative assistance. My lab mates Yong Li, Dongfang Bai, Camille Baelden, Dian Xu, Eric Senzer, Mathieu Picard, Yuan Wang, Tianshi Fang, Qing Zhao, Pasquale Totaro, Eric Zanghi have made my time in the lab more enjoyable.

Finally I would like to thank my family who provided me great support through the years of my stay in the US and all the friends I met at MIT that made my stay here more colorful.

Contents

List of Figures

List of Tables

Nomenclature

CA	crank angle
CAD	crank angle degree
RPM	revolutions per minute
TDC	top dead center
BDC	bottom dead center
FMEP	friction mean effective pressure
FLE	floating liner engine
TLOCR	twin land oil control ring
OD	outer diameter
HTHS	high temperature high shear

1. Introduction

1.1. Background

With the increased interests in reducing internal combustion engine fuel consumption and strengthened regulations on emission levels, automotive companies are putting in additional effort to optimize the engine power cylinder system to reduce the friction loss while trying to achieve an adequate oil control.

Mechanical friction loss is a major source of energy dissipation in the internal combustion engines that can consume up to 15% of the total energy input from fuel combustion [1]. Piston assembly friction is the major source of mechanical friction that contributes about 50% of the total mechanical friction loss. Ring friction can contribute about 50% of the piston assembly friction [2, 3].

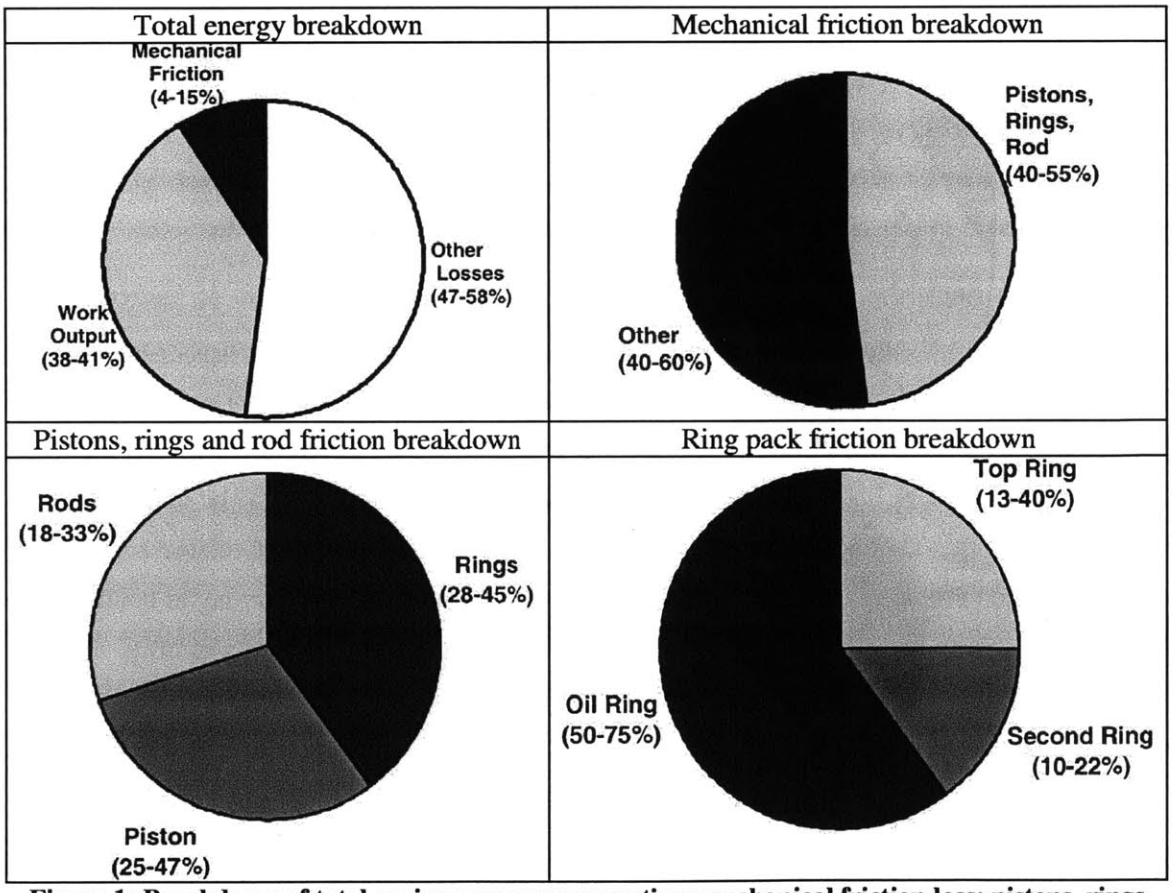

Figure 1: Breakdown of total engine energy consumption; mechanical friction loss; pistons, rings and rod friction; and ring pack friction [3]

1.2. Piston Rings

In the current piston assembly, three piston rings are usually used: the top ring, or the compression ring, seals the gas in the combustion chamber and controls blow-by; the second ring, or the scraper ring, acts mainly as secondary control of the upwards oil flows; and the oil control ring, below the top two rings, mainly controls the oil distribution on the cylinder liner.

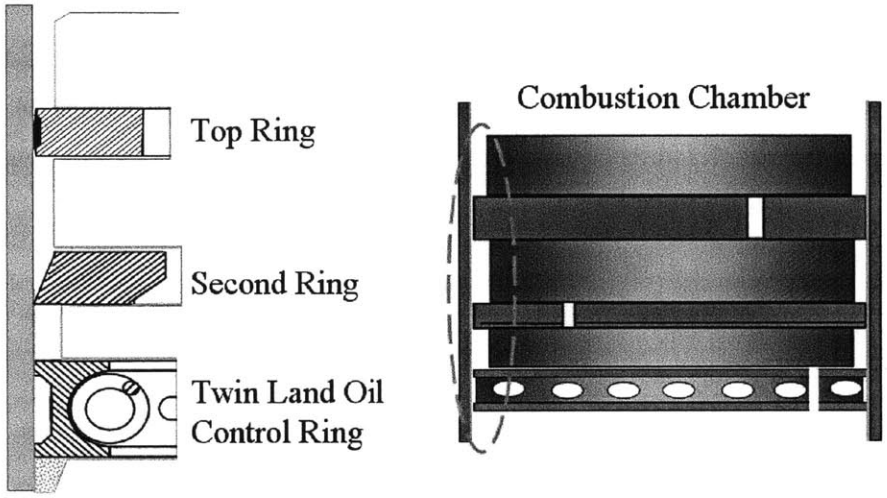

Figure 2: Piston rings on the piston assembly [4]

Among the piston rings, the friction and performance of the oil control ring is of particular interest. First, the ring tension of the oil control ring can be larger than the sum of the top two rings. Therefore, it can be the dominating contributor to the ring pack friction [3]. Second, the oil control ring limits the thickness of the oil film passing through it during piston downstrokes. The oil film left on the cylinder liner after the passage of the oil control ring becomes the oil supply for the top two rings. Therefore, the friction of the top two rings is highly related to the performance of the oil control ring [5]. In addition, the oil left on the liner above the oil control ring has the potential to travel up to the combustion chamber and to burn. The loss of oil to the exhaust increases oil consumption and the emission level. Certain inorganic components of the oil additives can poison the engine aftertreatment system and reduce its conversion efficiency [6, 7].

Various designs exist for oil control rings [8], and the oil control rings used in this work are two piece twin land oil control rings (TLOCR).

A TLOCR consists of a ring and a tension spring. The ring has two lands that are in contact with the mating cylinder liner surface during operation. Therefore, when fitted into the bore, the two lands usually have a flat profile that is parallel to the nominal plane of the liner after an extended period of operation. As a result, the geometrical variation of the liner roughness is solely responsible for generating hydrodynamic pressure when the ring is dragging oil through the rough liner [9]. The lubrication of the TLOCR thus involves strong interaction of the liner finish, the ring and the lubricants, which dictates the outcome of the ring pack friction and oil consumption in large part [10]. It is critical to establish an adequate understanding of the lubrication and friction of the TLOCR in order to realistically predict the friction of the entire ring pack and the effects of designs from rings, liner finish and lubricants [11].

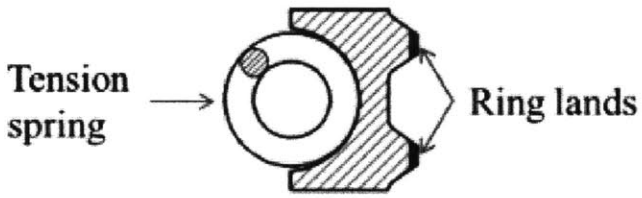

Figure 3: Two piece twin land oil control ring

1.3. Evolution of Cylinder Liner Surface

Traditionally, cylinder liners are manufactured through three steps: boring, base honing and plateau honing [12]. After the two-step base honing and plateau honing, the cylinder liner surfaces usually have smoother plateau areas and deep valleys [4].

Recently, new honing technologies have been applied to give cylinder liner surfaces the desired topography to enhance wear resistance and reduce oil consumption [13].

In reality, the geometry of the liner finish experiences constant change from interacting with the piston, rings and lubricants. From the functional point of view, the change may in general be divided into several stages. First, the change is at the level of the peaks of some individual asperities that are in direct contact with the piston and rings. The change also includes minor scratches that may be generated from the third-body interaction that involves worn particles, the

piston/rings and the liner. In the first stage, the main geometrical structure of the liner finish is not affected. It can be argued that this stage represents the commonly referred to break-in period. Then, in the second stage, the liner finish geometry may be stabilized for the entire engine life, which represents the best outcome. However, the liner finish may experience another stage of change, during which more and more vertical scratches are created on the plateau part of the surface. When more and more materials are removed, the relatively-large structure of the liner finish on the plateau part is modified [4]. As a result, flow resistance is reduced when the ring is dragging oil through the rough liner, and thus the ability of hydrodynamic pressure generation from the ring/liner interaction may be reduced. This reduction may result in more direct metal-metal contact between the rings and the liner, and therefore wear of the rings and the liner. Eventually the wear leads to another stage known as polishing when all the original liner finish features are removed. Then, most likely failure of the system will follow.

1.4. Experimental Study on Engine Power Cylinder System Tribology

From the experimental side, rotary bench tests [14, 15, 16, 17, 18] and reciprocating bench tests [19, 20, 21] were developed to study the basic friction and wear behavior of the cylinder and the ring material. The floating liner engine fired tests [14, 22, 23, 24, 25, 26, 27, 28, 29] were developed to measure the friction and wear related to the internal combustion engine power cylinder system.

The rotary bench tests are used in the automotive industry to measure wear, scuffing and the friction coefficient [14]. However, the tests cannot reflect the geometry of the components in an internal combustion engine. In addition, such tests usually have limited ability to measure hydrodynamic lubrication, which can be common in the lubrication between piston rings and cylinder liners.

Reciprocating bench tests have the ability to measure the friction behavior of real piston rings and cylinder liners. A modified Cameron-Plint high frequency friction machine can be used to study of the effects of oil properties [19, 30], new materials and coatings [14, 31] on engine friction and wear.

The reciprocating bench test machine generally consists of a fixed specimen, a moving specimen and the measurement system. The moving specimen is mounted on a carrier head and slides

against the fixed specimen. The load is applied on the moving specimen. A piezoelectric transducer is used for friction measurement.

Due to their convenience in modifying the applied load, oil supply and testing components, reciprocating bench tests are particularly helpful for the study of the friction mechanisms and factors affecting boundary or mixed lubrication with direct metal contact, such as the study of the lubricant additives and coating materials.

The floating liner engine (FLE) method has the ability to measure the piston assembly friction under engine operating conditions.

Takiguchi et al. modified the FLE system and used it to study the effects of the piston skirt design, lubricant film thickness distribution, oil viscosity, piston skirt profile and cylinder clearance on piston assembly friction under fired conditions [22, 23, 24, 25, 32]. The FLE method is able to encompass the effects from cylinder pressure variation, blow-by acting on oil distribution and fuel dilution. Its convenience in the piston, piston ring and cylinder liner sleeve replacement facilitates the study of the effects of the aforementioned engine components on friction.

Cho et al. [33] studied the lubrication behavior of a barrel-shaped oil control ring under the fully flooded condition using a modified FLE method that controlled the piston movement to be only in the vertical direction. Motoring tests were used in the study. This method is successful in eliminating the effects from piston skirt and isolating the friction from piston rings. Reasonable piston ring lubrication regime progression results from boundary lubrication to mixed lubrication to hydrodynamic lubrication were demonstrated. However, due to the limitation of the system, fired tests couldn't be conducted. In addition, the ring geometry, surface topography, oil properties and oil supply effects were not considered.

Shayler et al. studied the ring tension and piston skirt effects at a low temperature through a motoring test [34]. The work targets the cold start of the vehicle with an operating temperature and oil viscosity different from the normal vehicle operating conditions. Results and comparison of different ring tensions were used to interpolate the zero ring tension friction to identify the contribution from the piston skirt. This method provides a possible solution to isolate the friction from the piston skirt and piston rings during an experimental setup that the piston side force is

unavoidable. However, the reported results imply that at high oil viscosity, no consistent FMEP (friction mean effective pressure) variation trend is observed as the ring tension increases. Therefore, the interpolation cannot be conducted at such a regime [34].

1.5. Simulation of Piston Ring Pack Friction

Tian [5] built a piston ring pack model to study the performance of piston rings during different engine operating conditions. In this work, important factors including ring/liner lubrication, ring dynamics, ring/groove interaction, oil transportation and gas flow are considered.

Tian and Wong then concentrated on the TLOCR lubrication and replaced the hydrodynamic part of the TLOCR model with the deterministic correlation [35].

Chen [4] later improved the deterministic calculation in the TLOCR model initiated by Tian and Wong [35]. The deterministic TLOCR model developed by Chen [4] is based on the deterministic calculation method introduced by Li, Chen and Tian [36, 37]. The method calculates the oil transportation and the pressure generation between a flat surface and a rough surface under a reference sliding speed and a constant mean distance. A correlation method is introduced to calculate the hydrodynamic pressure generation ability of a ring-liner surface mating pair under different sliding speeds and oil film thicknesses [9].

The hydrodynamic pressure and shear stress are correlated with the sliding speed and the oil film thickness in the following form:

$$p_{hydro} = \frac{\mu U}{(\mu U)_0} p_0 \left(\frac{h}{\sigma_p} \right)^{-K_h} \tag{1}$$

$$f_{hydro} = \frac{\mu U}{h} \left(C_{f1} + C_{f2} e^{-C_{f3} \frac{h}{\sigma_p}} \right) \tag{2}$$

P_{hydro} and f_{hydro} stand for average hydrodynamic pressure and shear stress, respectively. P_0 and K_h are two characteristic constants. P_0 reflects the hydrodynamic generation ability of the ring and rough liner mating pair and K_h characterizes the speed of hydrodynamic pressure degradation as the ring and the cylinder liner separate from each other. μ and U are the instantaneous oil

dynamic viscosity and the ring sliding speed, respectively. μ_0 and U_0 are the reference oil dynamic viscosity and the reference ring sliding speed used in the deterministic calculation, respectively. h is the mean oil film thickness and σ_p is the cylinder liner plateau roughness. Thus the h/σ_p ratio represents the oil film thickness normalized by the cylinder liner plateau roughness. In the expression of hydrodynamic shear stress, C_{f1}, C_{f2} and C_{f3} are three non-dimensional parameters mainly decided by the liner roughness micro-geometry.

In addition to the aforementioned hydrodynamic part, the boundary contact pressure between a TLOCR and a liner surface is calculated using the Greenwood-Tripp method [38, 39]. The model has the following form:

$$P_C = K\ E\ F_{2.5}\left(\frac{h}{\sigma_p}\right) \tag{3}$$

$$K = \frac{8\sqrt{2}}{15}\pi\left(N\beta\sigma_p\right)\sqrt{\frac{\sigma_p}{\beta}} \tag{4}$$

$$E = \frac{2}{\left(\frac{1-\nu_1^2}{E_1} + \frac{1-\nu_2^2}{E_2}\right)} \tag{5}$$

where β is the asperity radius of the curvature; σ_p is the plateau roughness of the liner finish; N is the number of asperities per unit contact area; E_1 and E_2 are Young's modulus of the ring and the liner material; ν_1 and ν_2 are Poisson's ratios of the ring and the liner material;

and

$$F_{2.5}\left(\frac{h}{\sigma_p}\right) = \begin{cases} A\left(\Omega - \frac{h}{\sigma_p}\right)^Z & \frac{h}{\sigma_p} \le \Omega \\ 0 & \frac{h}{\sigma_p} > \Omega \end{cases} \tag{6}$$

where the function F2.5(h/σ_p) relates the probability distribution of the asperity heights; Ω=4.0, A=4.4068×10-5, and Z=6.804 are the coefficients for the convenience of the numerical calculation of the distribution function [38, 39, 40].

The load from the TLOCR is balanced by the sum of hydrodynamic pressure and contact pressure generated between the TLOCR and the cylinder liner.

The model input of the cylinder liner surface is usually obtained from the confocal microscopy measurement of a small patch on the cylinder liner, which is usually stitched together using many smaller patches of individual measurements. Figure 4 shows a typical cylinder liner surface input for the deterministic TLOCR model.

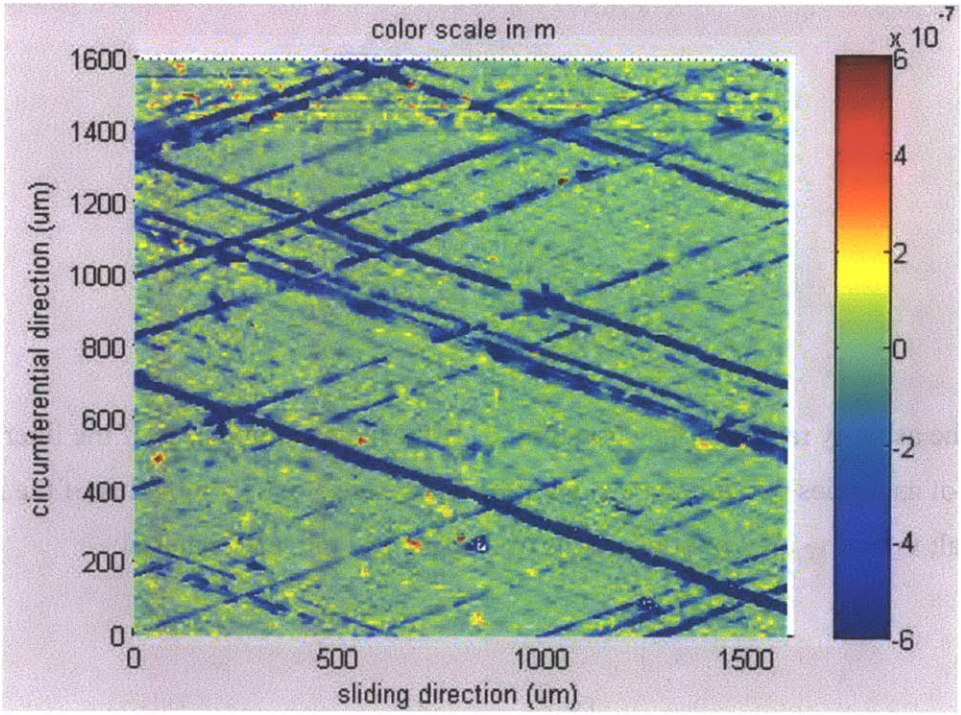

Figure 4: A typical confocal microscopy measurement of a cylinder liner surface patch

1.6. Instantaneous Stribeck Curve

The friction coefficient between the piston ring and the cylinder liner can be described by an instantaneous Stribeck Curve, as in Figure 5, which is derived from the original Stribeck Curve [40]. The X axis of the original Stribeck curve is the oil dynamic viscosity times the rotation

speed divided by the load, where the rotation speed is represented by revolutions per minute (RPM) for a bearing [40]. However, when applied to the internal combustion engines, at the same rotation speed in terms of RPM, the piston's linear speed varies based on its location. Therefore, in this work, the instantaneous piston speed is used to calculate the instantaneous Stribeck curve.

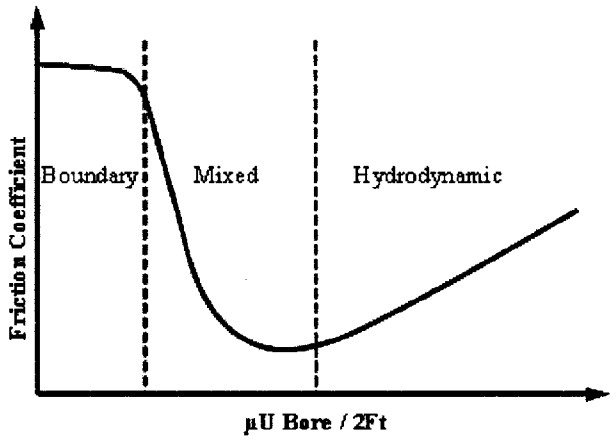

Figure 5: Instantaneous Stribeck curve indicating lubrication regimes

On the instantaneous Stribeck curve, the X axis is:

$$\frac{\mu U Bore}{2Ft}$$

where μ is the dynamic viscosity of the oil, U is the instantaneous piston linear speed, Ft is the ring tension in tangential force and Bore is the diameter of the engine cylinder.

The Y axis of the instantaneous Stribeck curve is the friction coefficient calculated from the friction data of each crank angle (CA).

It should be noticed that, for the X axis, the U is the instantaneous piston linear speed instead of the engine RPM. As a result, the measured data within one cycle can provide vast information for the instantaneous Stribeck curve calculation. The data measured at each CA can be used. As a

result, the accuracy of the system becomes critical. The first step before using the instantaneous Stribeck curve should be validating the reliability of the measurement results. The shapes of individual friction traces and the variations across different sets of measurement can be used as the initial check. If the system is accurate, experimental results of the same ring and liner but different ring tensions, operating temperatures and engine speeds should be able to fall onto the same instantaneous Stribeck curve. Therefore, the merging of instantaneous Stribeck curves is another validation tool for the system accuracy.

1.7. Objective of Thesis Work

Despite the past efforts, there remains a lack of detailed answers to the question of how would different factors affect the friction of the piston ring pack, especially the friction of the TLOCR under engine operating conditions.

The friction of the TLOCR is determined by factors including the TLOCR design, liner finish and lubricants. There has not been a coherent work employing both experimental and theoretical tools to study the combined effects of the aforementioned factors with extensive parameter ranges.

The objective of the present work is to study extensively how these three factors, the TLOCR design, liner finish and lubricant viscosity, affect the piston ring friction, with both experiments and modeling. In addition, the effects of liner finish changes, or break-in, on friction will also be investigated.

1.8. Organization of the Thesis

The second chapter of this thesis introduces the FLE system and the modification of the floating FLE system for TLOCR motoring tests.

The third chapter introduces the deterministic TLOCR model developed by Chen, Li and Tian [4, 36, 37]. Methods to properly prepare model inputs are discussed. This chapter also provides a model validation using the FLE system.

The fourth chapter discusses the practical challenges when using the deterministic TLOCR model to calculate the TLOCR friction. This chapter concentrates on surface variations across

the liners and their effects on the calculation. A multi-point correlation method is introduced and a calculation case is provided.

The fifth chapter introduces the effects from the ring land width and ring tension on TLOCR friction.

The sixth chapter discusses the cylinder liner roughness effects on TLOCR friction. The first part of the chapter introduces the study of liner break-in using liners covering a large range of roughness. The second part of the chapter discusses the effects of liner finish on TLOCR friction after the break-in is finished.

The seventh chapter discusses how to use the outcomes from the previous chapters to improve the ring/liner system design. An improved design is provided. Compared to the current industry norm, the improved design gives lower TLOCR friction and better oil control capability.

The last chapter summarizes and concludes the thesis, in addition to providing potential future work directions related to this topic.

2. The Floating Liner Engine (FLE) System

2.1. Original Floating Liner Engine Configuration

The FLE method is used in this work to measure the ring friction. The configurations of the FLE are provided in Figure 6 and Table 1.

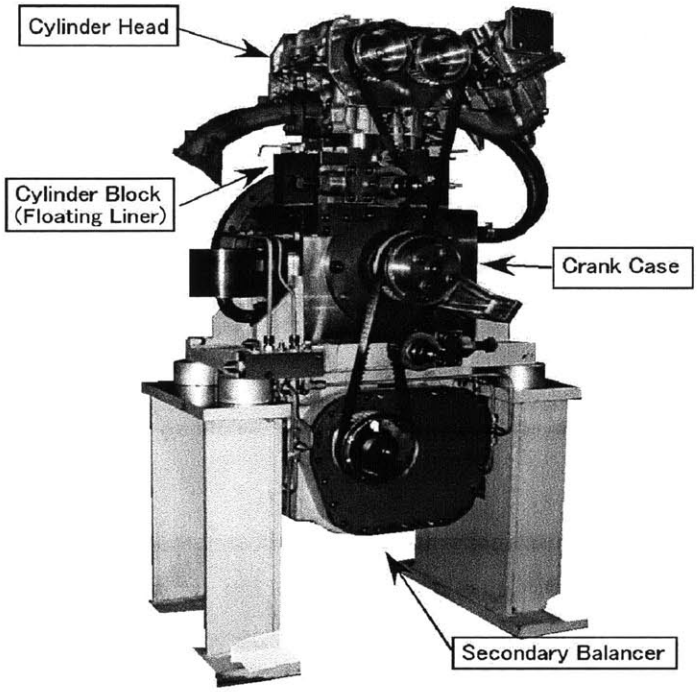

Figure 6: Floating liner engine

Table 1: Floating liner engine specification

Displaced volume	0.496L
Stroke	92.8 mm
Bore	82.5 mm
Compression ratio	10:1
Maximum BMEP	0.7MPa
Maximum engine speed	3000RPM

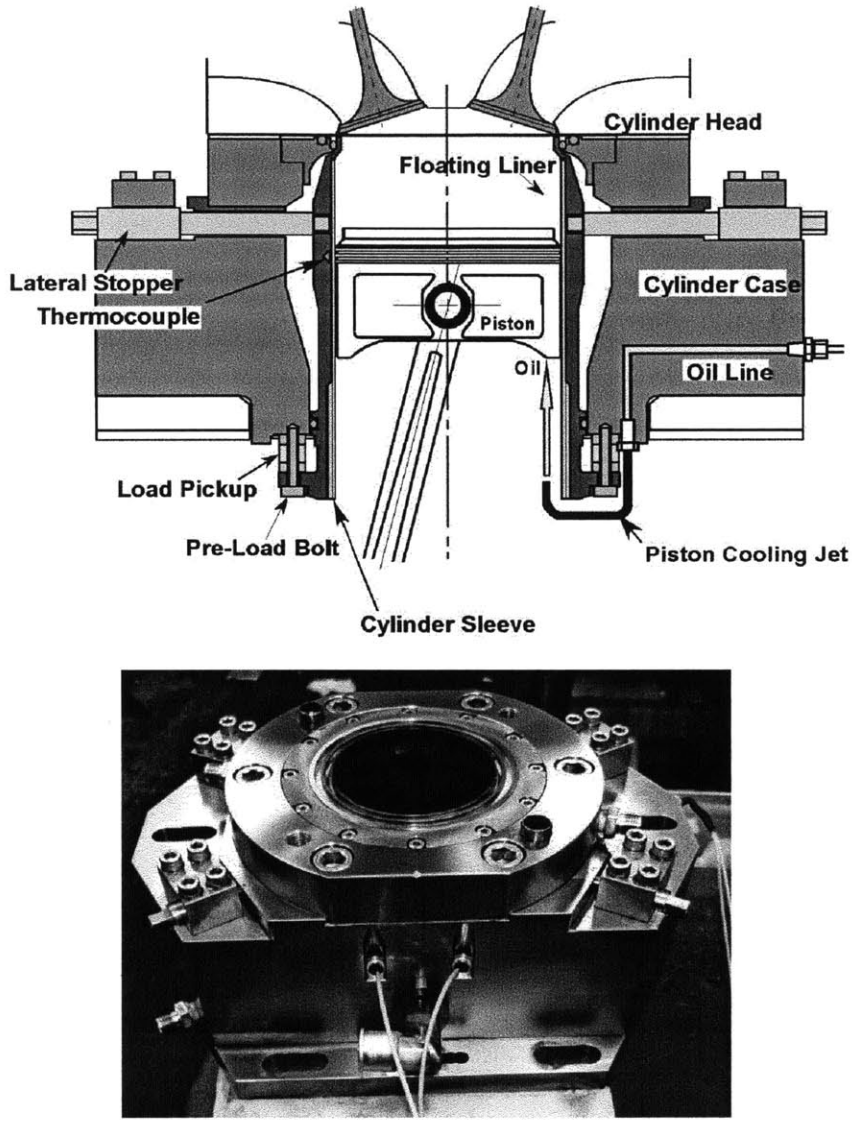

Figure 7: Cross section and block part of floating liner engine

The FLE was provided by Professor Masaki Takiguchi at Tokyo City University (formerly Musashi Institute of Technology) in 2009. Figure 7 shows the engine cross section and the FLE block. Vertically, the floating liner part is supported by two pre-load bolts at the thrust and anti-thrust side from the bottom. The two bolts are mounted on the cylinder block going through two piezoelectric force sensors, one on each side. The two load sensors at the bottom pick up the vertical micro movement of the floating liner due to the piston assembly friction. The lateral force from the piston is balanced by the four stick lateral stoppers at the top and a thin plate

shaped lateral stopper at the bottom. The cylinder sleeve is screwed onto the cylinder liner and can be easily replaced. The gas pressure in the combustion chamber and the coolant in the coolant jacket are sealed by two O rings at the top.

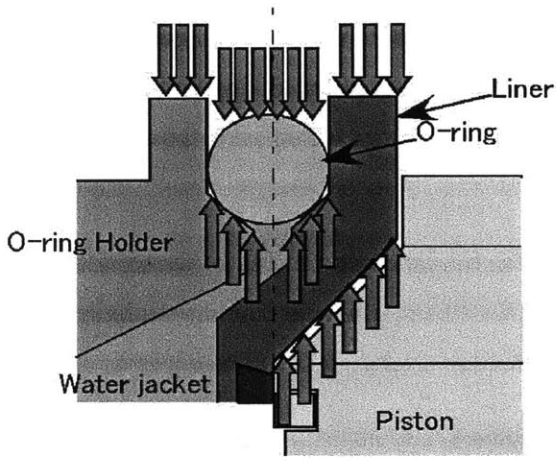

Figure 8: The mechanism of coolant seal and combustion chamber pressure balance [41]

The method by which the O-ring seals the coolant and the mechanism it balances the combustion chamber pressure are shown in Figure 8. The combustion pressure acting from above the O-ring should be evenly balanced by the O-ring holder and the top part of the liner from below the O-ring. By doing so, the net vertical force acting on the liner due to the combustion chamber pressure should be zero. Therefore, the combustion chamber pressure shouldn't affect the vertical friction force reading by the load sensors.

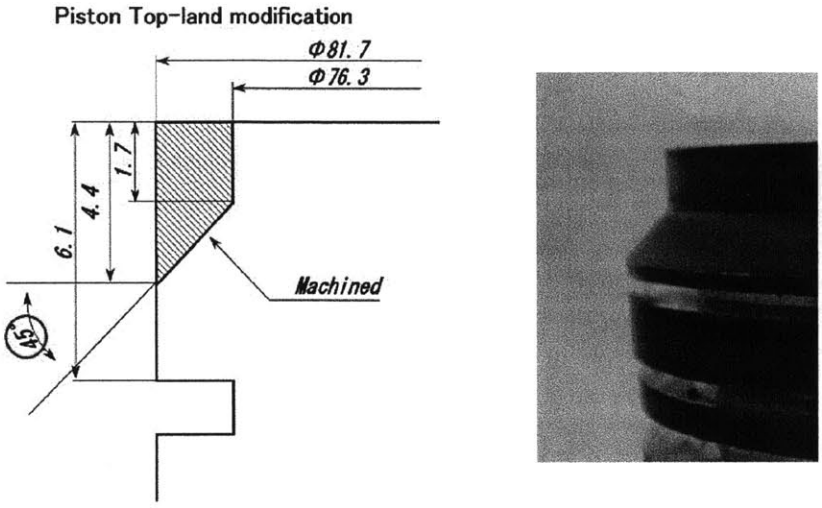

Figure 9: Modification of piston top land

In order to run experiment using the FLE, the top land of the piston needs to be modified as shown in Figure 9. The FLE requires the modification to balance the combustion chamber pressure.

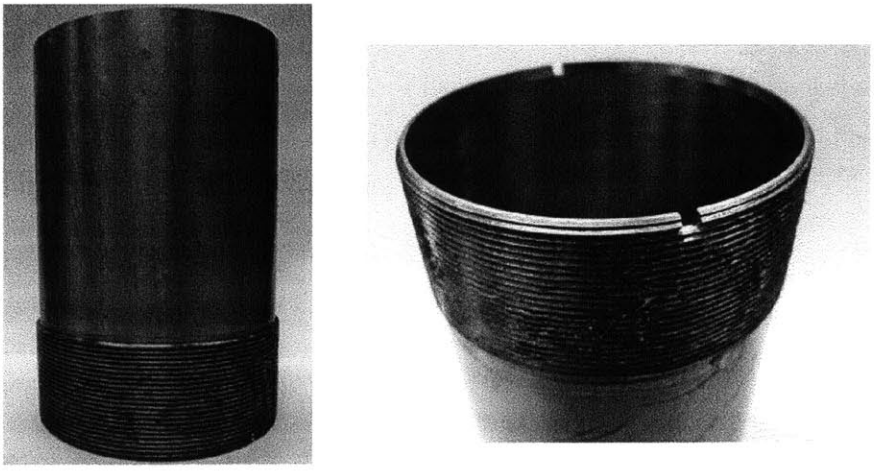

Figure 10: Cylinder sleeve of the floating liner engine

A cylinder liner sleeve is installed on the floating liner via the screw at the bottom of the sleeve, as shown in Figure 10. By changing the sleeves with different surface honing and finish, one can study the effects of the cylinder surface topography on piston ring pack friction.

2.2. Modification of Floating Liner Engine System

2.2.1. Engine Setup Modification

In order to maximize the fidelity of the measurement results on TLOCR friction, a special procedure was developed that involved the following items:

- Motoring tests were used
- The cylinder head was removed to eliminate the effect of combustion chamber pressure variation
- A 'small piston' with 100μm diametrical skirt clearance at the cold condition was used to reduce piston skirt friction
- Only one TLOCR was installed on the piston and the top two rings were removed
- The friction of the piston alone was measured to partially determine the piston skirt friction while the piston is running with the TLOCR
- The crankcase pressure of the FLE was fully released to eliminate the effect of crankcase pressure variation on the piezoelectric sensors reading

However, since the top four lateral stoppers are screwed in the floating liner body, the lateral stoppers have the potential to take part of the vertical friction force when the liner has dynamic movement. In addition, the piston alone friction may not be the same as the piston skirt friction when the piston is running with the TLOCR on. This topic will be discussed later in Section 2.2.4.

Figure 11 shows the modified FLE system.

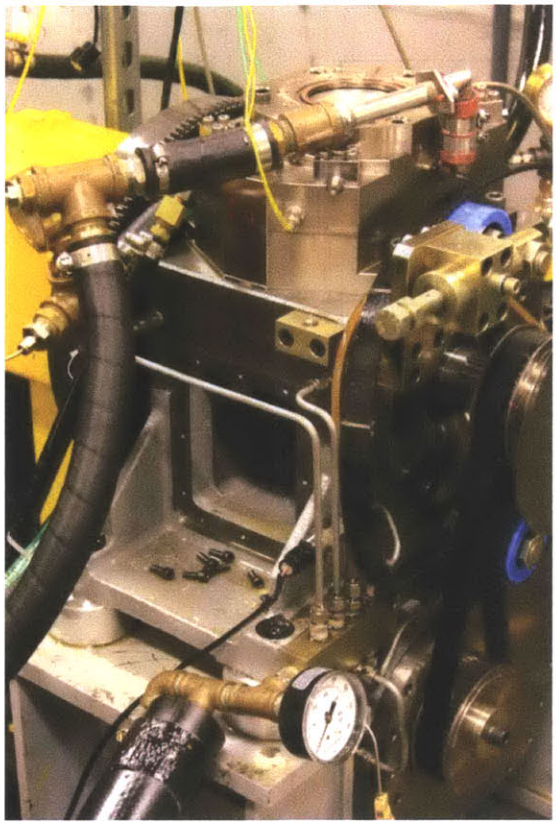

Figure 11: Floating liner engine setup for ring friction measurement under the motoring condition

The friction of a single TLOCR is small and therefore more sensitive to the FLE system dynamic effects resulting from piston secondary motion. Assuming the dynamic behavior of the FLE would be positively correlated with the engine speed, the engine speed was controlled to be below 1000RPM for the TLOCR-only friction study.

2.2.2. Crankcase Pressure Effect [42]

The load pickups of the FLE are two piezoelectric sensors mounted at the bottom of the liner, which are exposed to the crankcase pressure variation. Crankcase pressure variation causes excessive errors when reading friction forces.

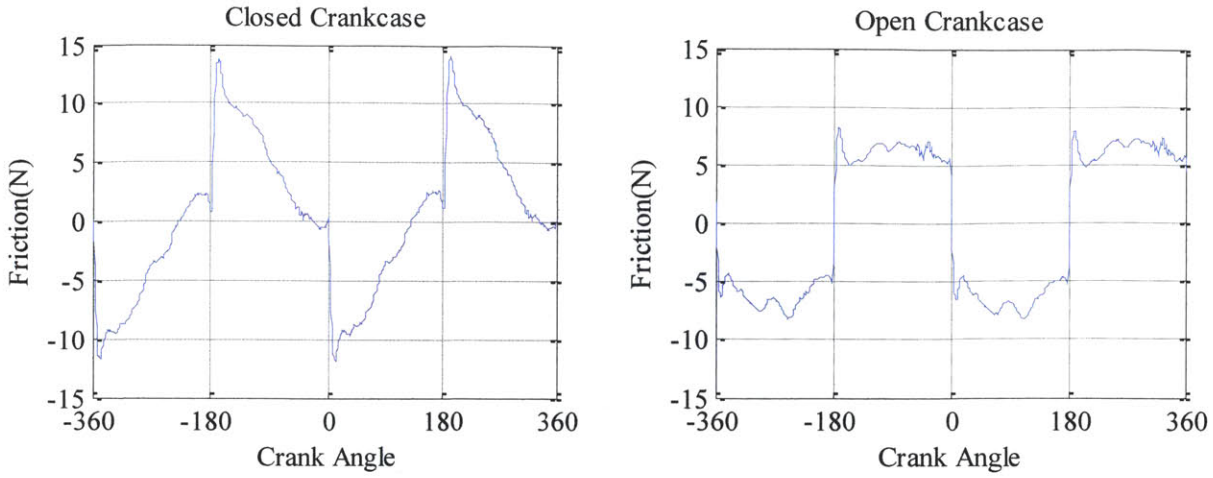

(a) Friction traces [42]

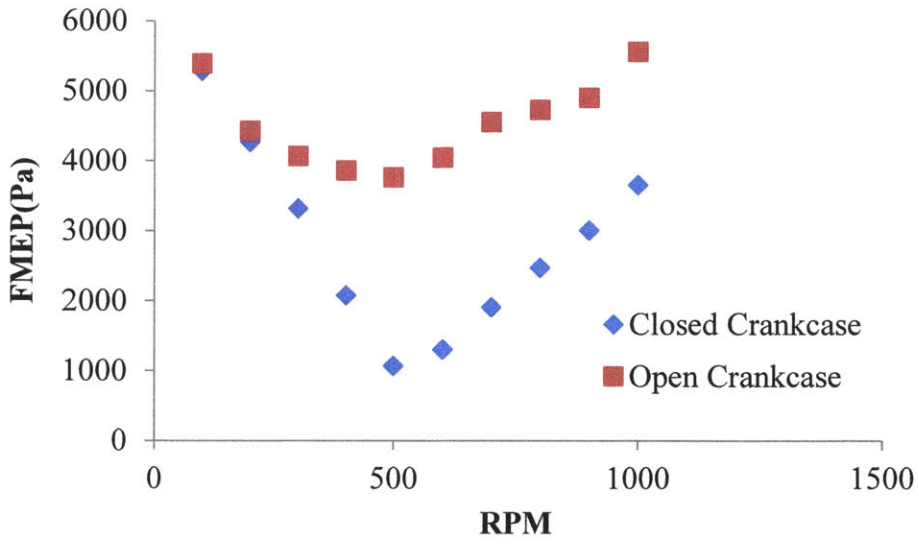

(b) FMEP

Figure 12: (a) Friction traces and (b) FMEP of 0.15mm land width 10.5N tension TLOCR at 1000RPM and 100°C before and after opening the crankcase

Figure 12 shows the experimental results under the same test setup and test conditions but one with closed crankcase and one with open crankcase. The friction trace difference is clear. The results suggest that the crankcase pressure variation can also be picked up by the load sensors if the crankcase is closed. The instantaneous friction values are inaccurate and the calculated FMEP is 3.65KPa when crankcase is closed compared to 5.56KPa when the crankcase is open.

The strong crankcase pressure variation may result from the limited crankcase volume and insufficient pressure ventilation.

As described by the instantaneous Stribeck curve, theoretically, when the piston speed is very low, the piston rings usually operate in the boundary lubrication regime. Contacts between the piston rings and the cylinder liner take place and bear the ring load. As a result, the total friction is usually high. As the piston speed begins to increase, the piston rings start to operate in a mixed lubrication regime. Hydrodynamic pressure starts to build up between the piston rings and the cylinder liner and takes part of the ring load. The boundary contact between the rings and the liner reduces, and the total friction reduces. As the piston speed further increases, the oil film completely separates the rings and the liner. The rings operate in a hydrodynamic lubrication regime. Viscous shear stress mainly contributes to the total friction between the rings and the liner. As the piston speed increases, the viscous shear stress and the total friction between the rings and the liner become larger.

Once the crankcase pressure is properly released, the friction trace demonstrates reasonable behavior: at the BDC and TDC regions where engine speeds are low, the piston ring operates in a boundary/mixed lubrication regime. Friction peaks at these regions are observed. As piston travels from the dead centers towards the mid-stroke, initially the friction drops and then increases. This can be explained by the instantaneous Stribeck curve. At dead centers where the piston speeds are low, little hydrodynamic pressure can be generated between the oil control ring lands and the cylinder liner surface. Thus the ring and liner contacting pair operates under a boundary contact-dominated regime. As the piston speed increases, hydrodynamic pressure starts increasing. As a result, boundary contact reduces and shear stress increases. At the initial stage when piston speed is relatively low, the benefit from reduced boundary contact outweighs the loss from shear stress, and the total friction decreases. While later at the mid-stroke, piston linear speed further increases. The increased shear stress outweighs the benefit from reduced boundary contact, resulting in a higher total friction force. The pattern of total friction increases as the piston speed increases is an indicator that the oil control ring operates in a hydrodynamic lubrication-dominated regime.

2.2.3. System Repeatability [42]

The repeatability of the modified system was examined by evaluating the variations of the cycle FMEPs calculated from the measured friction. In the tests, a TLOCR of 0.15mm land width and 10.5N tension was installed on the 100μm clearance piston. For the same test setup, engine speed was increased from 100RPM to 1000RPM at 100RPM intervals, and the process was repeated for 5 times.

The FMEP standard deviation over mean of the 5 sets of results at 100RPM, 300RPM, 500RPM, 700RPM and 1000RPM are shown in Figure 13. The results show that at 60°C, 80°C and 100°C, the standard deviation over mean of the 5 tests lies within 3% over the engine speeds up to 1000RPM. The results suggest that the modified FLE motoring system has good repeatability.

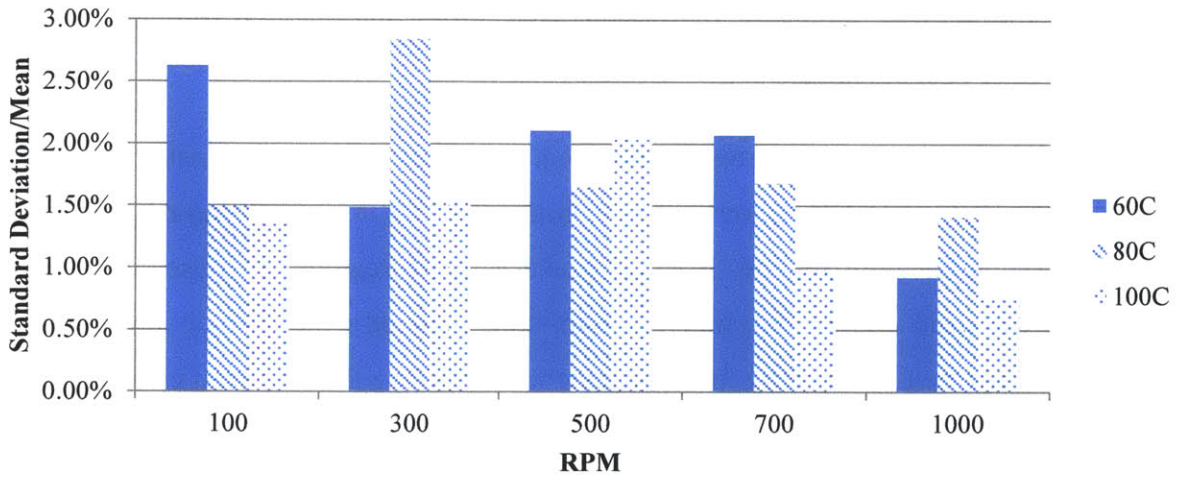

Figure 13: FMEP Standard deviation over mean of 5 sets of tests using the modified floating liner engine motoring system

For one set of test at each RPM, 28 cycles of friction data were recorded and the average FMEP of the 28 cycles was used to represent the FMEP at this RPM. Figure 14 shows the relative standard error (RSE) of the means of the 28 cycle FMEP results.

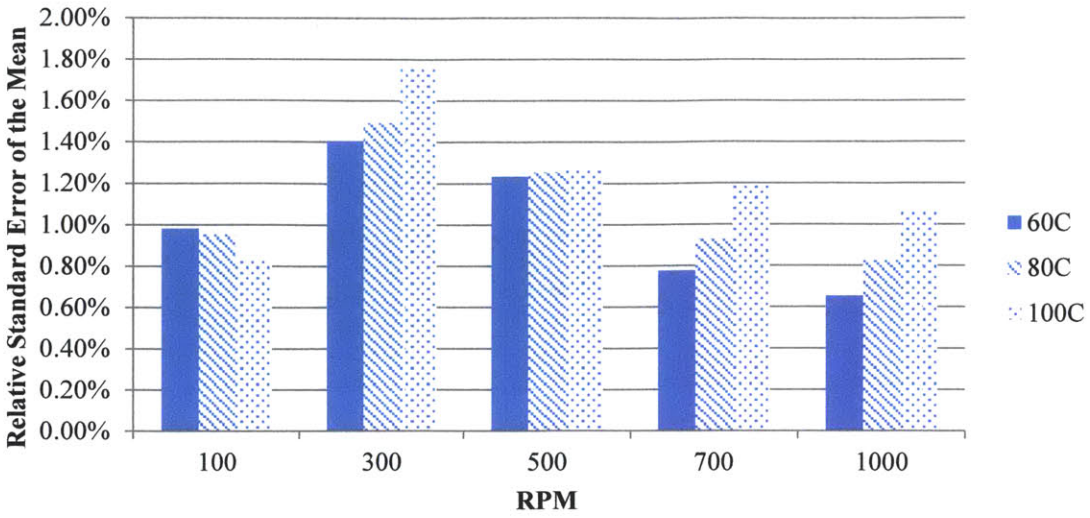

Figure 14: FMEP relative standard error of the mean of 28 cycles of data using the modified floating liner engine system for motoring tests

Figure 14 shows that at 60°C, 80°C and 100°C, the relative standard error of means of the tests at 100RPM, 300RPM, 500RPM, 700RPM and 1000RPM stay below 2%. The results indicate that the modified floating liner system demonstrates small system variations.

2.2.4. Piston Skirt and System Dynamic Effect [11]

Figure 15 shows the typical friction traces of the piston used in this study. In the piston friction tests, only a piston was installed on the crankshaft. All the piston rings were removed from the piston. Motoring tests were done with open cylinder head. The liner thrust side temperature was controlled to be 60 °C, 80 °C and 100°C. The engine speed increased from 100RPM to 1000RPM at 100RPM intervals.

It should be noticed that the oil distribution on the cylinder liner and the oil supply to the piston skirt are different with and without piston rings. As a result, the piston skirt friction without rings is different from that with a TLOCR. Nonetheless, this is the best option to experimentally determine the piston skirt friction. The results provide a first order approximation for the piston skirt friction in the case when both piston and piston rings are installed.

Figure 15 shows the piston friction at 100RPM, 500RPM and 1000RPM. The results in general show that piston friction increases with the piston speed. The effects of piston skirt friction

become stronger at mid-stroke and at higher engine speeds when hydrodynamic lubrication is dominant.

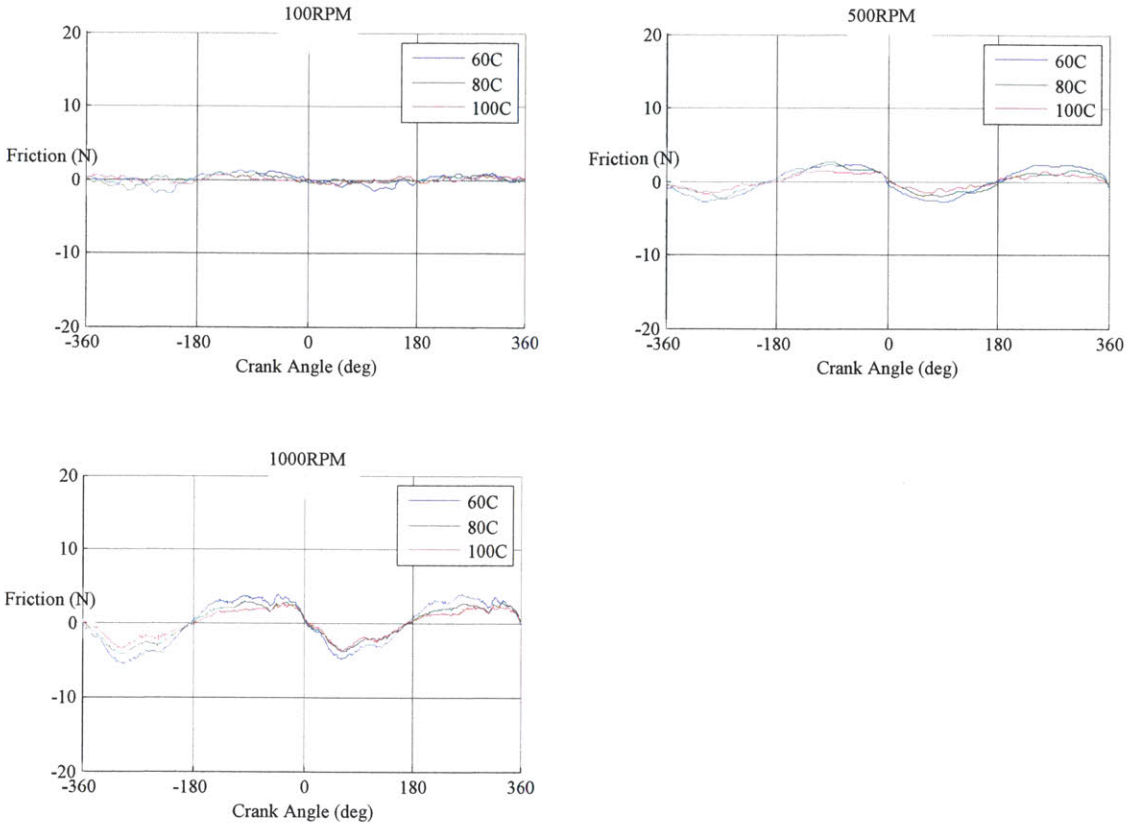

Figure 15: Friction trace results from the tests that only piston, no piston ring, is installed on the crankshaft

Figure 16 shows the friction difference of a piston with and without a 0.06mm land width TLOCR. It should represent the friction solely from the TLOCR. However, it is clearly shown that when the ring tension is 10.5N, the friction trace at the mid-stroke has abnormal behavior at engine speeds above 500RPM. At 1000RPM, from the start of the intake stroke (-360 crank angle degree, or -360 CAD), the friction increases with increased piston speed. The trend indicates the piston ring is operating in a hydrodynamic lubrication regime. The later sudden drop in friction at the mid-stroke cannot be explained solely by the hydrodynamic shear stress acting on the oil control ring. When the ring tension is increased to 28.5N, the piston friction effect is less obvious.

For the study of the TLOCR friction, the experimental instantaneous Stribeck curve should be calculated using the part of the friction results that are less affected by piston secondary motion. In the lower part of the strokes, piston speed is relatively low and piston oscillation is less strong. Therefore, friction from the lower part of the strokes should be used for instantaneous Stribeck curve calculation.

When the piston ring tension is small, the absolute value of the ring-only cycle FMEP results should be treated with caution. The mid-stroke friction, clearly affected by the piston secondary motion and lateral stoppers, has strong effects on the cycle FMEP values.

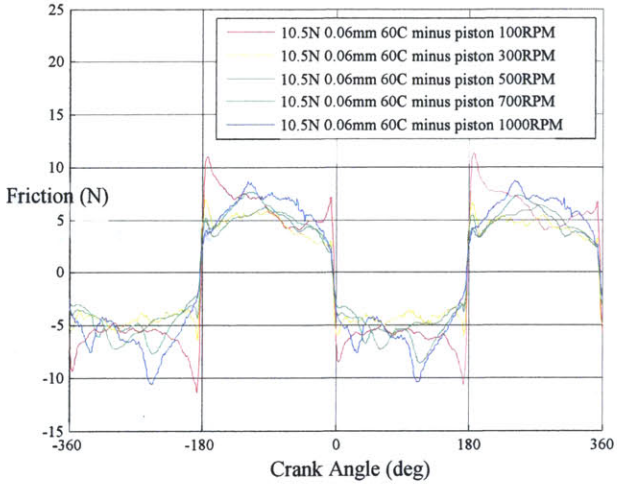

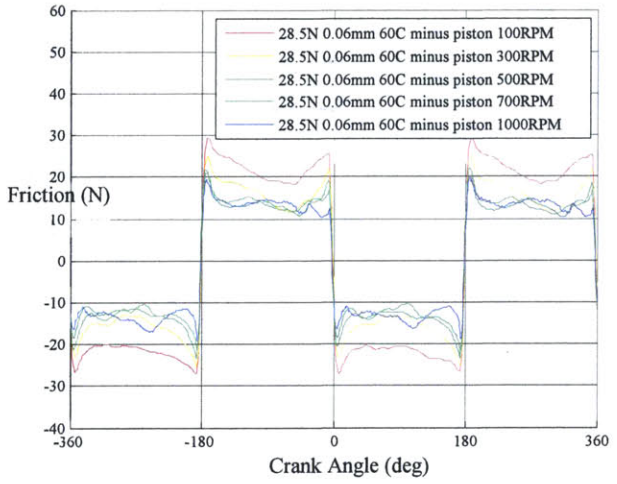

Figure 16: Friction trace difference between piston with installed TLOCR friction and piston-only friction, for 0.06mm land width TLOCR with 10.5N and 28.5N ring tension, respectively

2.3. Floating Liner Engine System Validation

2.3.1. TLOCR Profile

The FLE validation tests used 5W-30 oil. Only one TLOCR was used and the springs were changed to give different ring tensions. The selected 0.15 mm land width TLOCR was used for liner break-in over an extended length of time, which acted as lapping.

The ring profile measurement is shown in Figure 17. Figure 17 (a) shows that the land widths of both upper and lower land vary circumferentially. The mean land widths of the upper land and the lower land are also different. The 0.15mm value is merely a nominal value that best describes the ring profile. Figure 17 (b) and (c) show that the upper land and the lower land are well broken in and both have flat profiles.

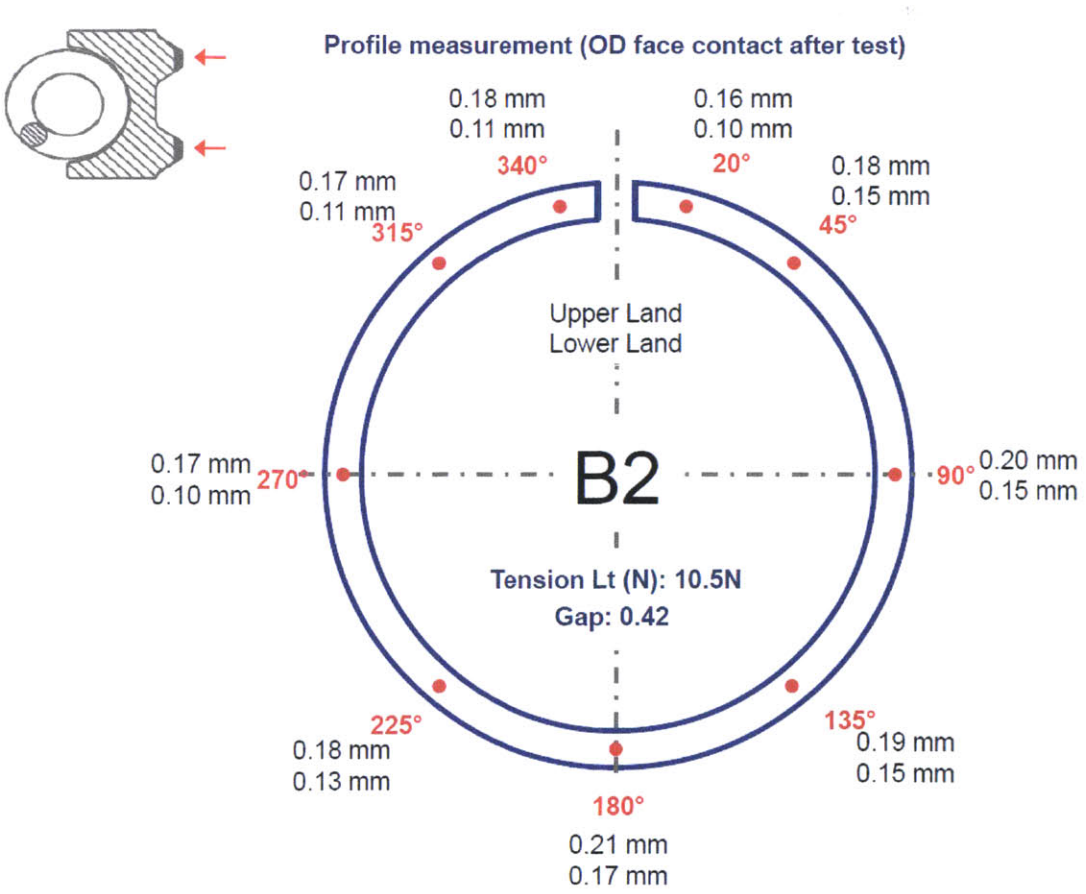

(a) Upper and lower land widths measured at different circumferential locations

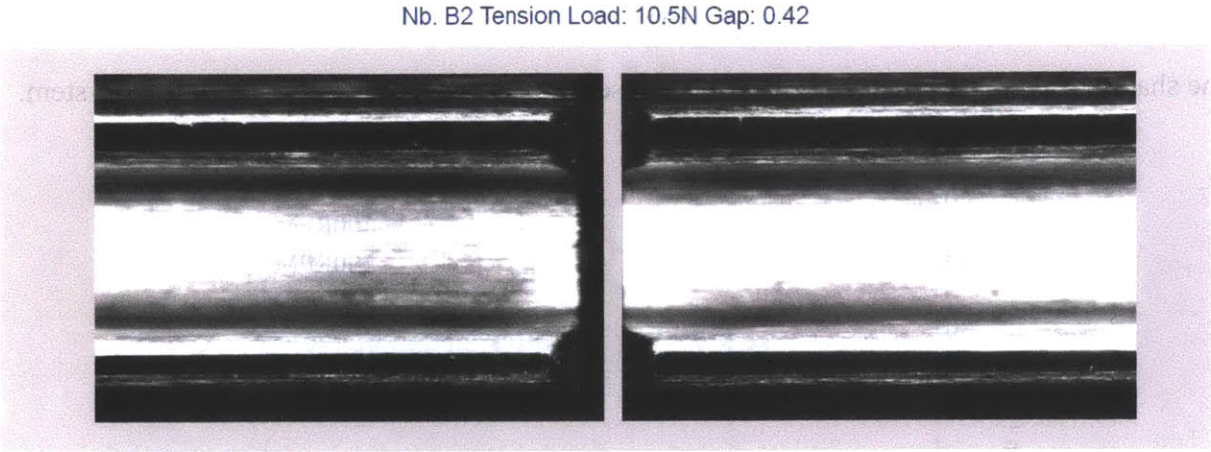

(b) Ring profile measurement at the ring gap

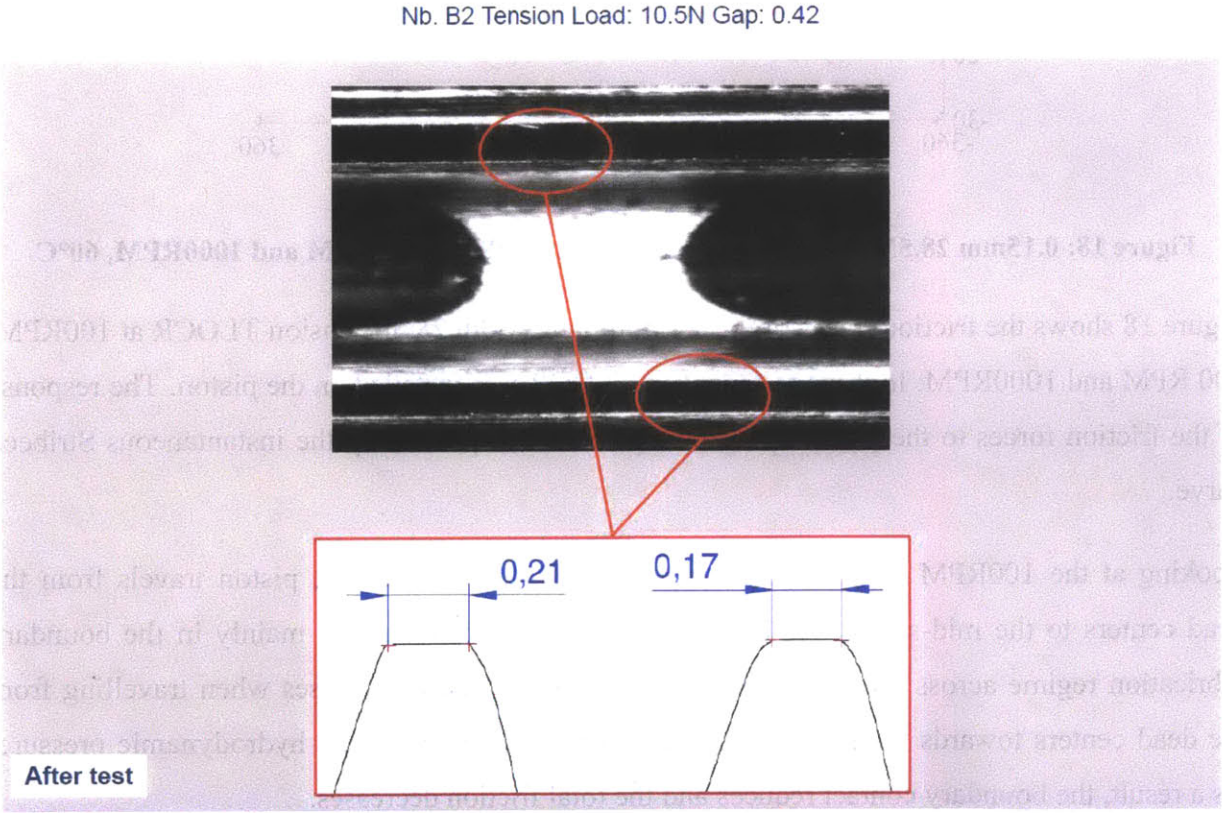

(c) Ring profile measurement opposite the ring gap

Figure 17: Profile measurement of a 0.15mm nominal land width TLOCR

2.3.2. Individual Friction Traces [11]

The shapes of the individual friction traces can serve as the first check of the modified system.

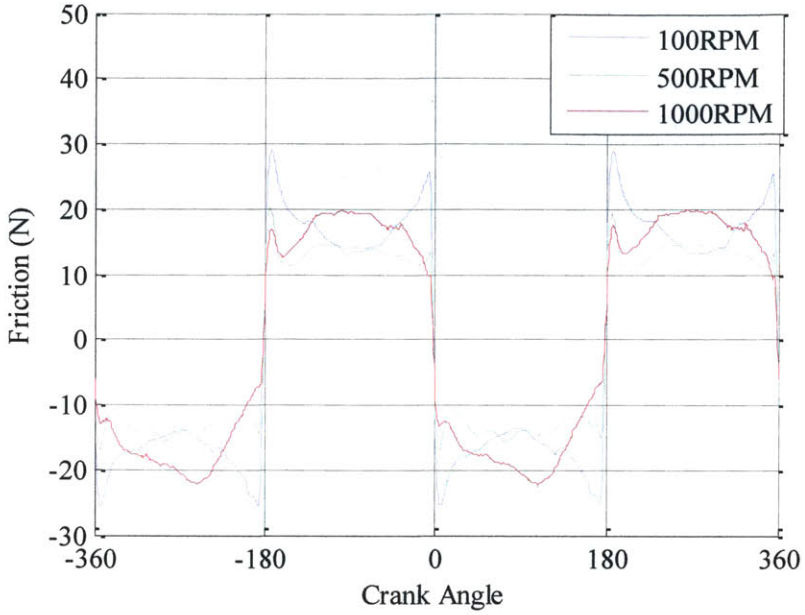

Figure 18: 0.15mm 28.5N TLOCR friction traces at 100RPM, 500RPM and 1000RPM, 60°C

Figure 18 shows the friction traces of the 0.15mm land width 28.5N tension TLOCR at 100RPM, 500 RPM and 1000RPM. In these tests, only a TLOCR was installed on the piston. The response of the friction forces to the piston speed change can be explained by the instantaneous Stribeck curve.

Looking at the 100RPM result, friction continuously decreases as the piston travels from the dead centers to the mid-stroke. At 100RPM, the TLOCR is operating mainly in the boundary lubrication regime across the entire stroke. As the piston speed increases when travelling from the dead centers towards the mid-stroke, the TLOCR generates higher hydrodynamic pressure. As a result, the boundary contact reduces and the total friction decreases.

At 500RPM, as the piston travels from the dead centers towards the mid-stroke, the friction initially decreases then increases. The trend indicates that at the mid-stroke, the TLOCR has passed the minimum friction coefficient point on the instantaneous Stribeck curve. Viscous shear stress is becoming the major contributor of the friction at the mid-stroke.

At a higher engine speed of 1000RPM, the friction at the dead centers is clearly lower than that at the mid-stroke. At the mid-stroke where the piston linear speed is high, the TLOCR is operating well into the hydrodynamic lubrication regime, and viscous shear stress is dominating.

At BDC and TDC regions, the engine speed approaches zero and boundary contact is most severe. Comparing the friction at the BDC and TDC regions across 100RPM, 500RPM and 1000RPM, the friction decreases as the engine speed increases. The benefit from increased hydro-pressure as the engine speed increases is obvious. At the dead centers, boundary contact still exists as the engine speed increases to 1000RPM.

At the mid-stroke, as the engine speed increases from 100RPM to 1000RPM, the friction first decreases then increases. At a very low engine speed of 100RPM, boundary contact is dominating even at the mid-stroke. As the engine speed increases to 500RPM, increased hydro-pressure lifts the ring and reduces the boundary contact. As the engine speed further increases to 1000RPM, increases in friction due to viscous shear stress outweighs the boundary contact friction reduction. As a result, at 1000RPM, the mid-stroke friction is higher than that at 500RPM.

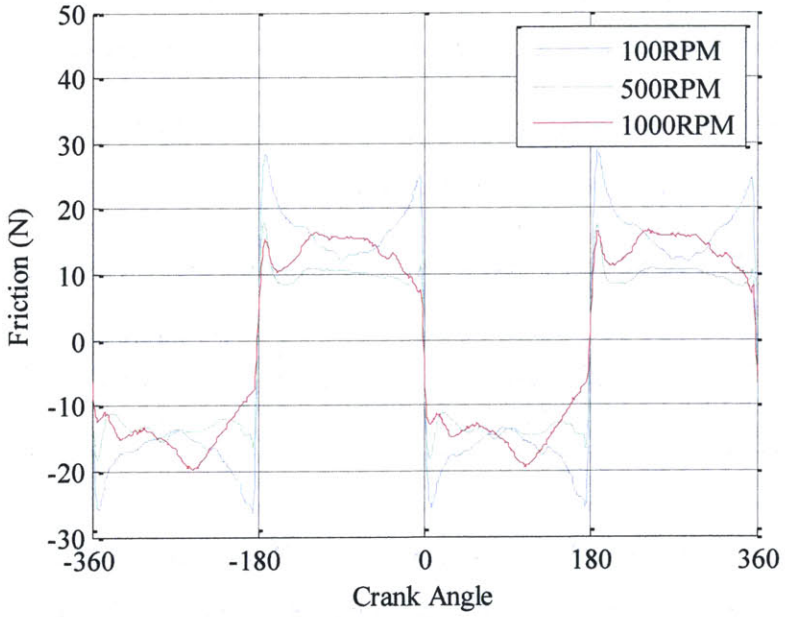

Figure 19: 0.15mm 28.5N TLOCR friction traces, after minus the corresponding piston friction, at 100RPM, 500RPM and 1000RPM, 60°C

Figure 19 shows the friction trace differences of the piston with and without the 0.15mm 28.5N TLOCR. It should represent the friction from the TLOCR only. Comparing Figure 18 and 19, it is shown that the piston friction is small relative to the 28.5N tension TLOCR friction. The effects from the piston skirt are mainly reflected at the mid-stroke of the 500RPM and 1000RPM friction traces. After the piston skirt friction is subtracted, the change of the TLOCR lubrication regime with respect to the piston speed remains the same.

2.3.3. Data Selection for the Instantaneous Stribeck Curve [11]

If the modified FLE system has good accuracy, for the same oil control ring profile and liner finish, the friction coefficient calculated from the friction results of different oil viscosity, engine speeds and ring tensions should be able to fall onto the same instantaneous Stribeck curve.

On the measured friction curves, the results close to the dead centers can be affected by the filtering process, because the friction is changing directions. Friction readings in the upper stroke can be more vulnerable to the effects from the lateral stoppers, whose extrusion may cause bore distortion. As a result, the friction results from 20 to 40CAD from the bottom dead center are selected to calculate the instantaneous Stribeck curve. This range should provide enough overlap on the instantaneous Stribeck curve between different test results, so that the accuracy of the experiment can be examined. Otherwise, a broader band of the friction results should be used.

The instantaneous Stribeck curve of a 0.15mm land width TLOCR was calculated with the friction results of the following tests, as shown in Table 2.

Table 2: Test results used to calculate the Instantaneous Stribeck Curve

Ring Type	Engine Speed	Temperature	Ring Tension
0.15mm land width TLOCR	100-1000RPM at 100RPM intervals	60°C, 80°C, 100°C	10.5N, 19.5N, 28.5N

For each ring type, the engine speed increased from 100RPM to 1000RPM at 100RPM intervals; the FLE thrust side temperatures were set to be 60°C, 80°C and 100°C; and the ring tensions were 10.5N, 19.5N and 28.5N.

2.3.4. Instantaneous Stribeck Curve Results

Figure 20 shows the instantaneous Stribeck curves of the 0.15mm land width TLOCR. Results from different ring tensions and temperatures can generally fall onto the same instantaneous Stribeck curves.

Taking the instantaneous Stribeck curve obtained from the friction test results of the 0.15mm 10.5N TLOCR at 100°C from 100RPM to 1000RPM as a baseline, the friction coefficient from the same TLOCR at 100°C but a higher engine speed can be obtained by reading along the instantaneous Stribeck curve further to the right, in which region the instantaneous Stribeck curve is represented by the 60°C and 80°C results. Although the maximum engine speeds at the 60°C and 80°C tests are also 1000RPM, the lower temperatures increase oil viscosity and extend the instantaneous Stribeck curve coverage range further to the right. Therefore, the aforementioned test method can extend the instantaneous Stribeck curve coverage range without going to high speeds.

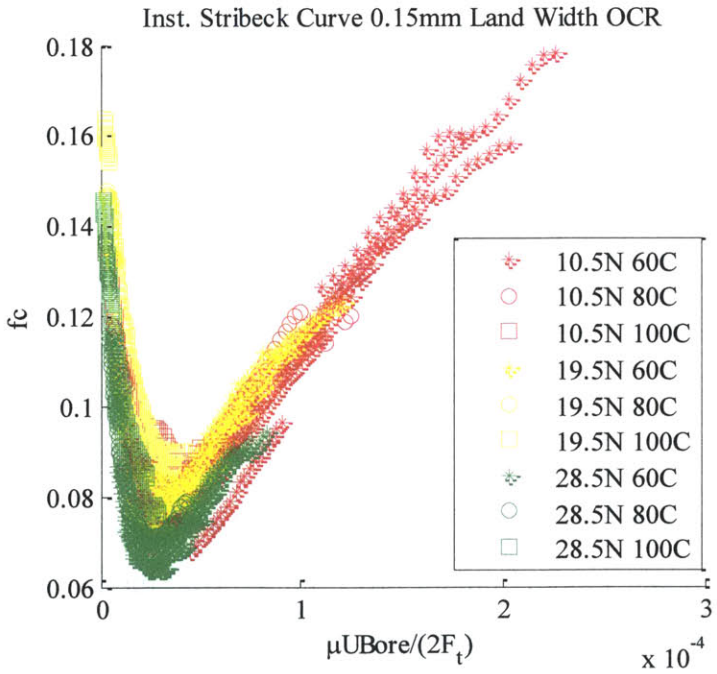

Figure 20: Instantaneous Stribeck Curve of 0.15mm land width TLOCR

Figure 21 shows the instantaneous Stribeck curve calculated using the original friction measurement minus the corresponding piston friction. The effect from the piston is observable. After subtracting the piston friction, the friction coefficient in the hydrodynamic lubrication

regime and the minimum friction coefficient in the mixed lubrication regime are lower. However, the friction coefficient results still generally fall onto the same instantaneous Stribeck curve.

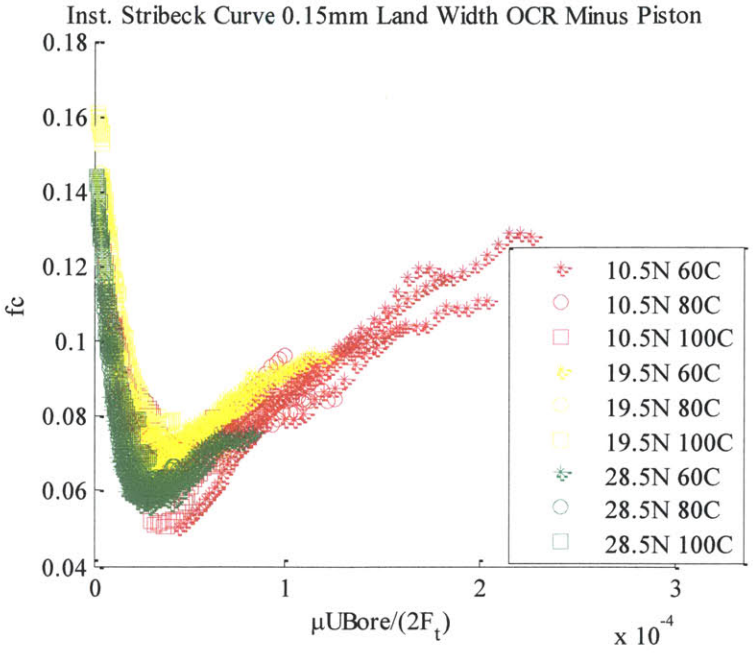

Figure 21: Instantaneous Stribeck Curve of 0.15mm land width TLOCR minus piston friction

2.3.5. Cycle FMEP

Cycle FMEPs can reflect the response of the piston ring friction to the engine speed change in an integral form. Figure 22 shows the FMEPs of the 0.15mm land width 28.5N tension TLOCR at 60°C from 100RPM to 1000RPM at 100RPM intervals. Both the original measurement results (with piston) and the results after subtracting the piston friction (without piston) are shown.

Under the specified conditions, the ring starts from a boundary lubrication-dominated regime at 100RPM. Gradually, it reaches the minimum FMEP in a mixed lubrication regime at a higher engine speed. Later when the engine speed further increases towards 1000RPM, viscous shear stress dominates and the total friction increases with the engine speed.

The piston has observable effects on the cycle FMEPs especially at higher RPMs where the skirt friction is higher. The general lubrication regime transition trend perseveres.

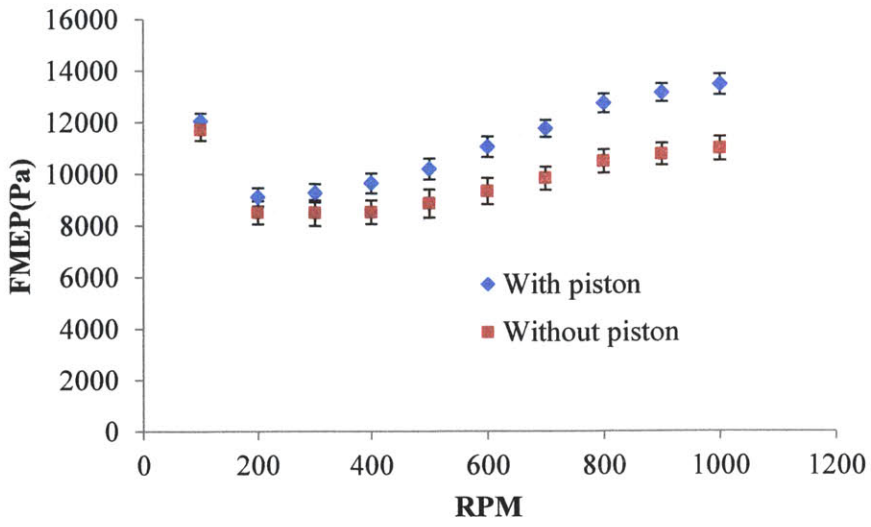

Figure 22: FMEPs of a 0.15mm land width 28.5N tension TLOCR with and without the piston at 60°C

2.4. Conclusion on Modified FLE Experiment

Therefore, when using the modified FLE system to study the TLOCR friction, the friction trace should be used as a first check for result reliability. The piston friction needs to be properly considered when calculating the TLOCR instantaneous Stribeck curve. After the piston friction is subtracted, the obtained cycle FMEPs and friction traces at the mid-stroke should be treated with caution, especially for TLOCRs whose friction values are small. Piston skirt shear stress, piston secondary motion and lateral stoppers can have strong effects on the TLOCR mid-stroke friction reading.

Following the aforementioned steps, the TLOCR friction traces from the modified FLE system can be well explained by the instantaneous Stribeck curve. The transition of lubrication regimes can be clearly seen from the friction traces and the FMEPs at different engine speeds. The instantaneous Stribeck curve calculated using friction results of different tests can generally fall together. The findings above contribute to the validation of the modified FLE system.

In addition, when the purpose of the study is to compare the friction between different TLOCR-liner mating pairs, friction trace differences can also be used. This method assumes that:

- the hydrodynamic shear stress acting on the piston skirt is not affected by the TLOCR type, and
- the effects from piston secondary motion are similar under the same engine speed.

Under the assumptions, taking the friction differences can mitigate the piston skirt and piston secondary motion effects.

3. The Twin Land Oil Control Ring Deterministic Model Validation

3.1. Previous Work

The deterministic TLOCR model developed by Chen [4] and the piston ring pack cycle model developed by Tian [5] are used to analyze different factors affecting ring friction. One key innovation of Chen's deterministic TLOCR model [4] is that it deterministically calculates the capability of cylinder liner's micro structure to generate hydrodynamic pressure. If a perfect flat ring dragging oil passes the liner, the hydrodynamic pressure generated between the ring and the liner should all contribute to the liner micro structure. Chen has provided an initial model validation using a typical plateau honing liner and 5W-30 fully formulated oil [4, 41].

The typical plateau honing surface measurement is provided in Figure 23:

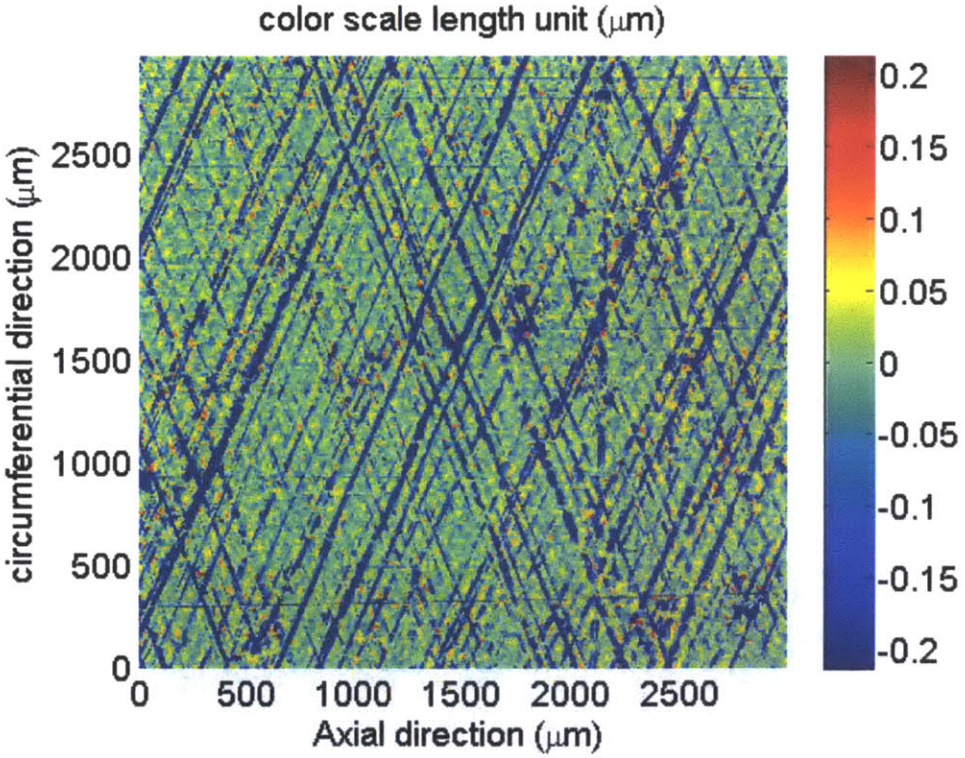

Figure 23: Surface structure of a typical plateau honing liner, measured with confocal microscopy [4, 42]

The current model validation will extend to a fine honing liner and extra thin oil.

3.2. Ring Selection

Two other TLOCRs in addition to the 0.15mm land width one are used in the experiments. Since the deterministic TLOCR model assumes flat ring lands, all three tested TLOCRs are well worn and the ring lands are almost flat. Figure 24 and Figure 25 show the ring profiles of the other two TLOCRs. It should be noticed that the land widths of the three rings are not perfectly uniform. In addition, only one land width input is allowed in the deterministic TLOCR model. Therefore, representative land widths are used to describe the three rings: 0.15mm, 0.23mm and 0.06mm, respectively. These are also the ring land width values used in the deterministic TLOCR model.

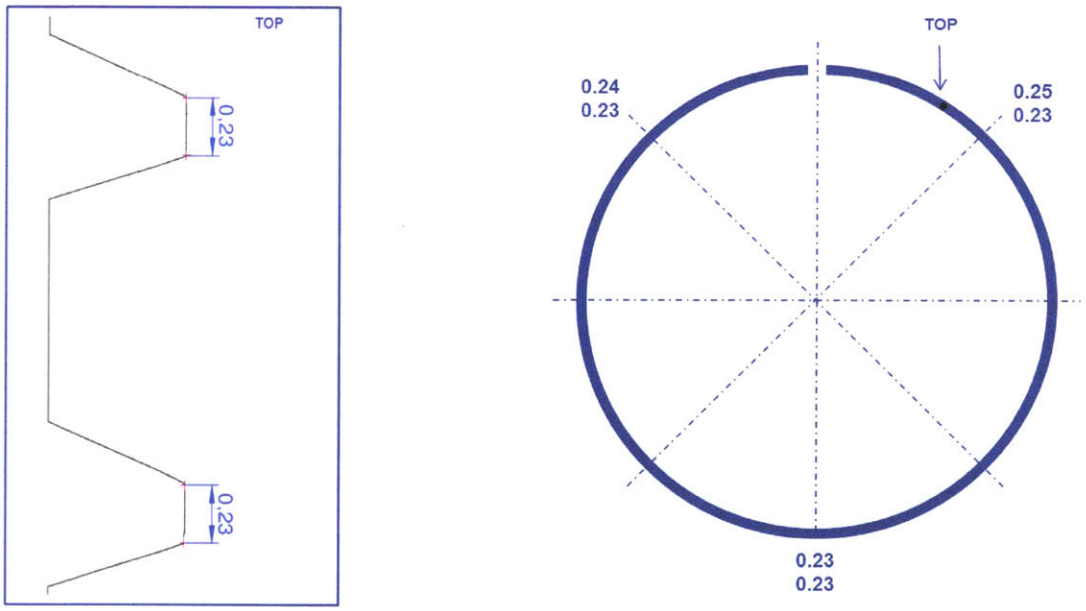

Figure 24: Ring profile of a 0.23mm land width TLOCR

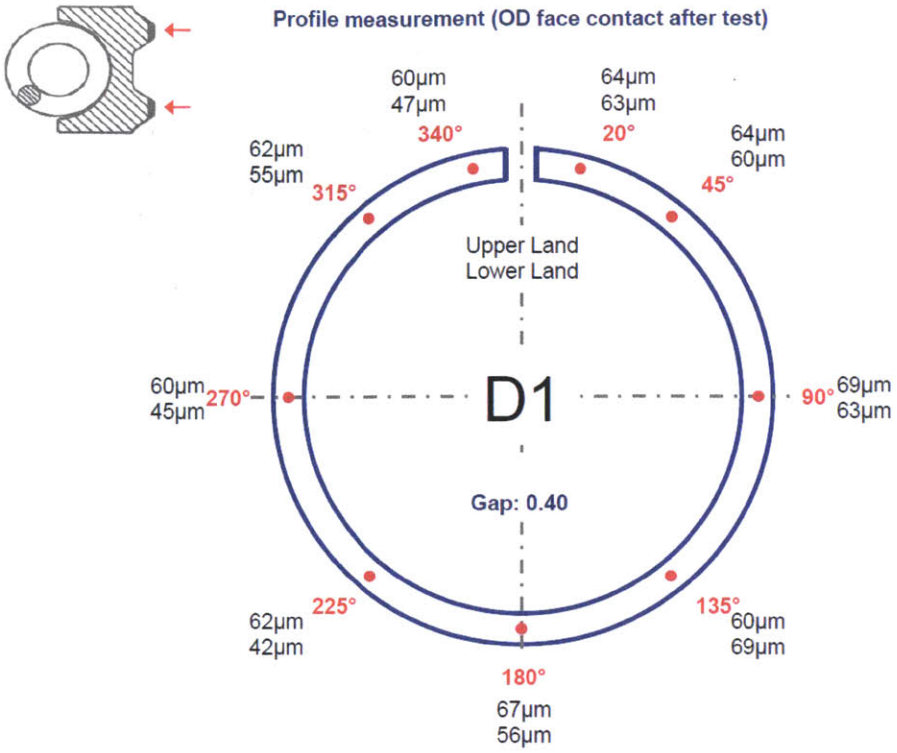

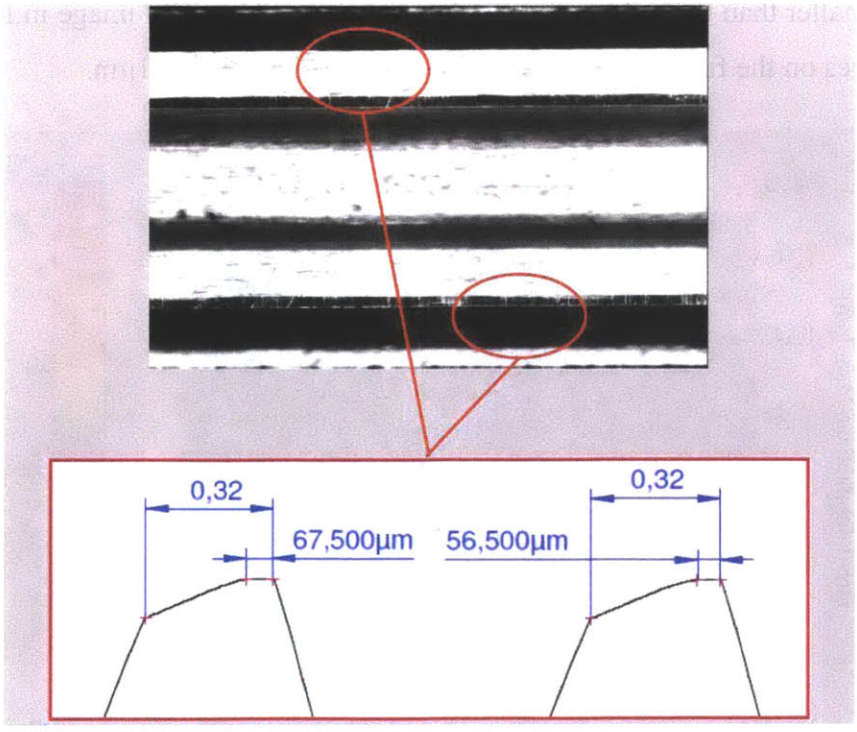

Figure 25: Ring profile of a 0.06mm land width TLOCR

In the experiments, the same rings are used but the springs are changed to give the TLOCRs different tensions. The tested TLOCR configurations are summarized in Table 3.

Table 3: TLOCR land width and tensions used in the experiments

TLOCR land width	Tensions
0.06mm	10.5N
0.15mm	10.5N, 19.5N
0.23mm	10.5N

It should be noticed that the 0.06mm and 0.15mm ring share the same 10.5N tension spring; while the 0.23mm ring uses its own 10.5N spring. In addition, the ring tensions are measured after the tests.

3.3. Cylinder Liner Surface Structure

Figure 26 shows the surface structure of the fine honing liner. The structure of the fine honing liner is much smaller than that of the typical plateau honing. The SEM image in Figure 27 shows that some grooves on the fine honing liner have widths at the order of 1μm.

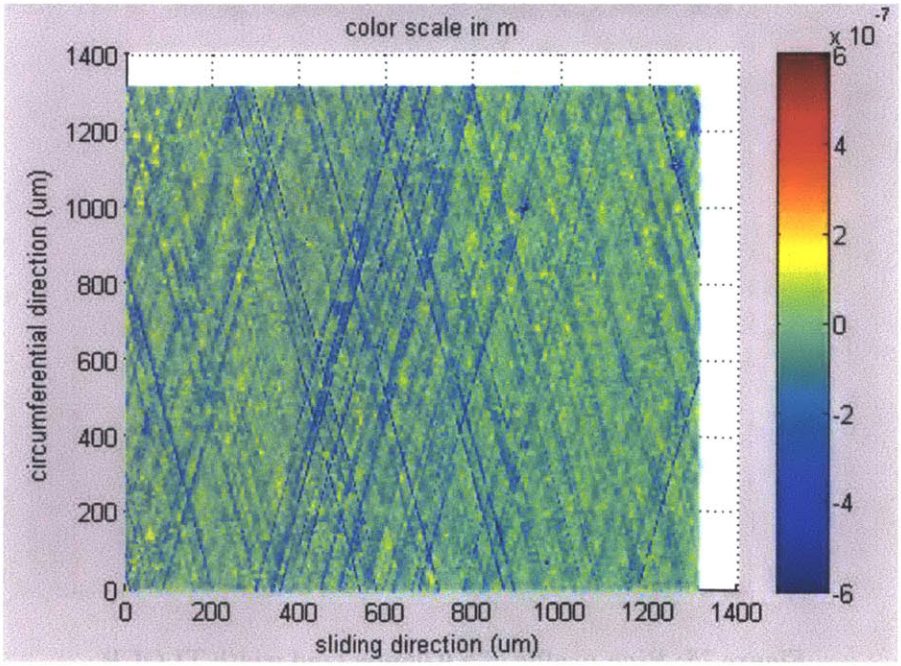

Figure 26: Confocal microscopy measurement with 0.37μm resolution of a fine honing liner

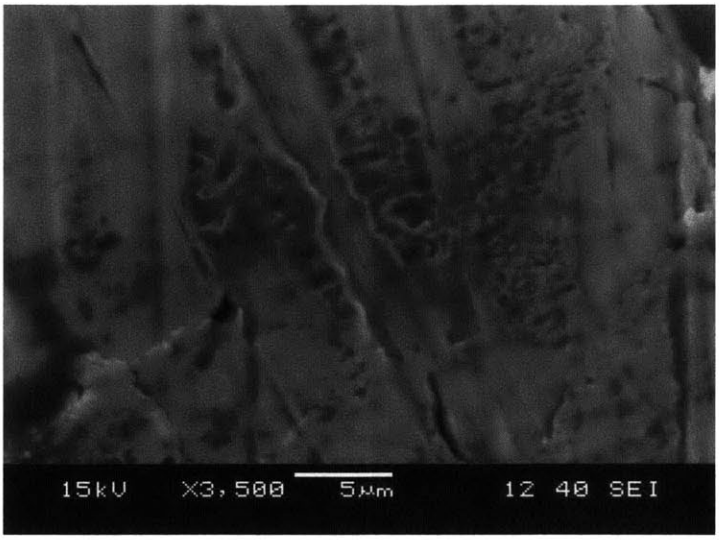

Figure 27: SEM measurement of the fine honing liner surface structure

Due to the small scale of its structures, the fine honing liner requires higher resolution confocal microscopy measurement for the deterministic TLOCR model input. Figure 28 shows the instantaneous Stribeck curves calculated using 0.37µm and 1µm resolution measurements as model inputs. The corresponding instantaneous Stribeck curve calculated using post break-in experimental results is provided as reference. It should be noticed that the piston friction was subtracted when calculating the experimental instantaneous Stribeck curve. The surface measurements used for model inputs were taken after the break-in process.

The comparison shows that a 1µm resolution cannot properly measure the fine honing liner surface structure. As a result, when studying the liners with fine honing, an objective length of 50x should be used to provide a higher resolution.

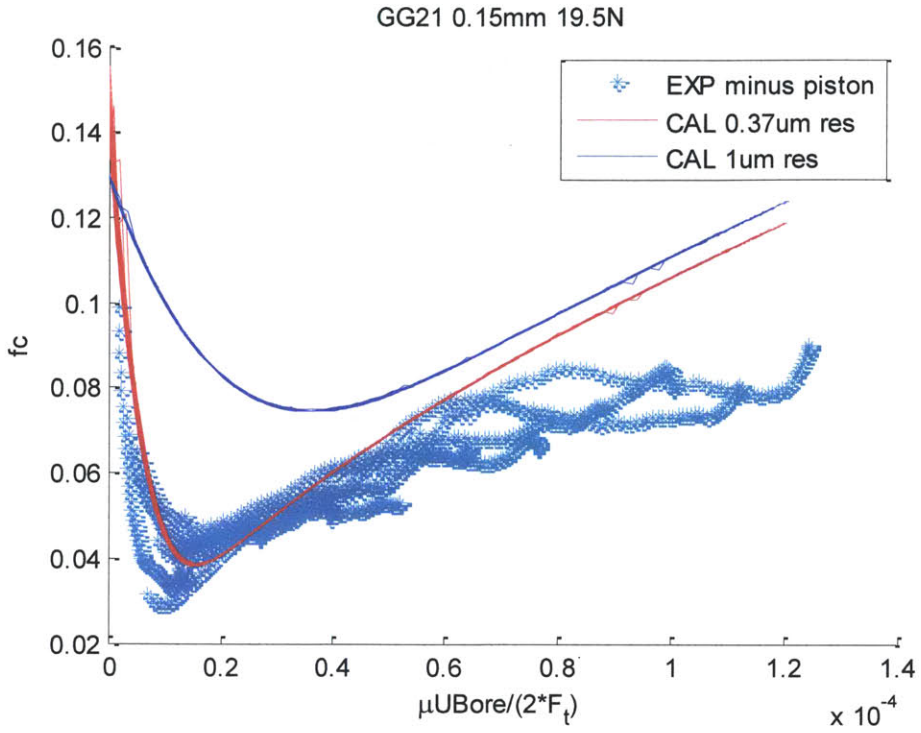

Figure 28: Effects of surface measurement accuracy on calculation results

Table 4 provides the surface statistics comparison between the plateau honing and the fine honing. The statistics show that the fine honing liner has both a smaller plateau roughness (σp) and a smaller surface roughness (Ra).

Table 4: Surface statistics of a typical plateau honing liner and fine honing liner

	Typical plateau honing	Fine honing
σp (micron)	0.071	0.049
Rpk(micron)	0.170	0.075
Rk(micron)	0.220	0.230
Rvk(micron)	0.994	0.261
Mr1(%)	7.527	4.618
Mr2(%)	77.353	81.875
Ra(micron)	0.196	0.089
Rq(micron)	0.501	0.125

3.4. Thin Oil Characteristics

The oil used in the experiment is specially formulated oil with a HTHS (high temperature high shear viscosity) of 1.4 mPa·s. The additive package of the oil is identical to that of the fully

formulated commercial oil. Only viscosity is reduced. The viscosity characteristics of the oil are provided in Figure 29.

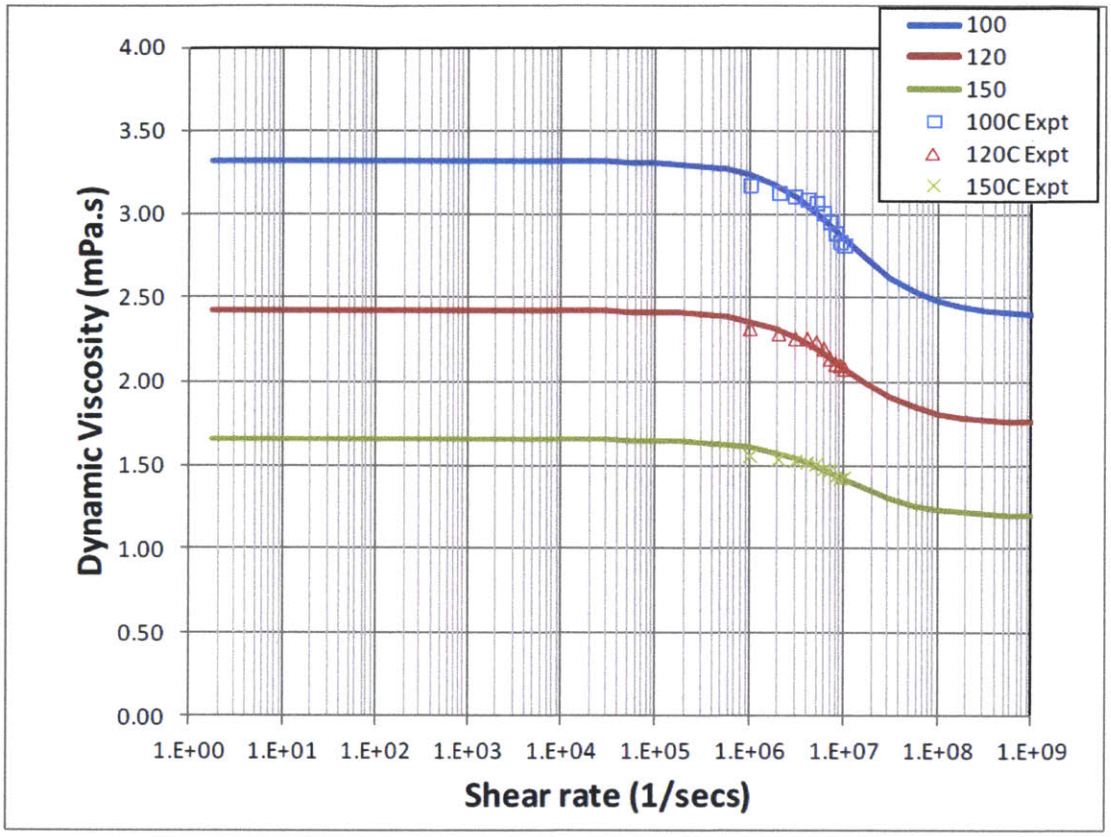

Figure 29: Oil viscosity characteristics of the HTHS 1.4 oil

For an internal combustion engine, the shear rate of the oil between the rings and the liner can usually exceed the 1.E+7 s^{-1} level in the mid-stroke region. In addition, the cycle FMEP is more affected by friction in the mid-stroke. Therefore, oil viscosity under high shear rate can be more related to the total ring friction. This topic will be discussed further in section 6.1.2.

3.5. Comparison between Experimental and Calculation Results

The friction traces comparison between experimental and calculation results at 100RPM, 500RPM and 1000RPM are provided in Figures 30 to 37. During the experiments, the liner temperatures were kept at 40°C, 60°C, 80°C and 100°C. The lower temperatures increase oil viscosity to move the ring operation towards the hydrodynamic regime. Original experimental friction results (Exp with P) and the results subtracted the piston friction (EXP w/o P) are compared with calculation results.

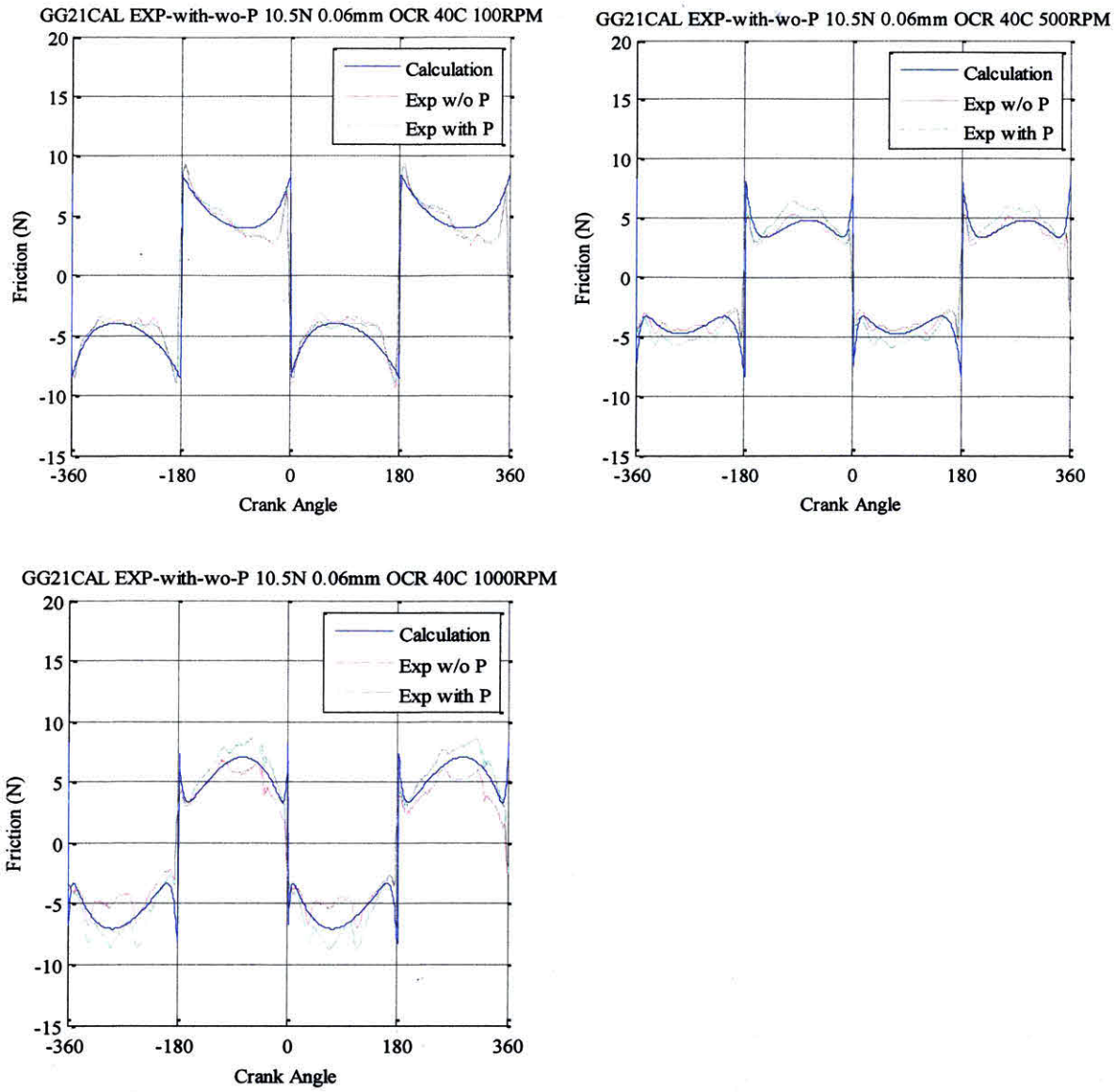

Figure 30: Friction comparison for 10.5N 0.06mm land width TLOCR, 40°C

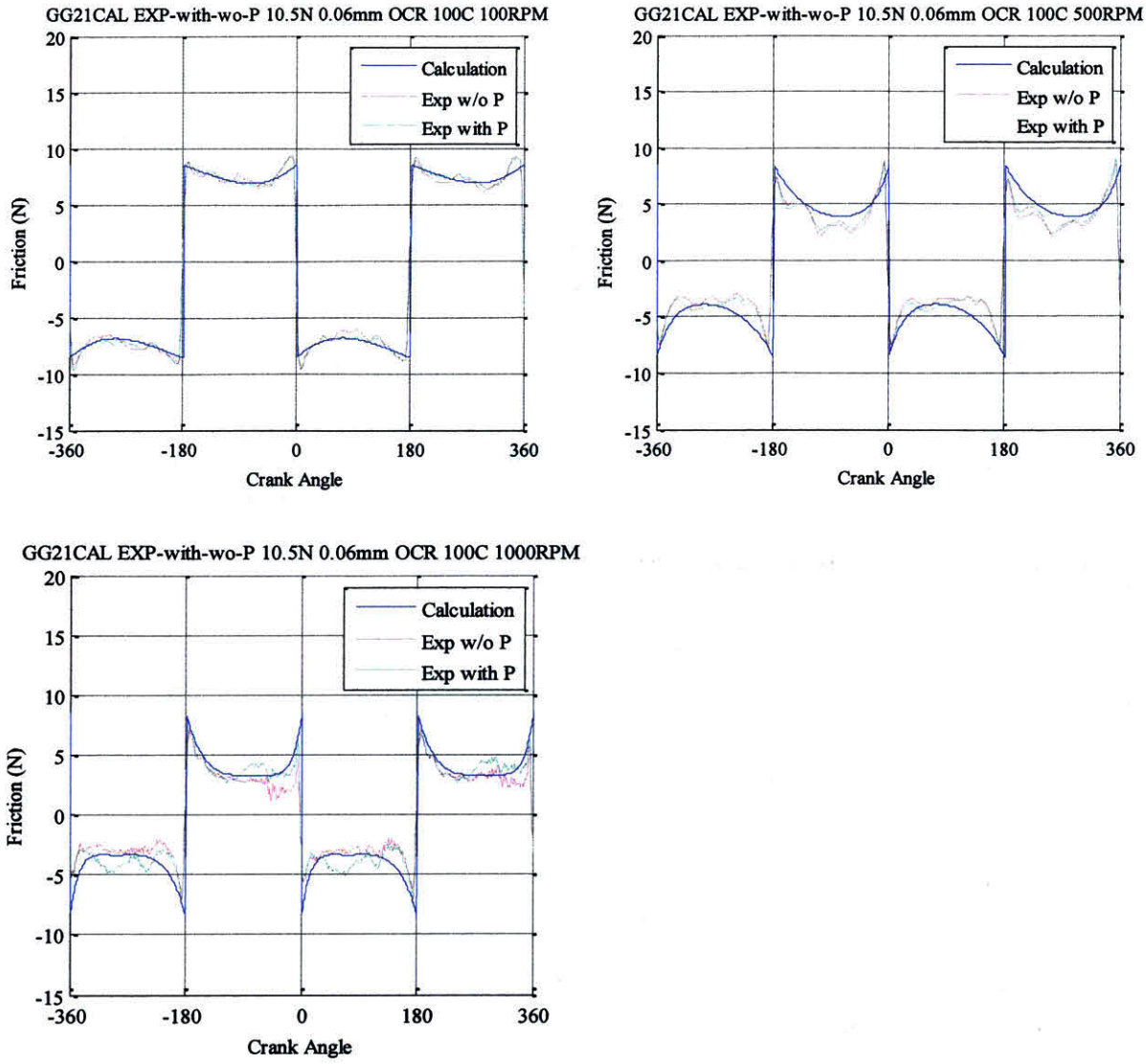

Figure 31: Friction comparison for 10.5N 0.06mm land width TLOCR, 100°C

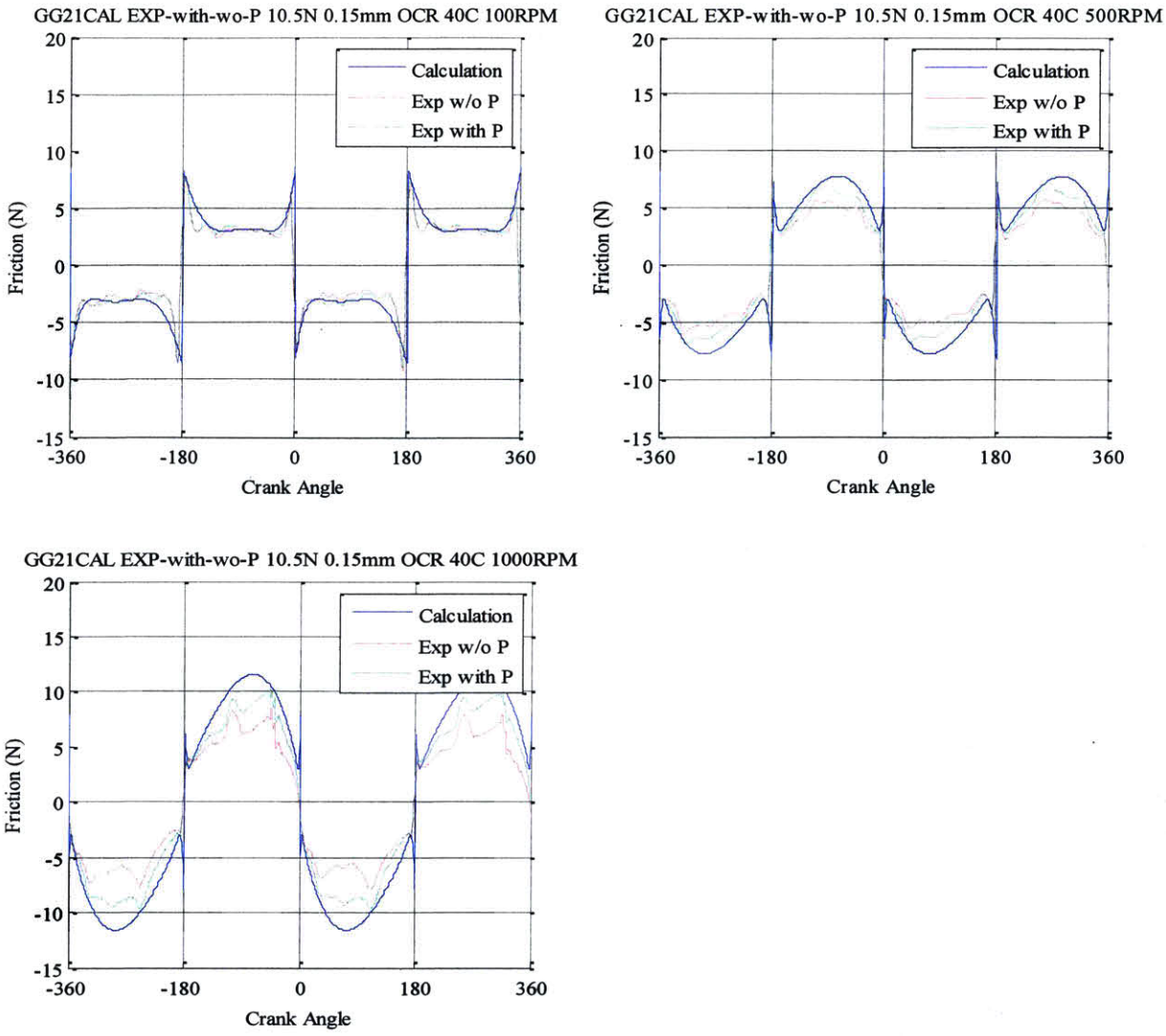

Figure 32: Friction comparison for 10.5N 0.15mm land width TLOCR, 40°C

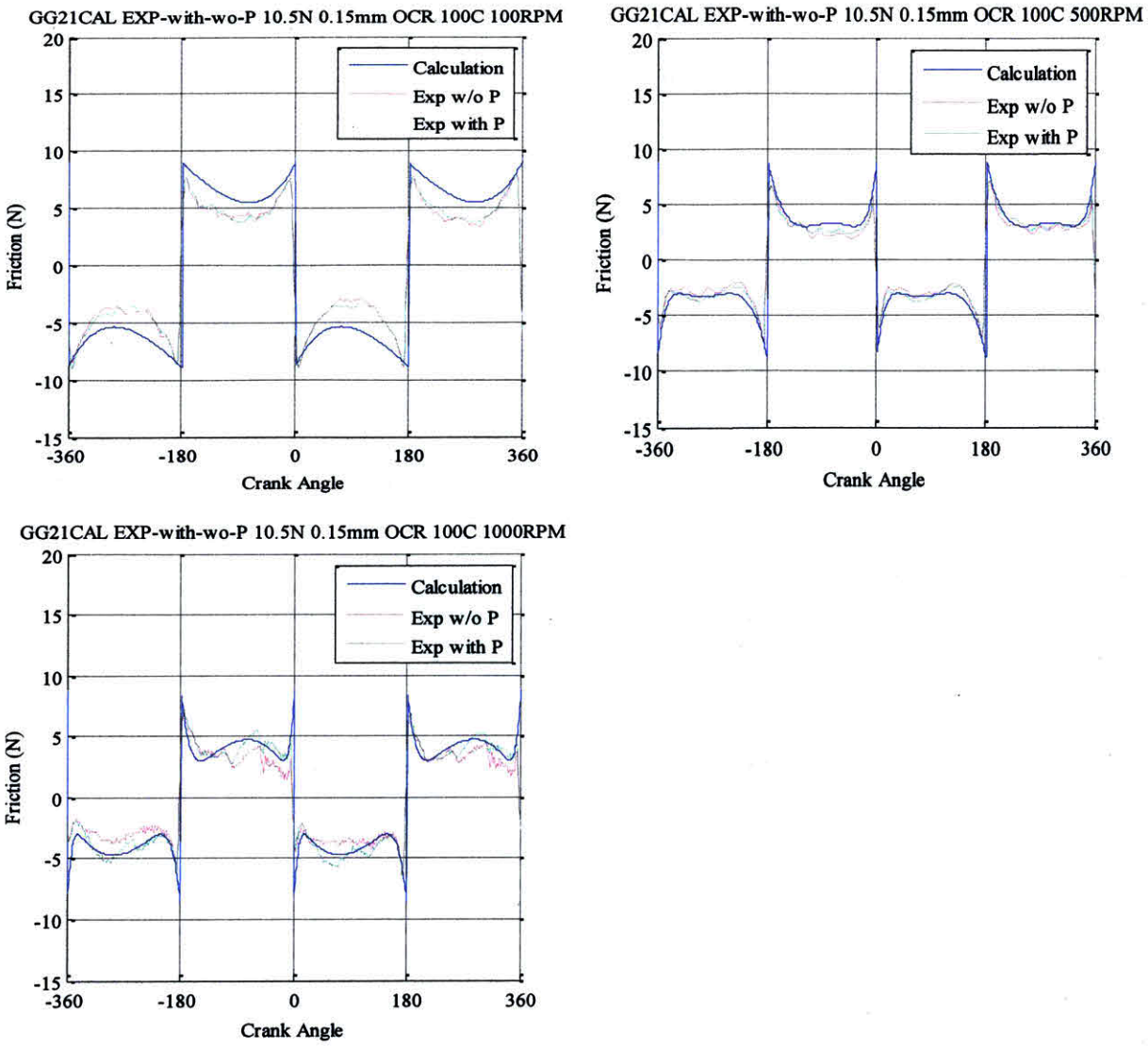

Figure 33: Friction comparison for 10.5N 0.15mm land width TLOCR, 100°C

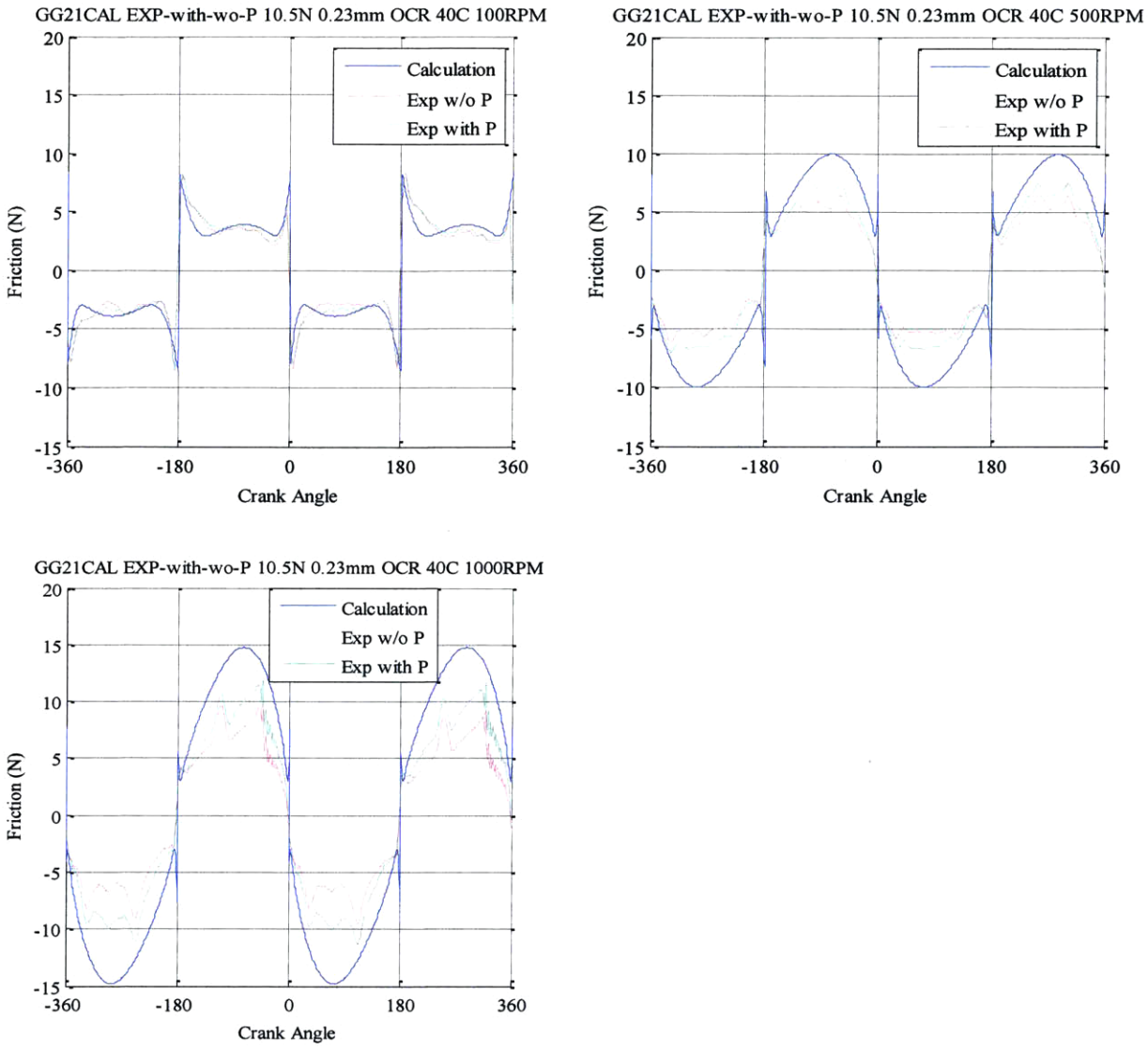

Figure 34: Friction comparison for 10.5N 0.23mm land width TLOCR, 40°C

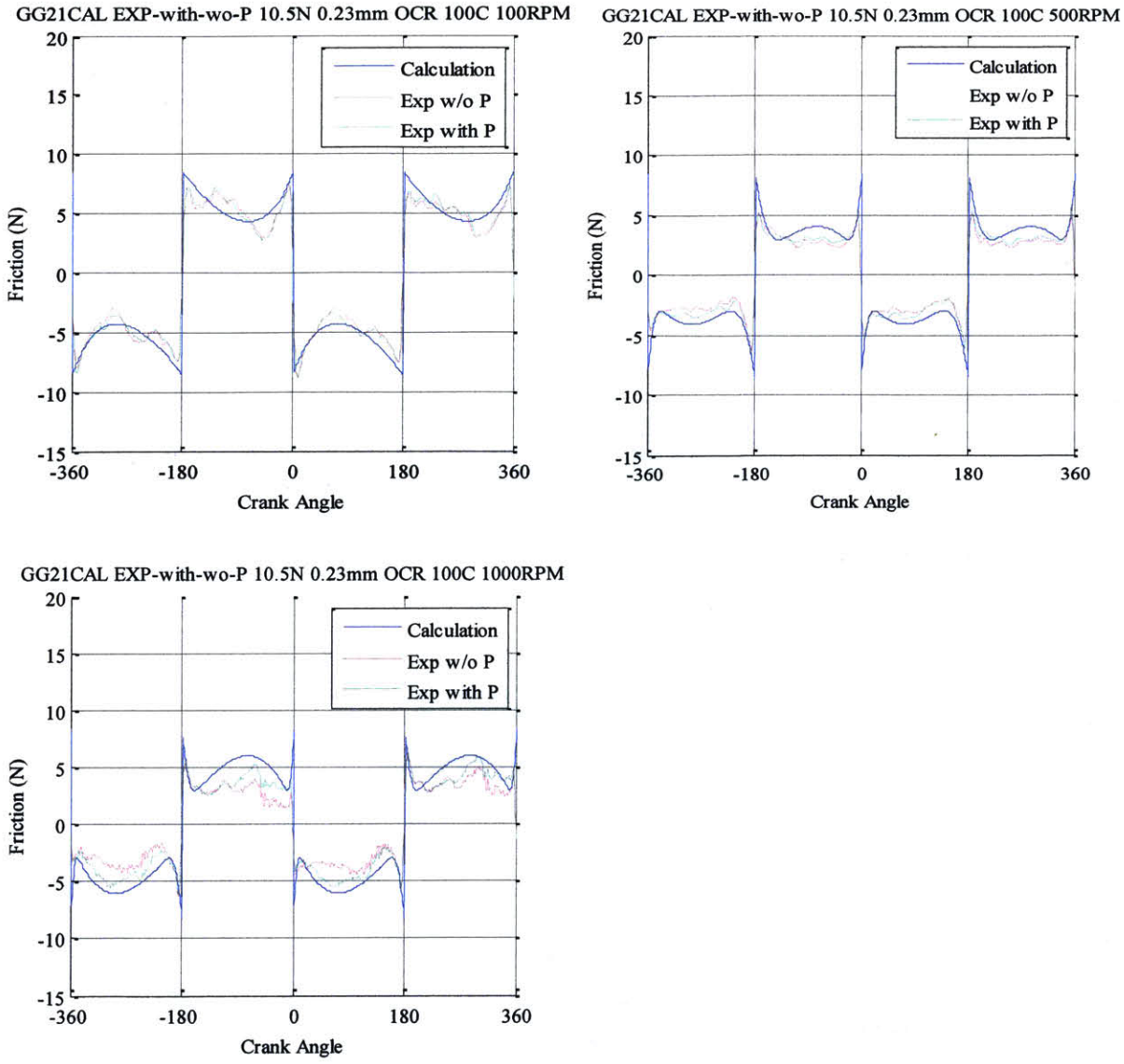

Figure 35: Friction comparison for 10.5N 0.23mm land width TLOCR, 100°C

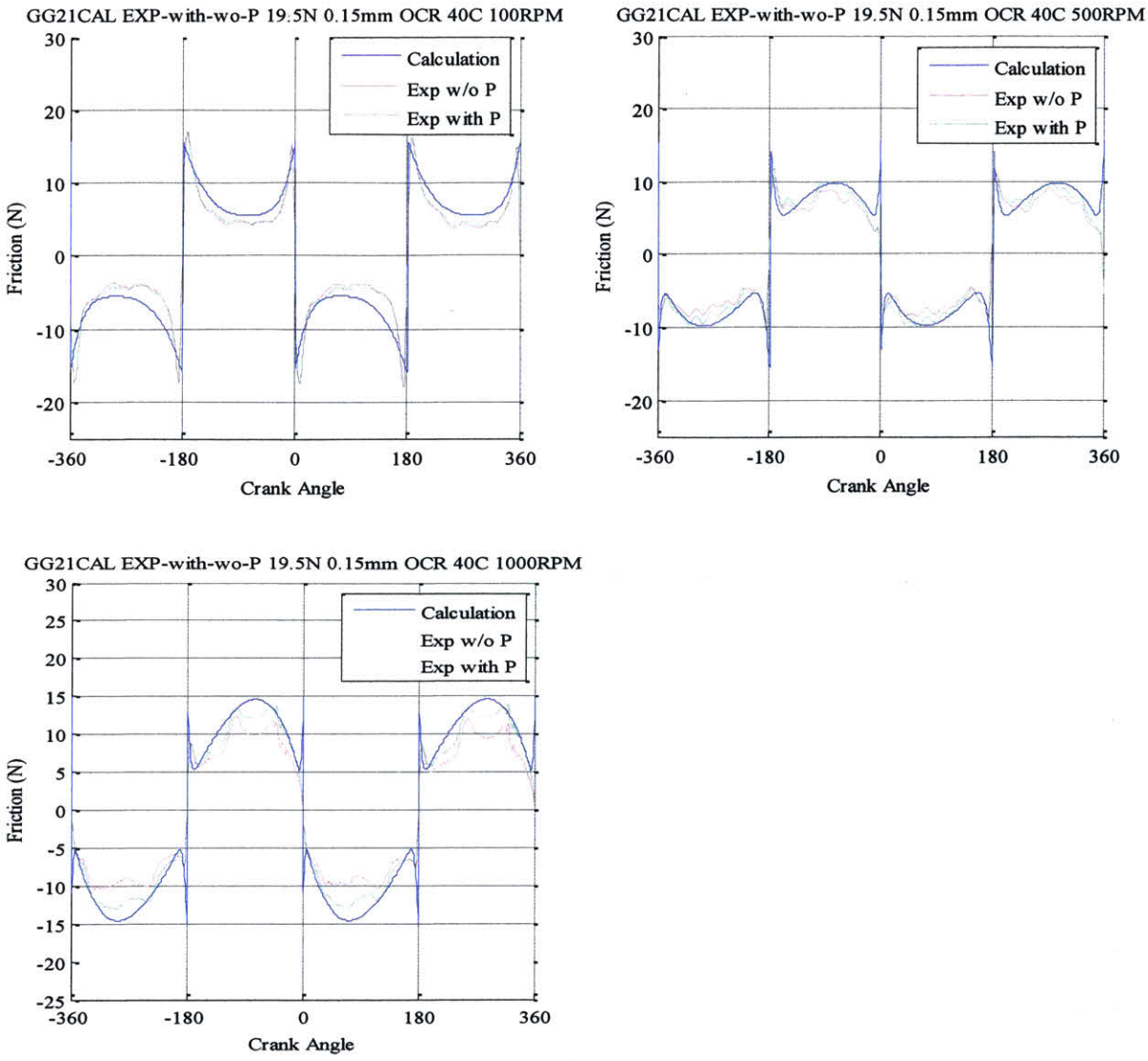

Figure 36: Friction comparison for 19.5N 0.15mm land width TLOCR, 40°C

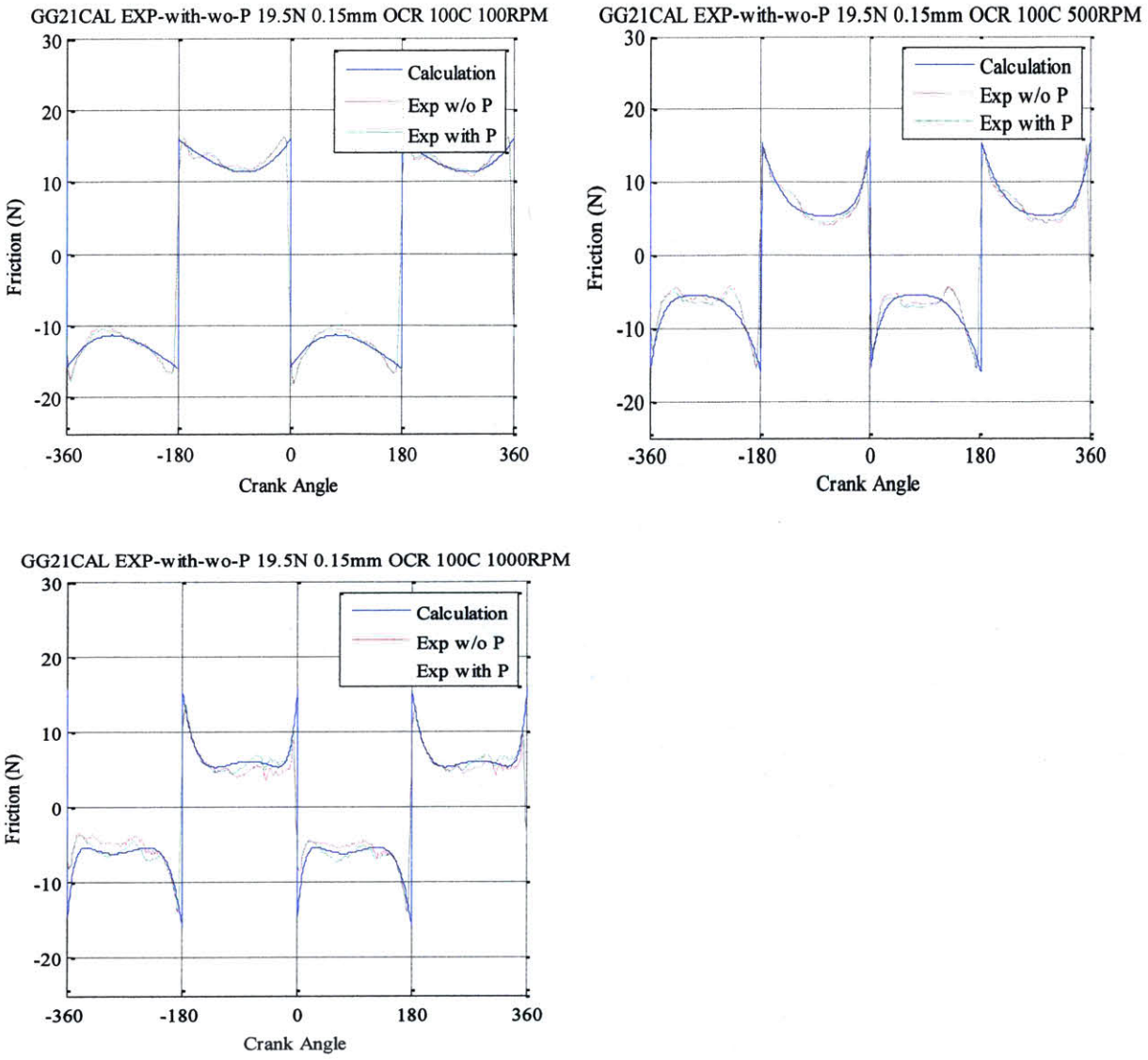

Figure 37: Friction comparison for 19.5N 0.15mm land width TLOCR, 100°C

All the experimental results from the three rings show clear lubrication regime transition from boundary lubrication to hydrodynamic lubrication. The hydrodynamic pressure generation ability of the liner surface micro-structure is shown. Calculation results show similar lubrication regime transition trend. Experimental and calculation results can generally match each other. However, certain deviations between the experimental and the calculation results are observed at the mid-stroke when the ring operates at the higher engine speed of 1000RPM. From the experimental side, the piston secondary motion grows stronger as the engine speed increases, especially at the mid-stroke. Taking the friction trace of 0.23mm 10.5N TLOCR at 40°C as an example, the sudden friction drop at the mid-stroke cannot be explained by normal lubrication regime

transition theory. Therefore, when using the measurement data to validate the model, the lower portion where piston secondary motion is minimal should be used.

The instantaneous Stribeck curves from the experiments and the calculations are compared in Figures 38 to 53. Experimental instantaneous Stribeck curves are obtained using results from 140-160CAD and 75-160CAD at engine speeds from 100RPM to 1000RPM at 100RPM intervals. (0CAD starts from the TDC.) The former one is intended to avoid the mid-stroke regions where the piston effects are strong. The latter one is intended to cover a larger lubrication regime and show the piston effects. In addition, the same ring test results at 40°C, 60°C, 80°C and 100°C are plotted together to show experimental self-consistency in addition to extending the lubrication regime when comparing with calculation results. Experimental results with and without the piston friction are both shown. The calculated instantaneous Stribeck curves use friction results of 80°C, engine speeds from 100-2000RPM or 100-3000RPM, so that the calculated and experimental instantaneous Stribeck curves cover a similar range.

0.06mm land width 10.5N tension TLOCR with piston friction:

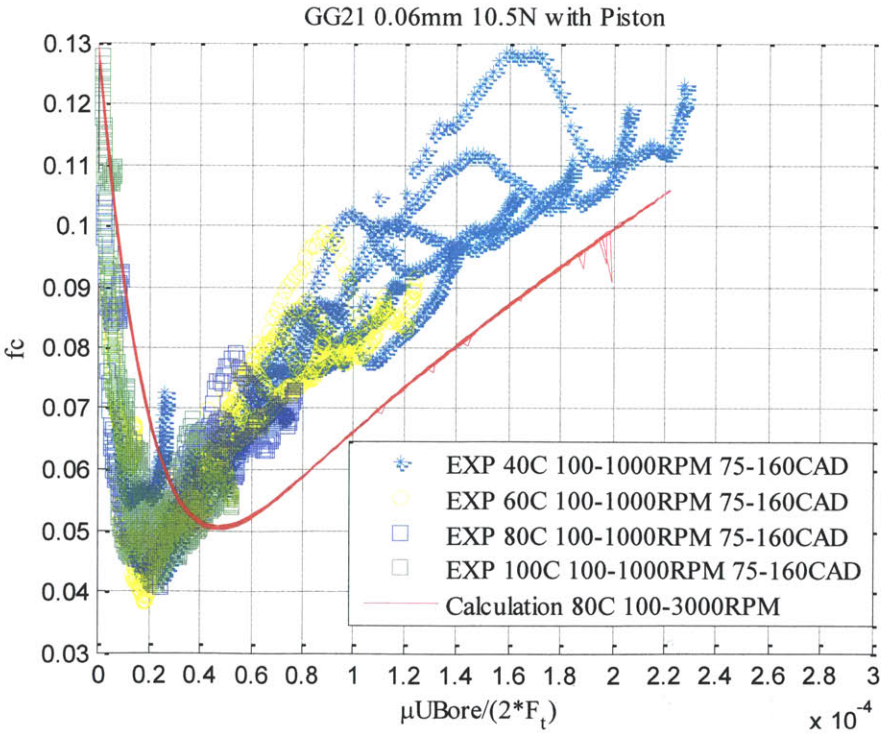

Figure 38: Instantaneous Stribeck curve, 0.06mm land width 10.5N tension TLOCR, experiment uses 75-160CAD results, with piston friction

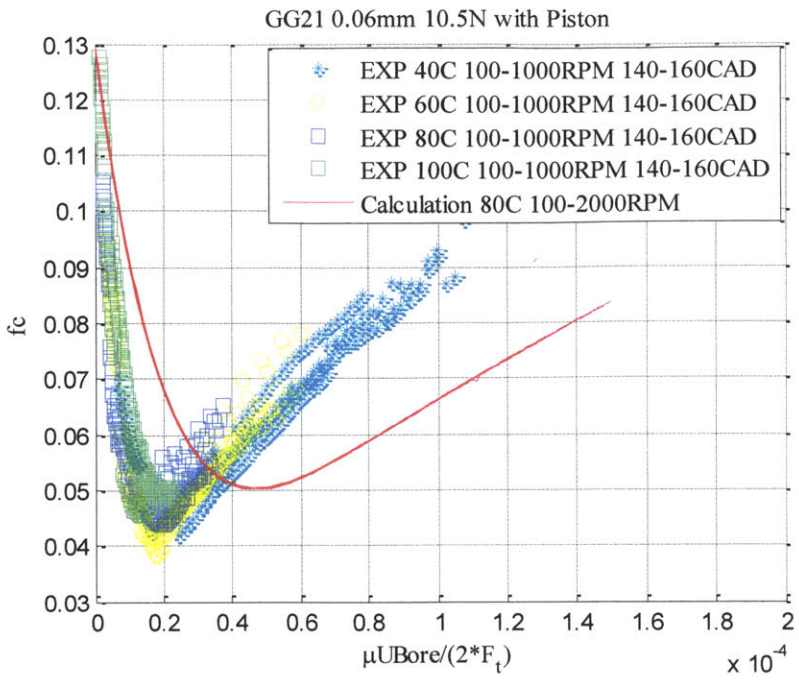

Figure 39: Instantaneous Stribeck curve, 0.06mm land width 10.5N tension TLOCR, experiment uses 140-160CAD results, with piston friction

0.06mm land width 10.5N tension TLOCR after subtracting piston friction:

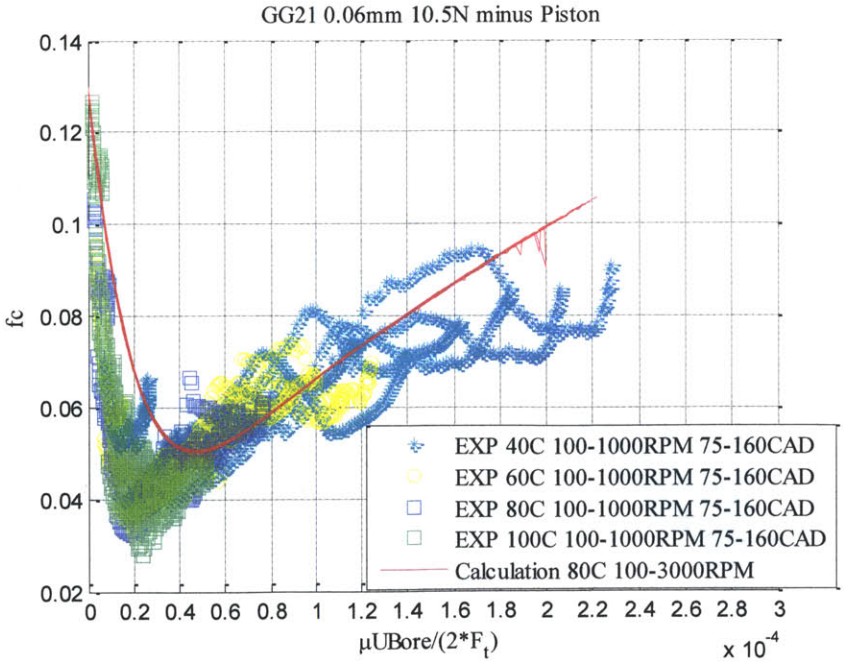

Figure 40: Instantaneous Stribeck curve, 0.06mm land width 10.5N tension TLOCR, experiment uses 75-160CAD results, after subtracting piston friction

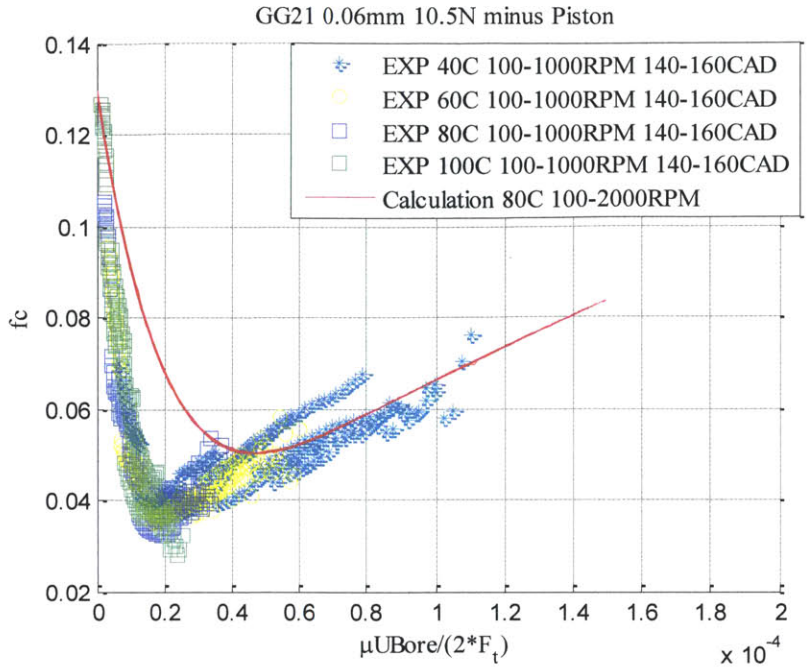

Figure 41: Instantaneous Stribeck curve, 0.06mm land width 10.5N tension TLOCR, experiment uses 140-160CAD results, after subtracting piston friction

0.15mm land width 10.5N tension TLOCR with piston friction:

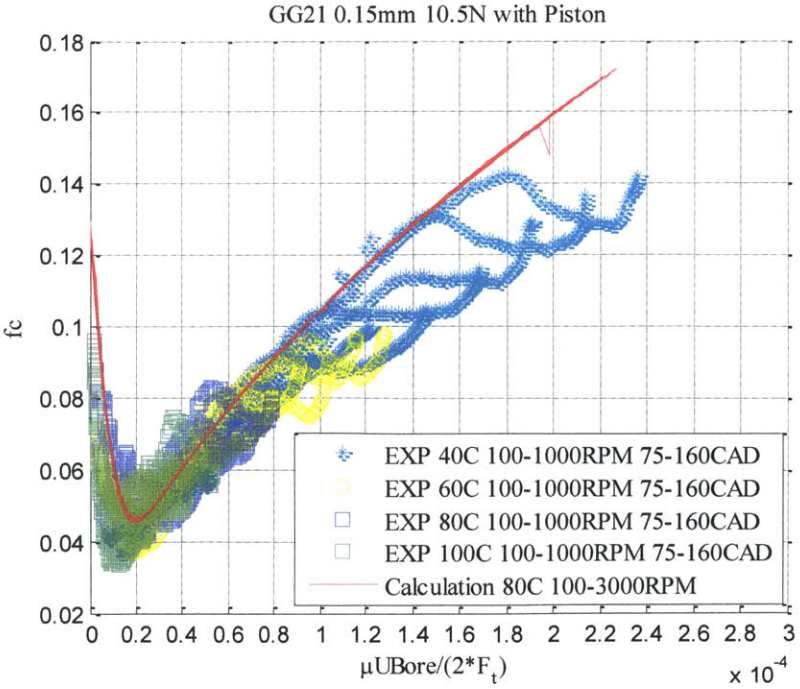

Figure 42: Instantaneous Stribeck curve, 0.15mm land width 10.5N tension TLOCR, experiment uses 75-160CAD results, with piston friction

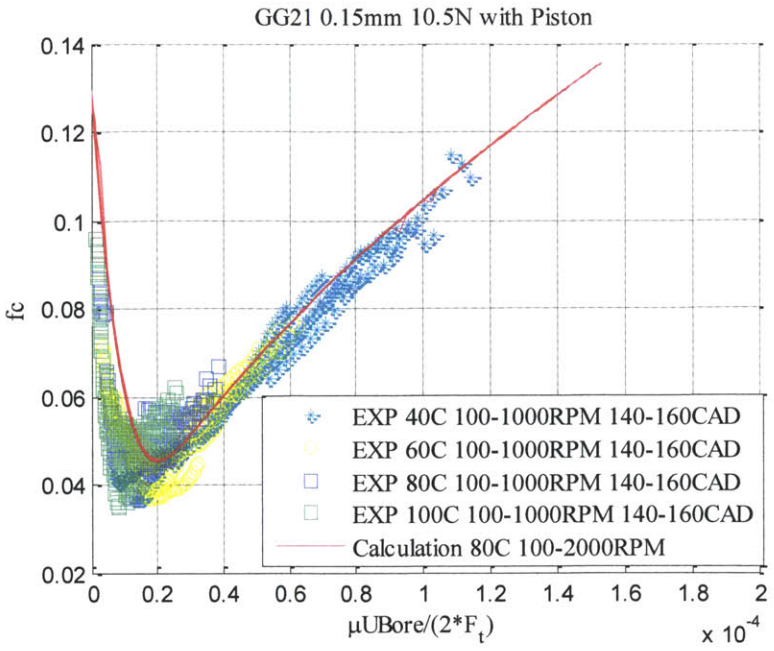

Figure 43: Instantaneous Stribeck curve, 0.15mm land width 10.5N tension TLOCR, experiment uses 140-160CAD results, with piston friction

0.15mm land width 10.5N tension TLOCR after subtracting piston friction:

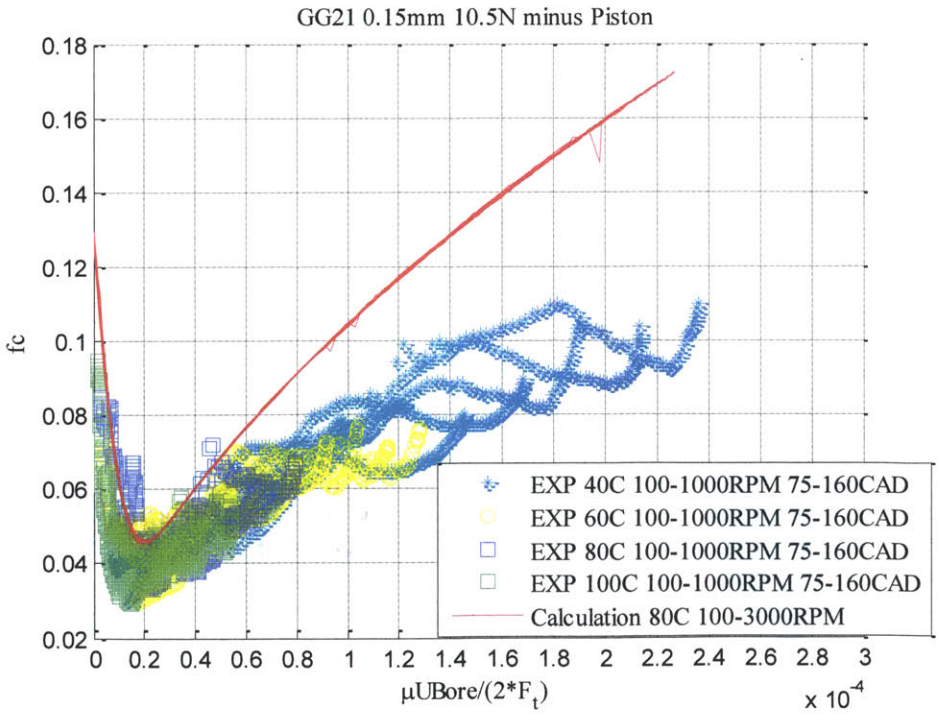

Figure 44: Instantaneous Stribeck curve, 0.15mm land width 10.5N tension TLOCR, experiment uses 75-160CAD results, after subtracting piston friction

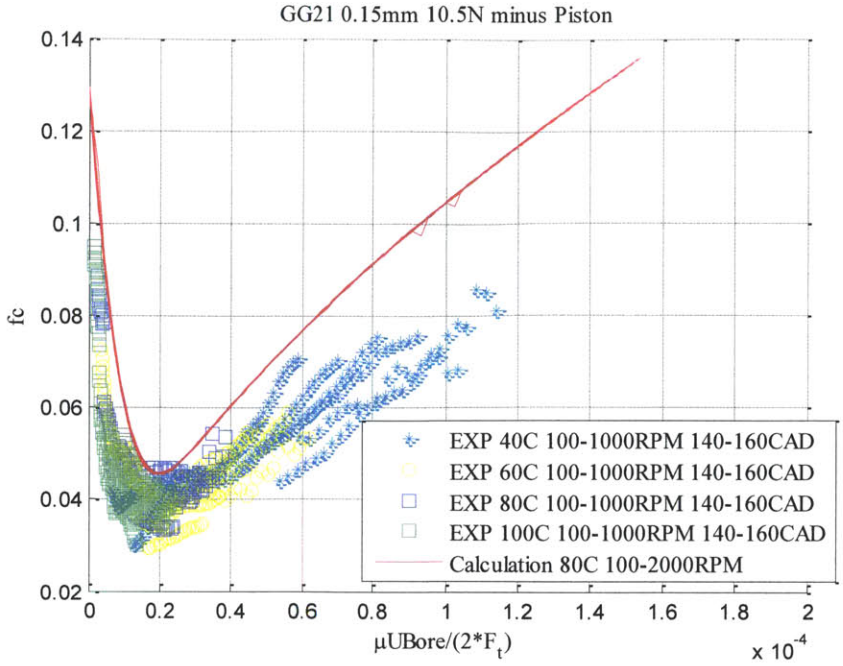

Figure 45: Instantaneous Stribeck curve, 0.15mm land width 10.5N tension TLOCR, experiment uses 140-160CAD results, after subtracting piston friction

0.15mm land width 19.5N tension TLOCR with piston friction:

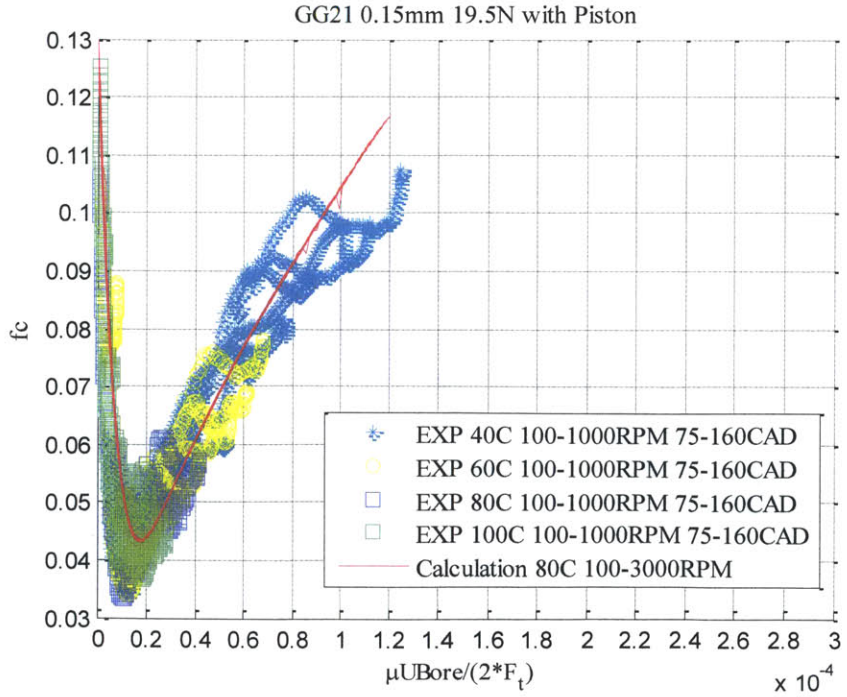

Figure 46: Instantaneous Stribeck curve, 0.15mm land width 19.5N tension TLOCR, experiment uses 75-160CAD results, with piston friction

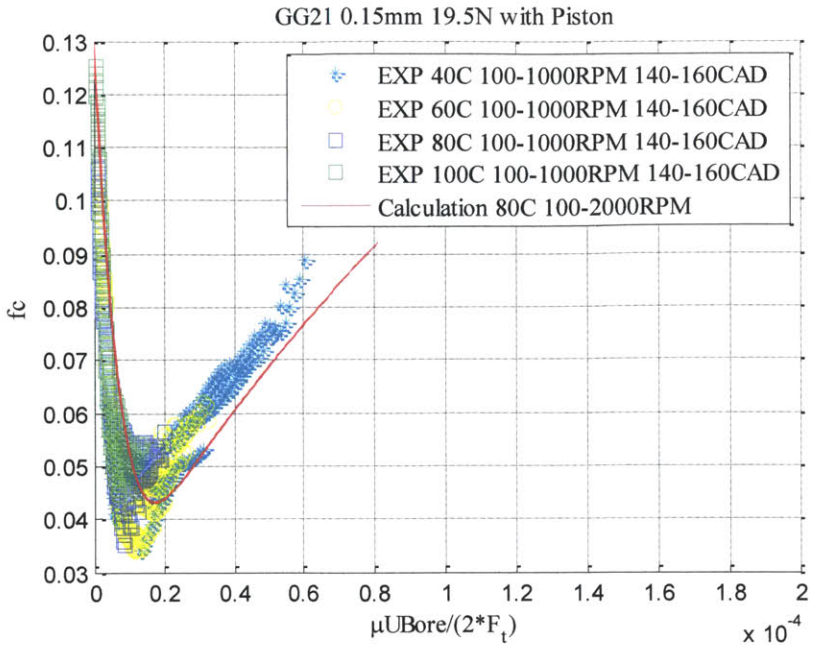

Figure 47: Instantaneous Stribeck curve, 0.15mm land width 19.5N tension TLOCR, experiment uses 140-160CAD results, with piston friction

0.15mm land width 19.5N tension TLOCR after subtracting piston friction:

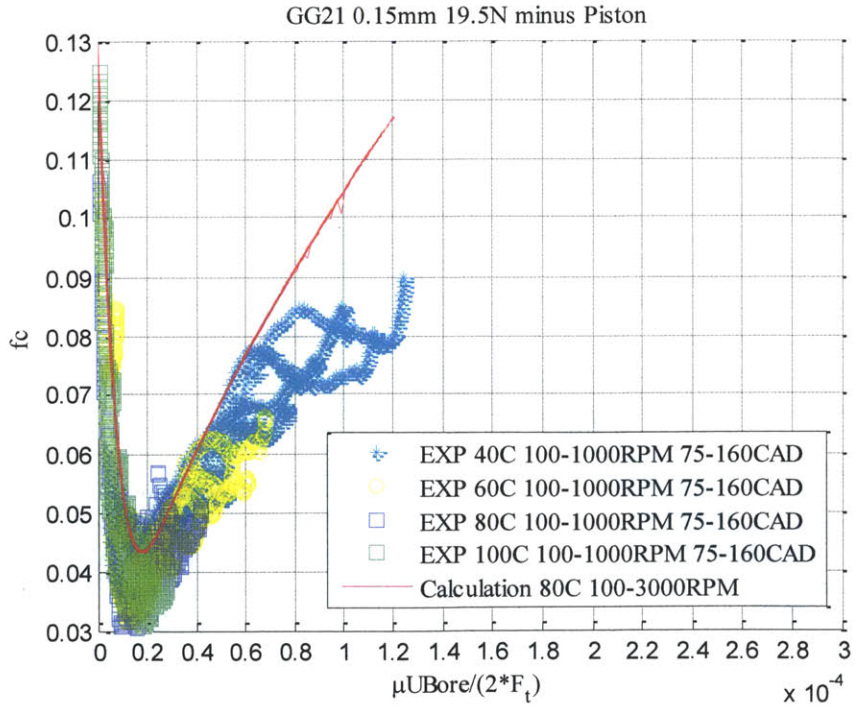

Figure 48: Instantaneous Stribeck curve, 0.15mm land width 19.5N tension TLOCR, experiment uses 75-160CAD results, after subtracting piston friction

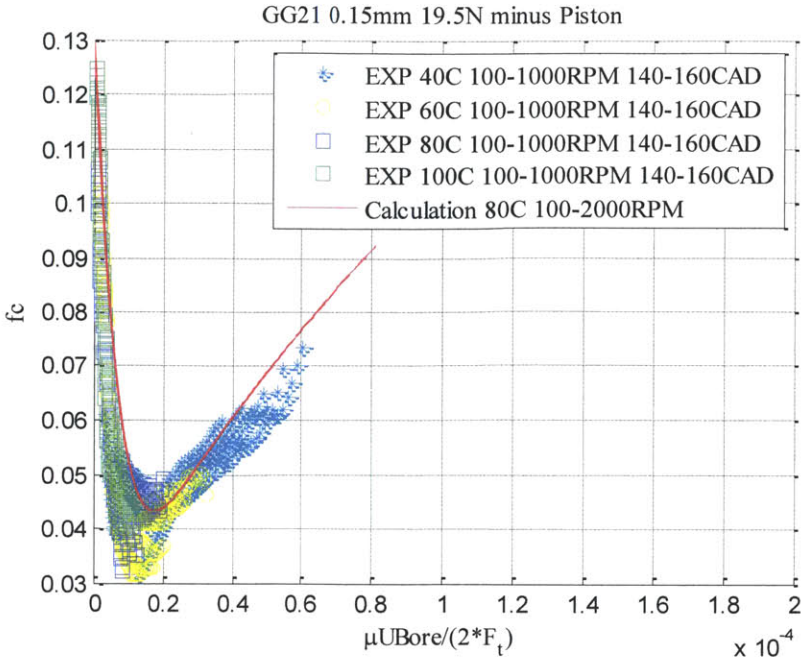

Figure 49: Instantaneous Stribeck curve, 0.15mm land width 19.5N tension TLOCR, experiment uses 140-160CAD results, after subtracting piston friction

0.23mm land width 10.5N tension TLOCR with piston friction:

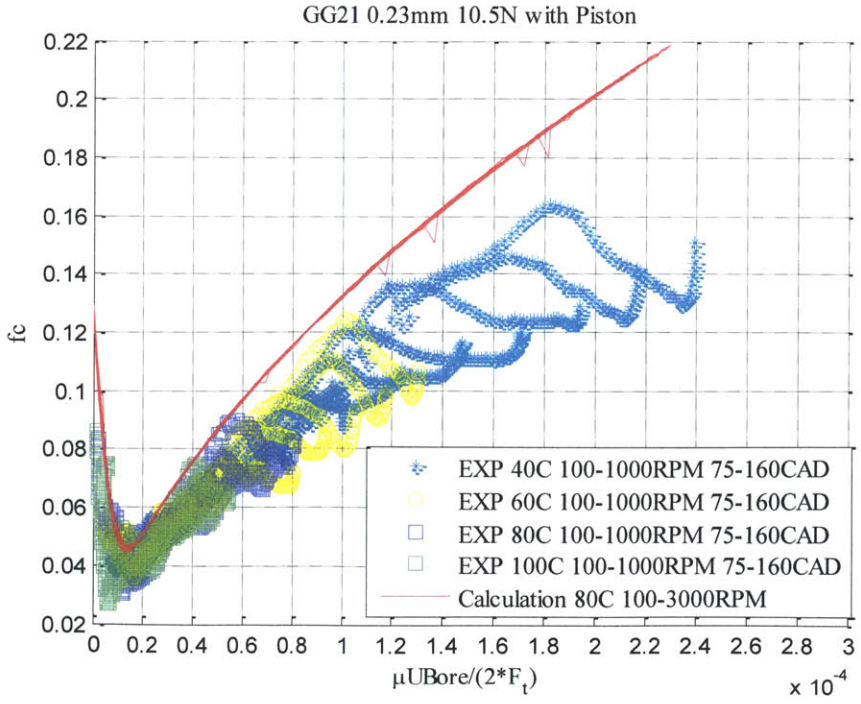

Figure 50: Instantaneous Stribeck curve, 0.23mm land width 10.5N tension TLOCR, experiment uses 75-160CAD results, with piston friction

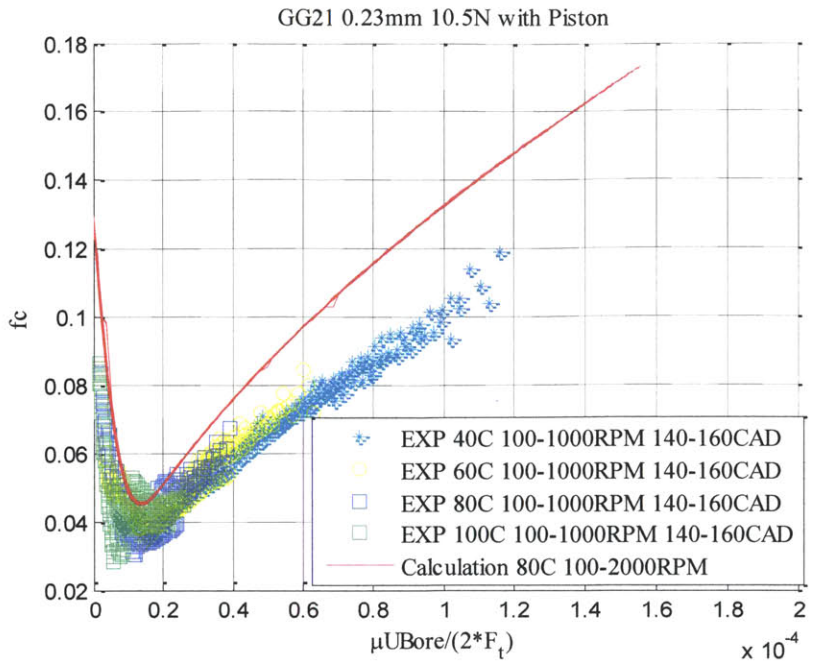

Figure 51: Instantaneous Stribeck curve, 0.23mm land width 10.5N tension TLOCR, experiment uses 140-160CAD results, with piston friction

0.23mm land width 10.5N tension TLOCR after subtracting piston friction:

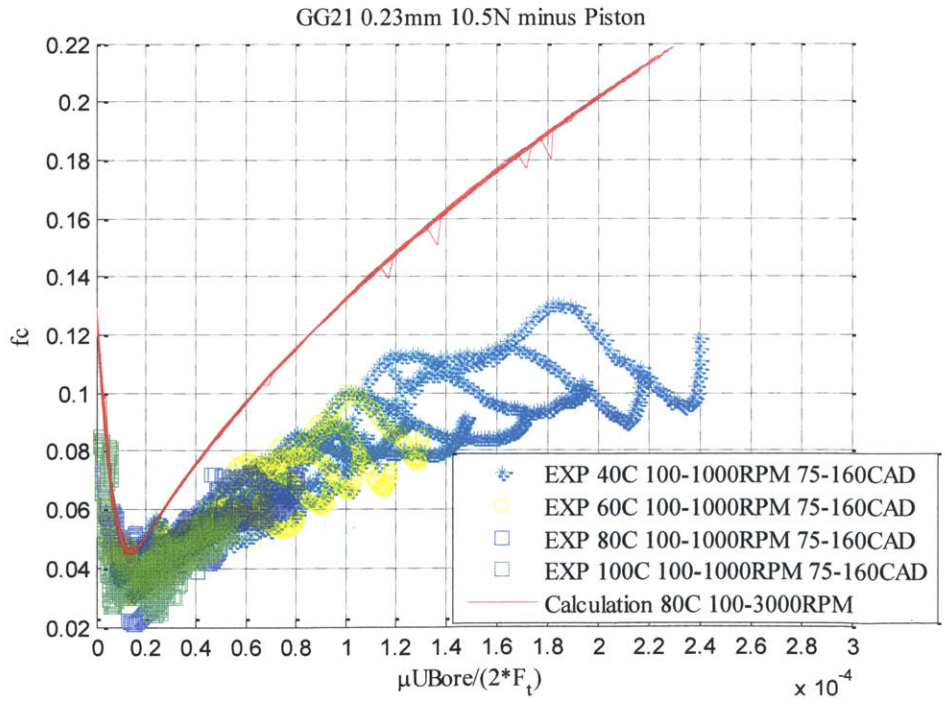

Figure 52: Instantaneous Stribeck curve, 0.23mm land width 10.5N tension TLOCR, experiment uses 75-160CAD results, after subtracting piston friction

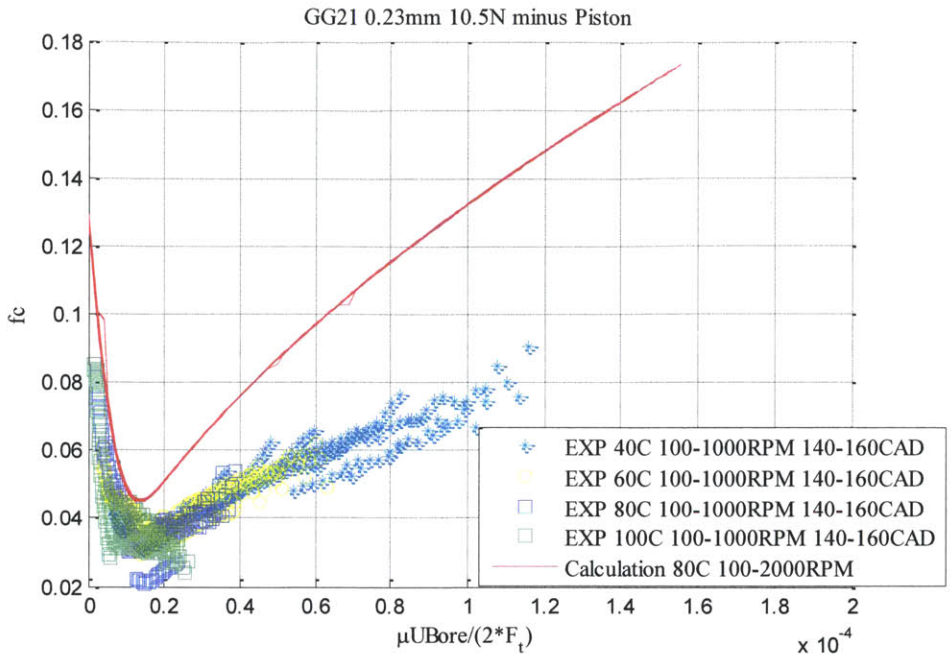

Figure 53: Instantaneous Stribeck curve, 0.23mm land width 10.5N tension TLOCR, experiment uses 140-160CAD results, after subtracting piston friction

3.6. Conclusion on the Deterministic TLOCR Model Validation

The instantaneous Stribeck curves from the experimentation and the calculation show similar minimum friction coefficient values and locations. The lubrication regime transition behavior, from boundary lubrication to hydrodynamic lubrication, is predicted by both experimental and calculation results.

Figures 41, 45 and 53 show the instantaneous Stribeck curves of the 0.06mm, 0.15mm and 0.23mm land width TLOCRs with 10.5N tension, after subtracting the piston friction, respectively. Comparing the three figures, both the experimental and calculation results indicates that as ring land width decreases, the minimum friction coefficient location moves rightwards, and the minimum friction coefficient increases.

A certain deviation in terms of absolute friction coefficient value exists between the experimental and calculation results, and the piston skirt friction effect is obvious.

First of all, the friction of the piston skirt is different with and without the TLOCR. When the TLOCR is installed, the oil accumulated below the TLOCR provides good lubrication to the piston skirt in the upstrokes. In addition, the oil distribution on the liner is different. So the piston skirt friction should be smaller when the TLOCR is installed, which partially explains why the calculation results match better with experimental results with the piston for 0.15mm and 0.23mm land width TLOCRs.

In addition, the ring land width input has a strong effect on the calculation results. This is especially true for the ring with a smaller land width of 0.06mm: a 0.01mm land width difference will cause an observable deviation in the calculation results. From the measurement, the upper ring land width varies between 0.06mm and 0.07mm at different locations. A larger ring land width can lead to higher friction once the ring operates in the hydrodynamic lubrication regime. This topic will be discussed in detail in section 5.1.

Furthermore, the top four lateral stoppers that are screwed in the liner can withstand some of the friction forces. Although, from the experimental results, the load sensors are sensitive enough to the vertical movement and should respond to most of the friction forces, uncertainties still exist around lateral stoppers. By the current practice of limiting the engine speed and concentrating on the lower stroke friction where the piston side force is minimal, the lateral stopper effect is mitigated to a minimal level. However, uncertainties should still be recognized.

Considering the uncertainties around the experimental and calculation inputs, the deterministic TLOCR model can reasonably predict the hydrodynamic pressure generation ability of a ring/liner mating pair. The deterministic TLOCR model and the piston ring pack model will be used to further study the factors affecting piston ring friction.

4. Practical Challenges for Applying the Deterministic TLOCR Model

4.1. Surface Calculation Uncertainties: Introduction

When studying the friction between piston rings and cylinder liners using the deterministic TLOCR model, a small patch of the liner is measured as model input. However, after an extended period of operation, the liner surface roughness at different locations is usually different. Identifying a single patch with a limited size (usually a square of a few millimeters) that can faithfully represent the surface roughness and wear of the entire surface can be hard to achieve.

4.2. Surface Roughness Effects on Contact Model

The boundary contact model inputs are strongly related to the surface roughness and wear conditions. Different measurement spots on the same liner surface can result in significant variations in the boundary contact pressure calculation.

For this study, on each liner sleeve, 4 spots were measured after all the tests were finished. The four locations are: thrust side close to top dead center (TDC Thrust), thrust side close to bottom dead center (BDC Thrust), thrust side close to mid-stroke (Mid Thrust) and pin side close to mid-stroke (Mid Pin). Figure 54 shows the surface measurement results. Table 5 shows the plateau roughness σ_p and the surface roughness R_a of the measured points on the three liner sleeves. It can be observed that both the plateau roughness and the surface roughness have apparent variations across different measurement locations.

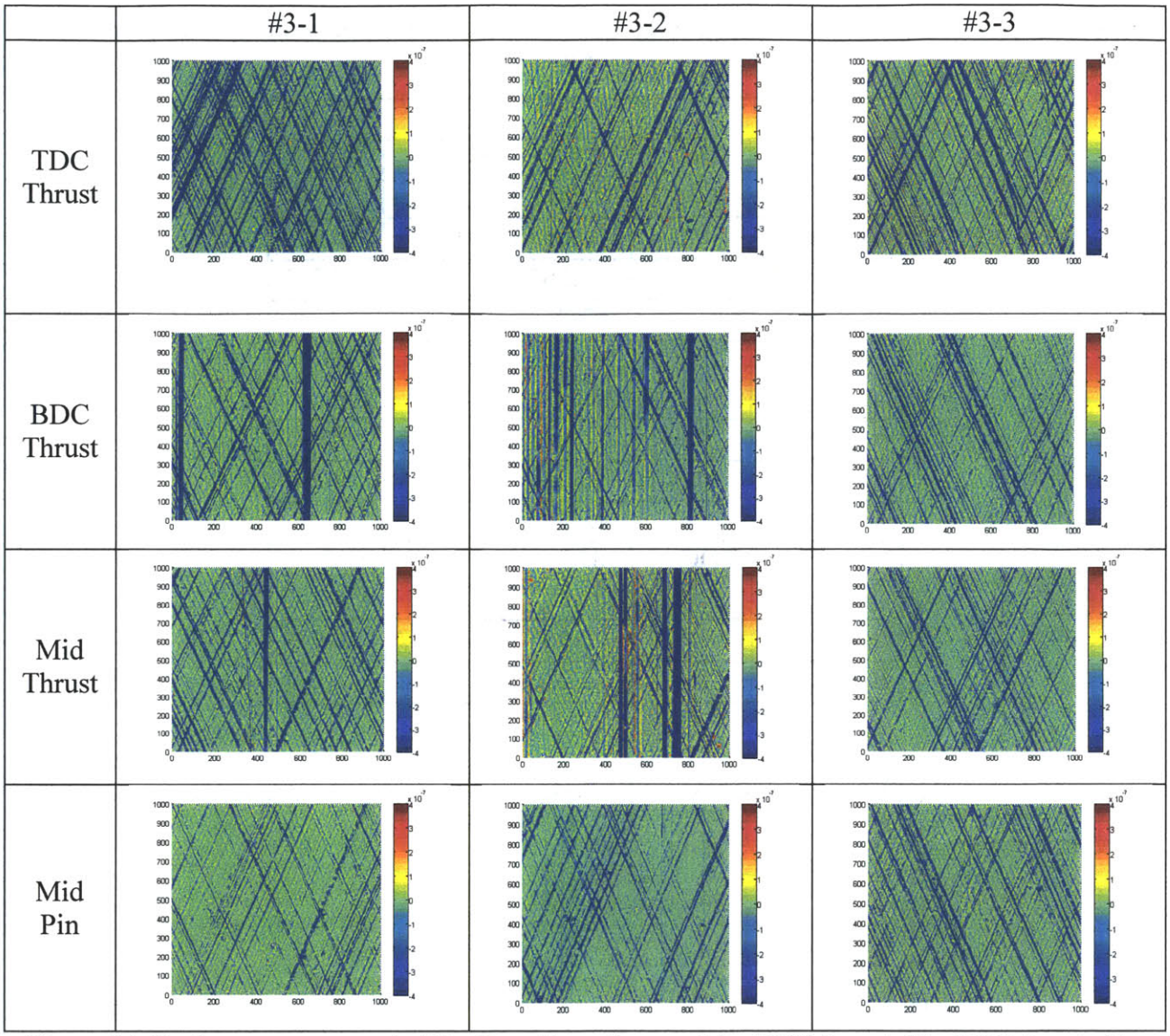

Figure 54: Surface measurement of the three liner sleeves at the TDC thrust side, BDC thrust side, mid-stroke thrust side and mid-stroke pin side, sling direction from top to bottom. Each patch is about 3mm by 3mm and the color bar unit is in meter.

Table 5: Plateau roughness and surface roughness of the three liner sleeves measured at 4 different locations

#3-1				
	TDC Trust	BDC Trust	Mid Thrust	Mid Pin
σ_p (μm)	0.071	0.058	0.063	0.055
Ra (μm)	0.568	0.363	0.346	0.201
#3-2				
	TDC Trust	BDC Trust	Mid Thrust	Mid Pin
σ_p (μm)	0.092	0.08	0.116	0.041
Ra (μm)	0.301	0.247	0.314	0.267
#3-3				
	TDC Trust	BDC Trust	Mid Thrust	Mid Pin
σ_p (μm)	0.124	0.063	0.067	0.078
Ra (μm)	0.611	0.286	0.282	0.31

Figure 55 shows the FEMP calculation results using the mid-stroke pin side measurement of the three liner sleeves.

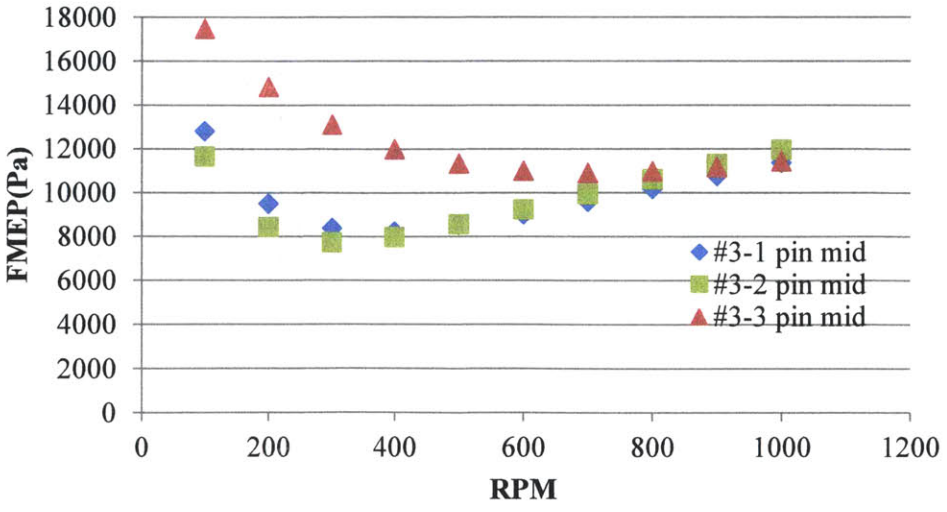

Figure 55: FMEP calculation results of the three liner sleeves using the mid-stroke pin side surface measurement as input

The calculation results show that the FMEPs of the three liner sleeves have large variations at lower engine speeds. As the model consists of the contact module and the hydrodynamics module, an analysis of the FMEP contribution from each module can provide more insight.

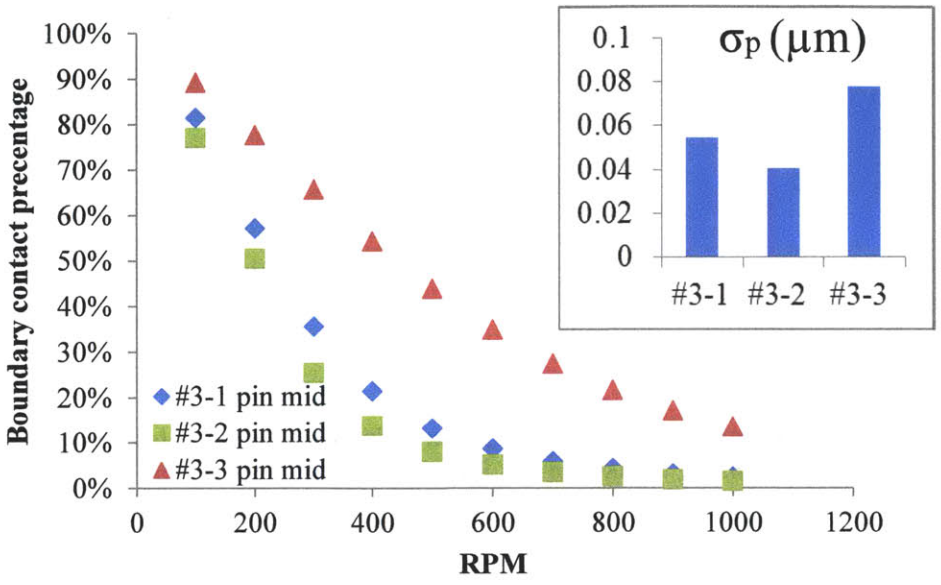

Figure 56: FMEP contribution from contact model and plateau roughness of the three surfaces measured at mid-stroke pin side

Figure 56 shows that at lower engine speeds, the FMEPs are mainly from boundary contact. As the engine speed increases, the FMEP contribution from boundary contact reduces. Therefore, the variations at the low engine speeds mainly result from the contact model. In addition, the values of plateau roughness of the three liner sleeves covary with their 100RPM FMEPs. Across all engine speeds tested, boundary contact has the greatest contribution to the FMEP at 100RPM. A study concentrating on 100RPM FMEPs can help identify the deciding factor when boundary contact is dominating.

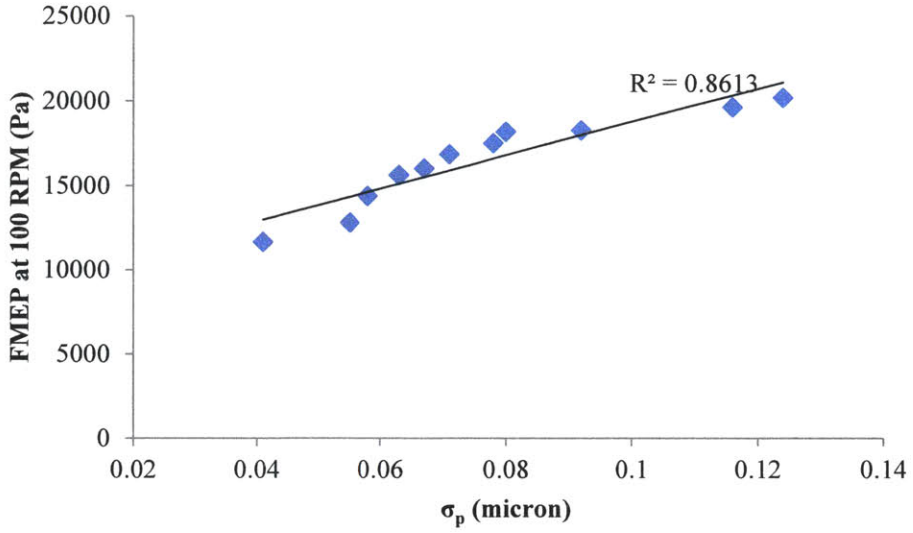

Figure 57: Correlation of FMEPs at 100RPM and plateau roughness (σ_p), FMEPs at 100RPM calculated using measurement from all 12 spots on the 3 liner sleeves

Figure 57 uses 100RPM FMEPs to represent boundary contact FMEPs, plotting against the plateau roughness (σ_p) of all 12 measured spots. The figure shows that boundary contact FMEPs are strongly correlated with the surface plateau roughness (σ_p).

Therefore, when boundary contact is dominating the total friction, liner surface plateau roughness (σ_p) can be the decisive factor to the friction loss of the ring/liner contacting pair.

4.3. Surface Roughness Effects on Hydrodynamic Model

Figure 58 shows the instantaneous Stribeck curves obtained from the calculation results that use different liner locations' surface measurement as inputs. The curves are compared with the instantaneous Stribeck curve obtained from the experimental results.

The solid lines represent the calculation results, and the marks represent FLE experimental results. The FLE tests used a 0.06mm land width TLOCR, and the springs were changed to give the TLOCR different tensions. Lowering the liner temperature to 40°C and 60°C can extend the hydrodynamic regime covered by the instantaneous Stribeck curve. It should be noticed that for the experimental instantaneous Stribeck curve, the piston friction was subtracted and friction results of 20-40CAD from the BDC were used.

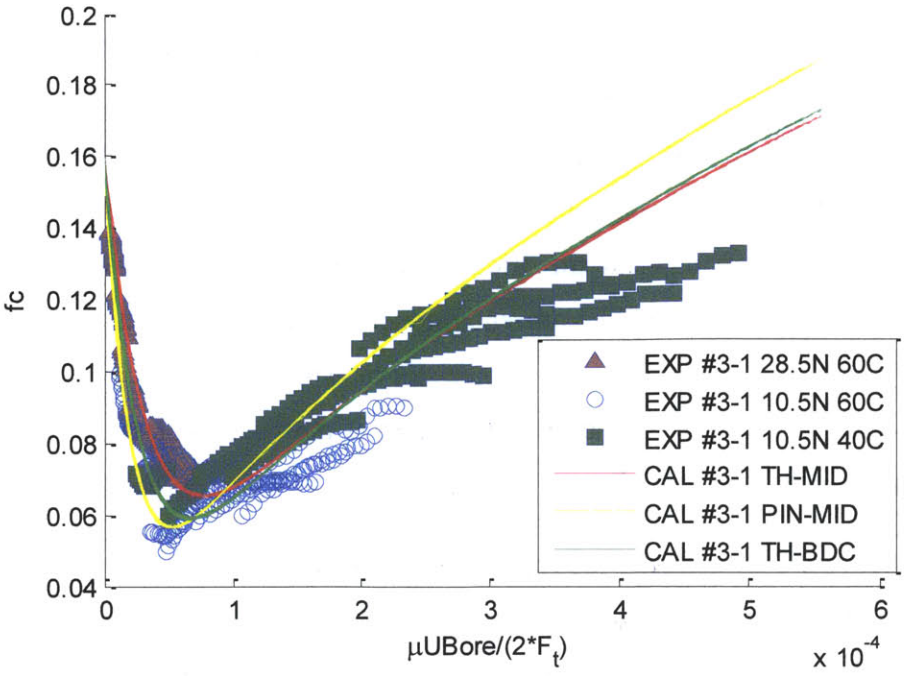

Figure 58: Instantaneous Stribeck curve from 0.06mm land width TLOCR model results using different surface inputs, compared with FLE results

Figure 58 indicates that the hydrodynamic pressure generation ability and the shear stress calculated based on a small patch can deviate from the surface average values.

It is worth noticing the thrust side BDC surface input gives the calculation a good match with the experimental results, which are also from the BDC region. The observation further suggests that the deterministic TLOCR model can faithfully represent the hydrodynamic pressure generation ability of a given surface input. However, results deviation is observed due to different surface inputs. The challenge now becomes how to find an input correlation that can represent the average hydrodynamic pressure generation ability of the entire surface.

4.4. Multi-Point Correlation Method

Section 3 shows the consistency between the measurement and the calculation in a local area, indicating the credibility of the model. A further question is how well the model can predict FMEP, which is dominated by the friction at the mid-stroke and affected by the surface roughness at all the locations.

Figure 59 shows the experimental results of the FMEP trend of the 0.06mm land width 28.5N tension TLOCR on three liners. The #3-1 and the #3-3 liners were broken in using the 0.06mm land width 28.5N tension TLOCR under the motoring condition. During the break-in process, the FLE thrust side temperature and the oil jet temperature were kept at 60±1°C, and the engine speed was kept at 100RPM. Every half an hour, the engine speed was increased from 100RPM to 1000RPM at 100RPM intervals, and the friction was recorded. After friction recording, the engine speed returned to 100RPM. The aforementioned process continued for 15 hours for the #3-1 liner sleeve, and 10 hours for the #3-3 liner sleeve. The friction forces at different engine speeds stabilized within the time frame. FMEP results of the #3-1 liner after 10-hour and after 15-hour break-in are used. The #3-3 liner friction results after 10-hour break-in are used.

The #3-2 liner sleeve was operated with various rings under both motoring and fired conditions for extended periods. For the purpose of the current study, the #3-2 liner sleeve was run under the same motoring condition with that of the #3-1 and the #3-3 sleeves for 5 hours. The last set of friction results from 100RPM to 1000RPM was used for comparison. The piston friction was subtracted from the TLOCR friction results.

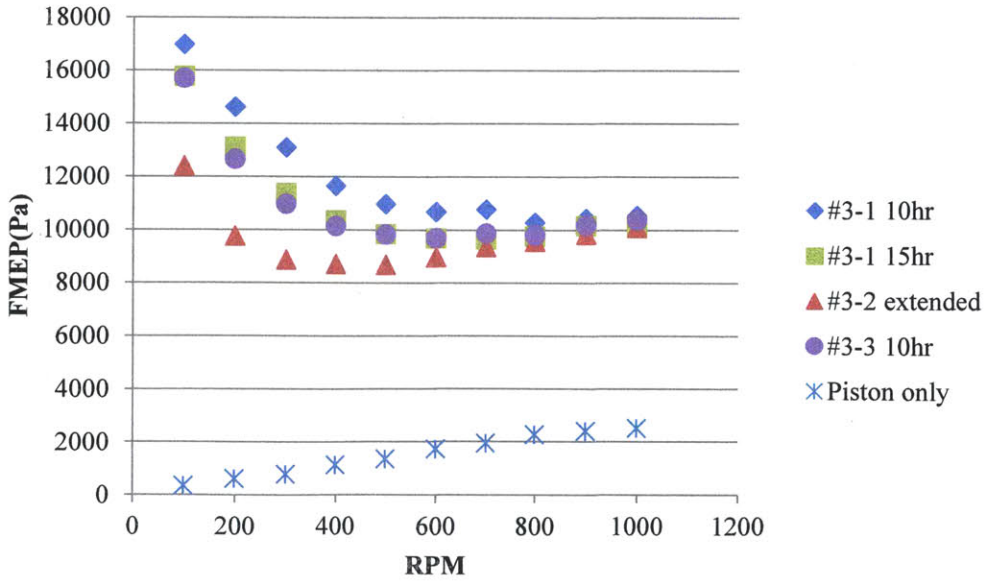

Figure 59: Experimental FMEP trend of the 0.06mm land width 28.5N tension TLOCR on three liners of the same honing, at 60°C

The experimental results in Figure 59 show that at higher RPMs, the FMEPs of different liner sleeves but the same honing in addition to the same sleeve but different break-in length are

converging. The implication of this evidence is that in an average sense, hydrodynamic behavior of the three sleeves with the same honing is the same and the difference in FMEP is made by the asperities in contact.

Therefore, the following multi-point method is proposed to predict the FMEP of the TLOCR. First, an overall hydrodynamic pressure (shear-stress) relation with the ring-liner clearance based on all the reasonable spots should be obtained. Then, as the plateau roughness is changing during break-in, plateau roughness can be changed in certain ranges to predict the evolution of FMEP during break-in.

The multi-point correlation method needs to first define a representative plateau roughness (σ_{p0}) and plateau ratio (r_{pl0}). These two values can be obtained by averaging the results from different measured spots.

$$r_{pl0} = \frac{\sum_{i=1}^{N} r_{pl,i}}{N} \tag{7}$$

$$\sigma_{p0} = \sqrt{\frac{\sum_{i=1}^{N} r_{pl,i}\sigma_{p,i}^2}{\sum_{i=1}^{N} r_{pl,i}}} \tag{8}$$

In equations 7 and 8, $\sigma_{p,i}$ and $r_{pl,i}$ are plateau roughness and plateau ratio of each selected small surface patch. The patch selection criteria are: 1) the patch should not have through scratch in the sliding direction; and 2) the patch should be able to reflect the intended honing pattern.

Then, the pressure (and shear-stress) and nominal clearance relationship from all the patches with normal wear should be calculated using the deterministic model [4, 8]. Single correlations in the form of equation (1) and (2) are obtained, with σ_p replaced by σ_{p0}.

Figure 60 shows the correlations of hydrodynamic pressure (and shear stress) with the clearance.

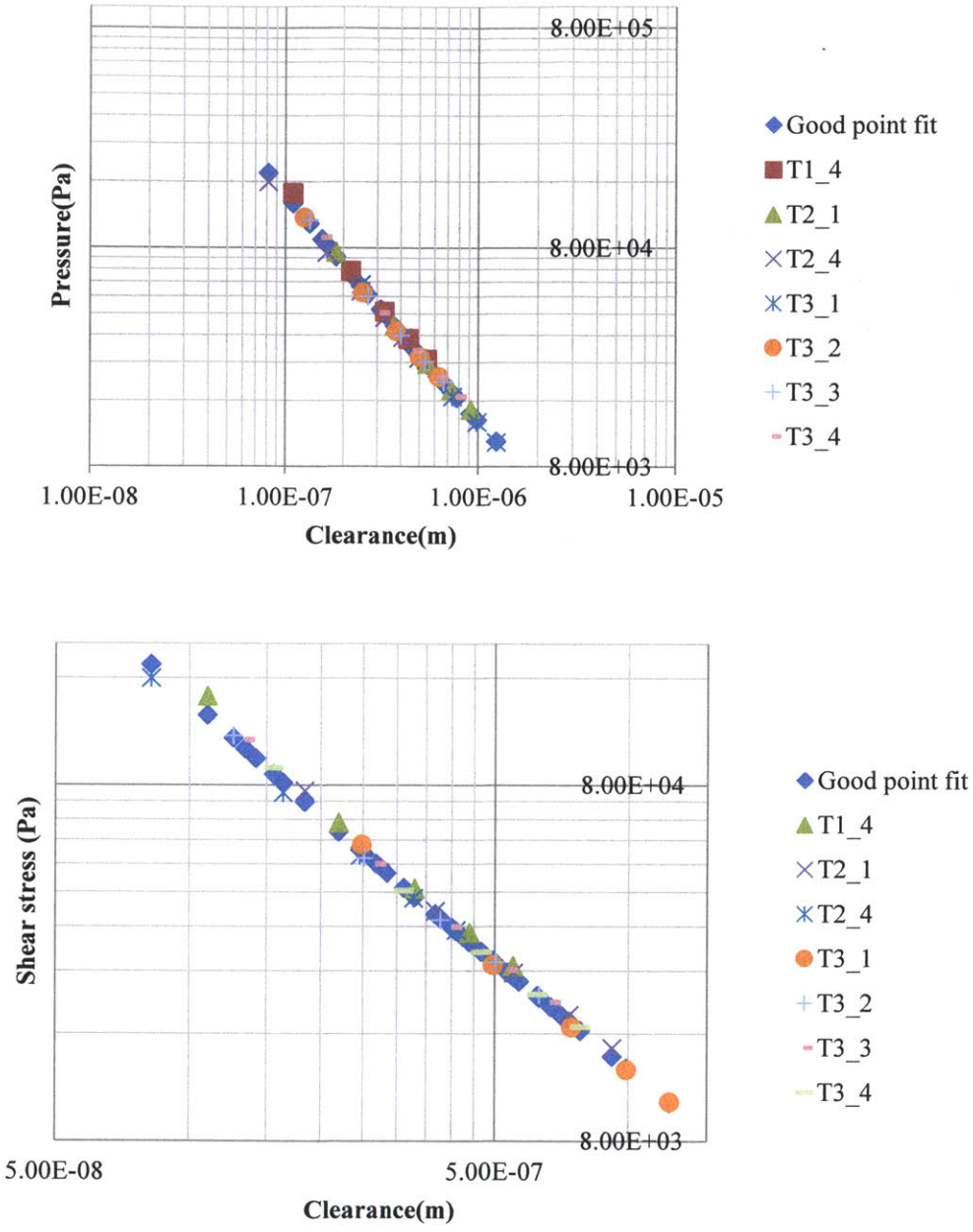

Figure 60: Correlations of hydro pressure (and shear stress) and clearance. In the legend, sleeve 1, sleeve 2 and sleeve 3 are #3-1, #3-2, #3-3 liner sleeve, respectively; the second digit of 1, 2, 3 and 4 represent TDC thrust side, BDC thrust side, mid-stroke thrust side and mid-stroke pin side, respectively.

The robustness of the multi-point correlation method was tested. In addition to the correlation obtained from all reasonable spots (good points), all spots including those with severe scratches were used to obtain another correlation. Figure 61 shows the FMEP results from both inputs.

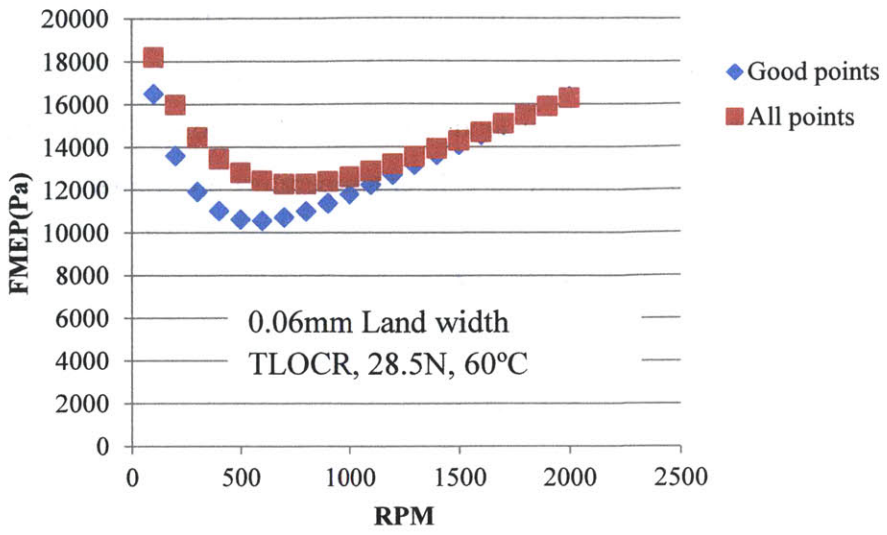

Figure 61: FMEP calculated with 'good points' and 'all points' correlation inputs, using multi-point correlation method

Figure 61 shows the FMEPs of the 0.06mm land width 28.5N tension TLOCR at 60°C. Calculations using correlations from only good points and all points predict the same FMEPs at higher RPMs where hydrodynamic shear stress is dominant. At lower RPMs where asperity contact happens, deviations in the plateau roughness result in differences in FMEPs.

Therefore, when the surface roughness changes across the liner, the multi-point correlation method is robust in predicting hydrodynamic pressure generation ability (and shear stress) of a certain type of surface honing. The effects of changing surface roughness on boundary contact can be reflected by changing the plateau roughness input.

Experiments suggest limited hydrodynamic behavior change over the break-in period and with different liners of the same honing. Thus, the multi-point correlation method can be used to best represent the hydrodynamic behavior of a certain honing. The boundary part is dependent on the exact stage of the asperity wear.

4.5. Multi-Point Correlation Case Study

The following case compares experimental results with calculations that use multi-point correlation inputs.

Figure 62 shows the friction-difference comparison between the experimental and the calculation results. The friction-differences are obtained by subtracting the 0.06mm land width 10.5N tension TLOCR friction from the 0.06mm land width 28.5N tension TLOCR friction. Friction-differences at 500RPM and 1000RPM at a 60°C liner temperature are shown.

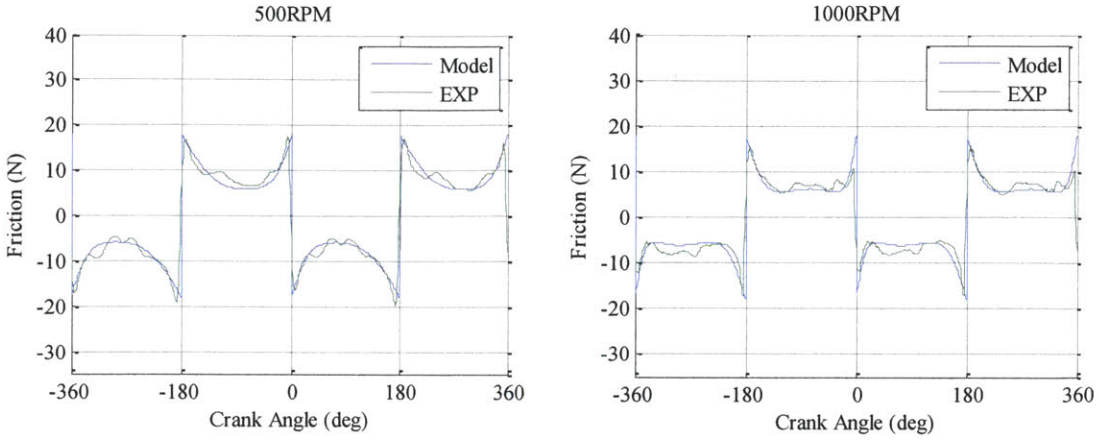

Figure 62: TLOCR model (Model) and experimental (EXP) friction difference between 28.5N 0.06mm land width TLOCR and 10.5N 0.06mm land width TLOCR at a 60°C liner temperature, 500RPM and 1000RPM, respectively

In the comparison shown in Figure 62, FLE piston secondary motion effect is alleviated by using friction difference comparison. The surface variation effects on the calculation are mitigated by using the multi-point correlation input. After efforts from both sides, good agreement between the experimental and model results is observed.

Figure 63 shows the FMEP comparison between experimental and calculation results. In Figure 63, the piston friction was subtracted from the experimental results. In the experiment, the same ring was used and springs were changed to give the ring different tensions.

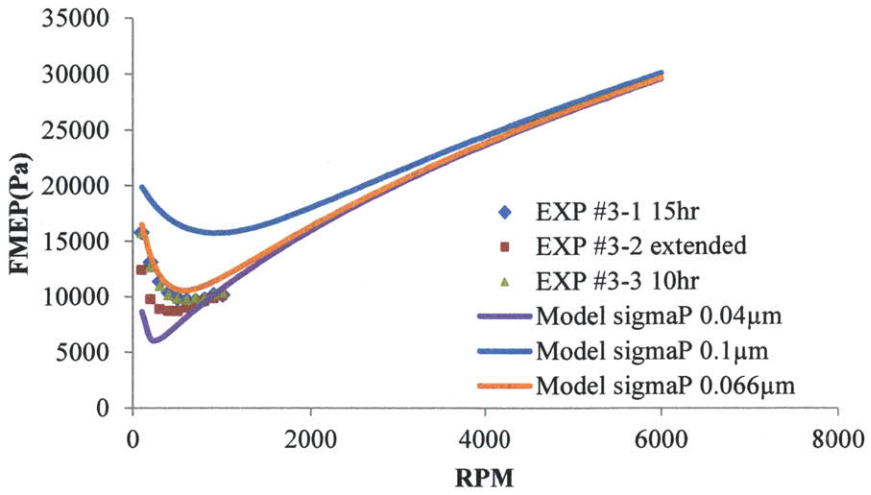

Figure 63: Experiment and multi-point correlation model comparison of FMEP of 0.06mm land width TLOCR, model plateau roughness (sigmaP) ranges from 0.04μm to 0.1μm.

Figure 63 demonstrates the effects of liner plateau roughness change over the break-in period. The model calculates the FMEPs of the TLOCR under the same hydrodynamic pressure – clearance correlation but three different σ_p: 0.04μm, 0.066 μm and 0.1μm. It indicates the evolution of FMEPs when contacting asperities are still evolving. The figure shows that hydrodynamic lubrication is robust to the asperity contact change in the break-in process. The boundary contact is continuously changing and can be represented by the plateau roughness evolution in the model. Model predictions cover the experimental results variations due to boundary contact change.

4.6. Conclusion

In conclusion, the multi-point correlation method can be used when the surface roughness variation is significant across different measurement patches across the same liner. The hydrodynamic pressure generation ability of the liner is preserved by keeping the same pressure-clearance correlation. Changing plateau roughness can reflect surface change due to break-in or across different parts of the liner.

5. Ring Design Effects

5.1. TLOCR Land Width Effect

In order to study the effects from the TLOCR land width, two TLOCRs with land widths of approximately 0.06mm and 0.15mm were used for the tests. The profiles of the two rings are shown in Figure 17 and Figure 25. Due to manufacturing tolerance, the ring land widths are not uniform circumferentially. Best ring land width approximations were used to name the oil control rings. Springs of three tensions, 10.5N, 19.5N and 28.5N, were used in the tests to fit in the two rings. The springs are interchangeable for these two kinds of rings. Table 6 shows the test setup for the oil control rings.

Table 6: Oil control ring land width effect test matrix

Ring Land Width	Ring Tension		
0.06mm	10.5N	19.5N	28.5N
0.15mm	10.5N	19.5N	28.5N

The FLE tests were run at 60°C, 80°C and 100°C for each ring configuration. Figure 64 shows the FMEP result comparisons between the two types of rings with different tensions at 60°C.

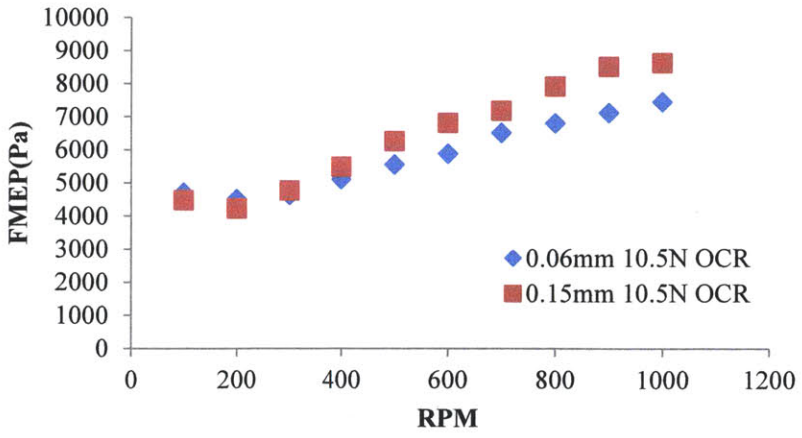

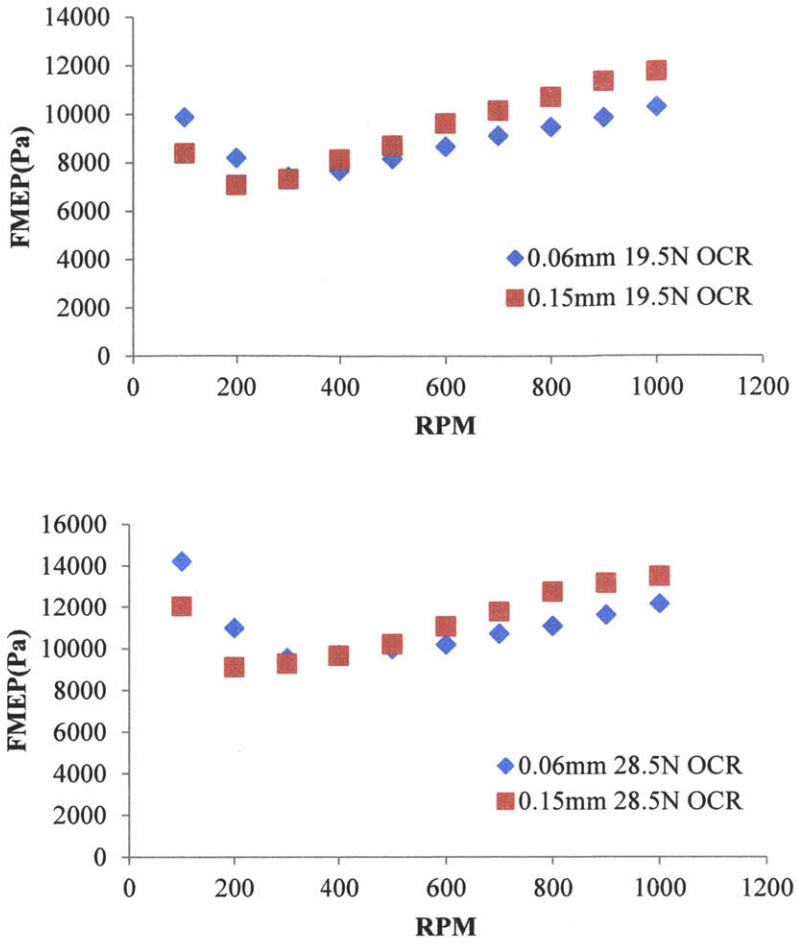

Figure 64: 0.06mm and 0.15mm land width oil control ring FMEP comparison at 60°C, for 10.5N, 19.5N and 28.5N ring tensions

From the FMEP results at different engine speeds, general 'Stribeck curve' shaped results can be observed at all the plots. At low engine speeds, the FMEP decreases as the engine speed increases. After reaching a minimum value, the FMEP starts to increase as the engine speed increases. At low engine speeds, boundary and mixed lubrication dominate in the entire cycle. Under such conditions, a larger land width can provide extra hydro-lift that increases the oil film thickness between the ring and the liner. As a result, boundary contact and total friction are reduced. Figure 65 shows the calculated minimum oil film thickness (MOFT) between the ring and the liner.

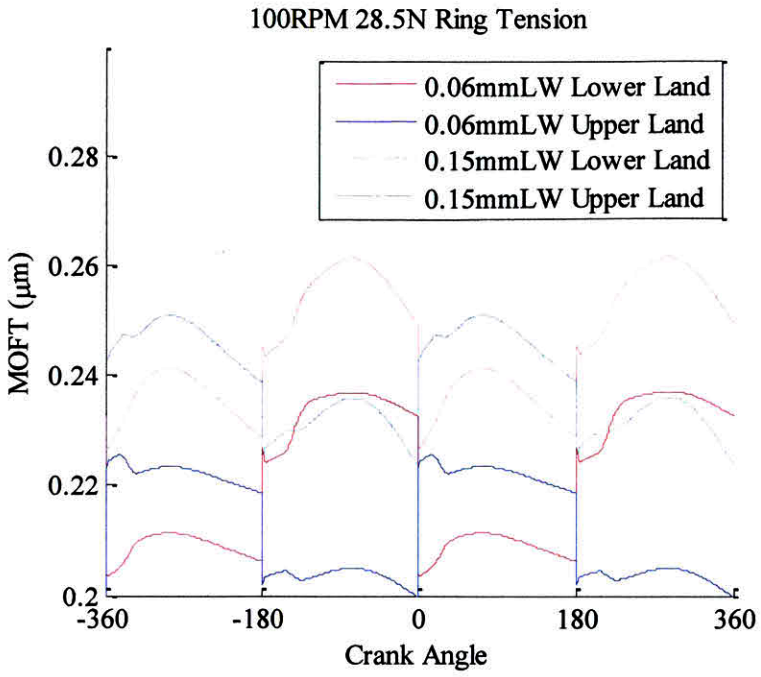

Figure 65: Minimum oil film thickness (MOFT) allowed passing lower land and upper land of the 28.5N, 0.06mm and 0.15mm TLOCR at 100RPM, calculation results

Once the ring enters a hydrodynamic lubrication-dominated regime, a higher engine speed causes the increase of the oil shear stress. A larger land width can increase the hydrodynamic pressure generation ability of the ring/liner mating pair, reflected as P_0 in equation (1). As a result, the 0.15mm land width TLOCR leads to a larger oil film thickness than that of the 0.06mm land width TLOCR. The shear stress from the oil is lower for the larger land width TLOCR accordingly. However, P_0 and the oil film thickness do not increase proportionally with the land width. The decreased shear stress cannot compensate for the extra ring land area that is exposed to the shear stress. As a result, the total friction increases with the land width.

The change of the 'hydro pressure generation ability characteristic constant' (P_0) as the ring land width changes is shown in Figure 66. Figure 67 shows the calculated minimum oil film thickness (MOFT) between the lower land and the upper land of the TLOCRs and the liner. The TLOCRs have a same ring tension of 28.5N but two different land widths, 0.06mm and 0.15mm. The engine speed is 1000RPM.

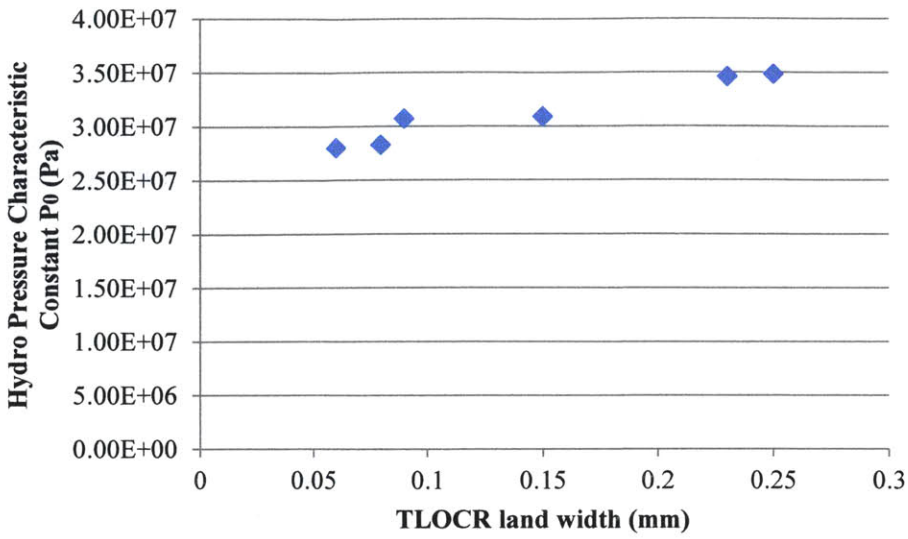

Figure 66: The change of hydro pressure characteristic constant P_0 with TLOCR land width

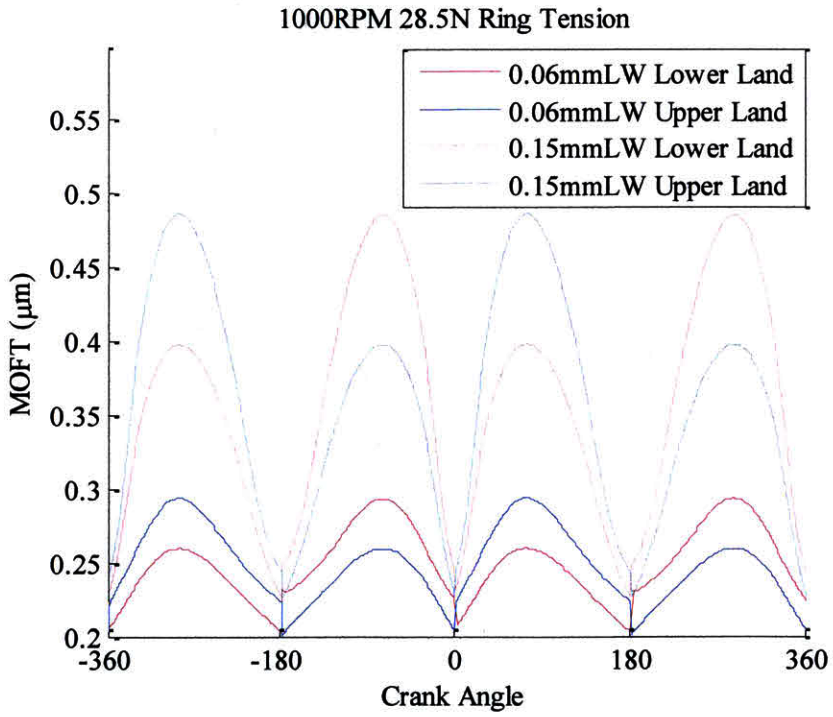

Figure 67: Minimum oil film thickness (MOFT) allowed passing lower land and upper land of the 28.5N, 0.06mm and 0.15mm TLOCR at 1000RPM, calculation results

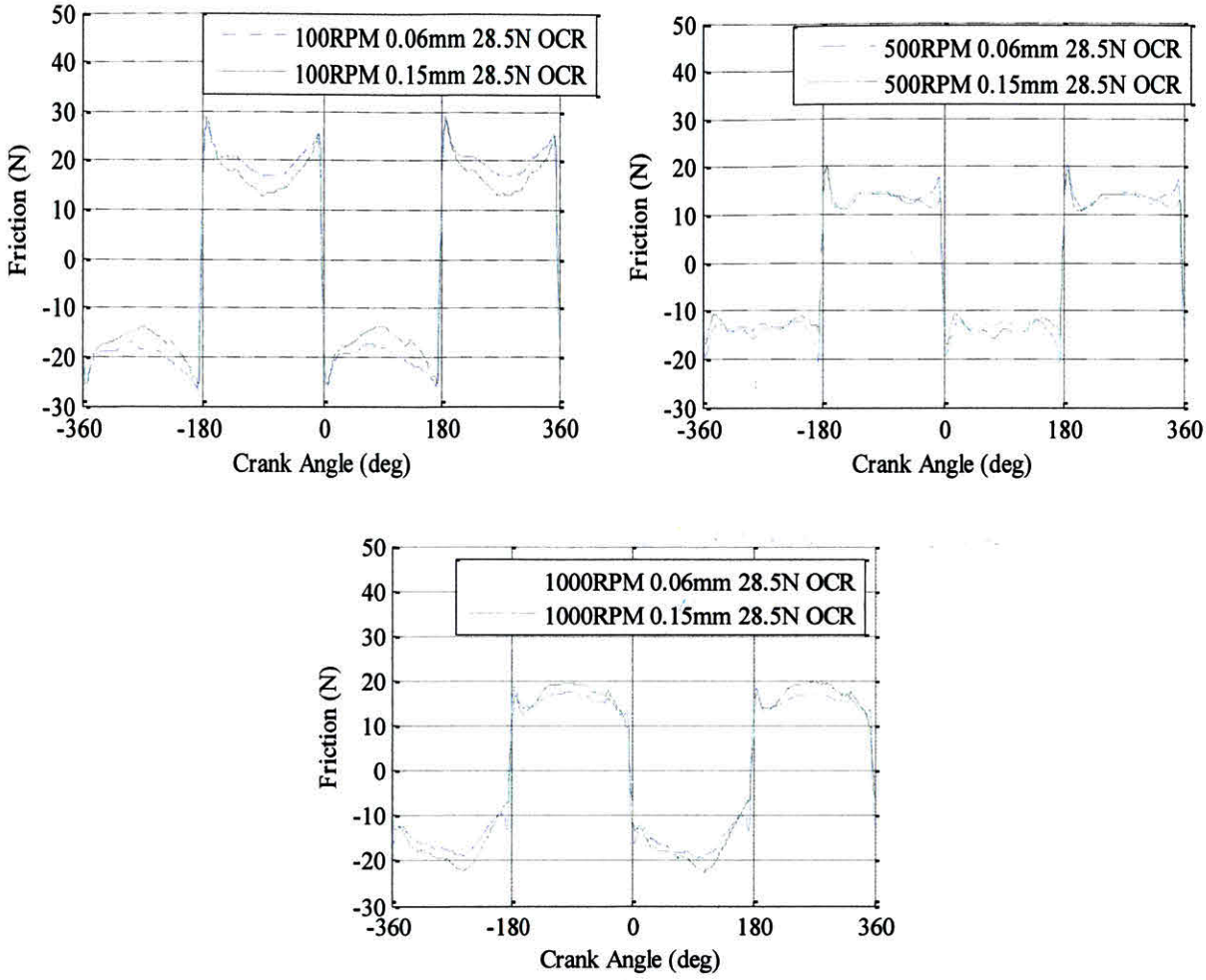

(a) Experimental results

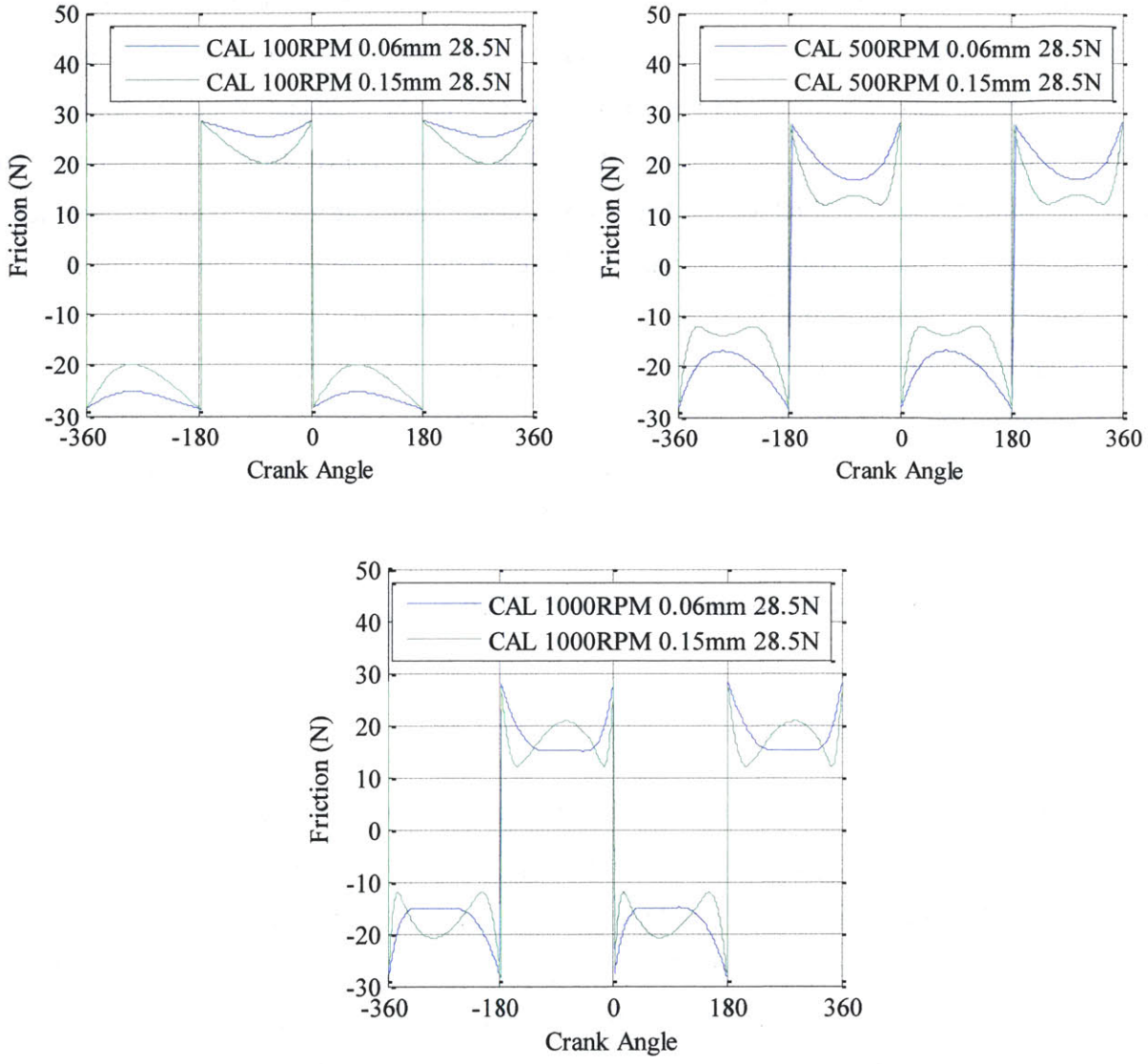

(b) Calculation results

Figure 68: 0.06mm 28.5N TLOCR and 0.15mm 28.5N TLOCR friction traces comparison at 100RPM, 500RPM and 1000RPM, 60°C, (a) experimental results, (b) calculation results

The effects of the ring land width can also be observed from individual friction traces. Figure 68 (a) shows the measured friction trace comparison between the 0.06mm land width and 0.15mm land width TLOCRs at 100RPM, 500RPM and 1000RPM. The tensions for both rings are 28.5N. The engine thrust side temperature is 60°C. At 100RPM, the 0.15mm TLOCR has lower friction than the 0.06mm TLOCR across different parts of the stroke. Under a low engine speed of

100RPM and relative large ring tension of 28.5N, TLOCRs of the two land widths both operate at a boundary to mixed lubrication regime. A larger ring land width, 0.15mm, increases the TLOCR's ability to generate hydro-lift force and reduces boundary contact. As a result, the total friction of the 0.15mm TLOCR is lower at 100RPM across the entire stroke. As engine speed increases to 500RPM and 1000RPM, the benefit of a larger land width still exists near the dead centers. However, at the mid-stroke, the friction forces mainly come from hydrodynamic shear stress. A larger land width results in larger hydrodynamic friction and total friction. Figure 68 (b) shows the calculation results using the same parameters with the experiments. The calculations also show that at the boundary to mixed lubrication regime, a larger ring land width reduces boundary contact and total friction; while at the hydrodynamic lubrication regime, a larger ring land width increases total friction.

5.2. Calculation Sensitivity on Ring Land Width

In the TLOCR manufacturing process, the ring tension can be controlled to be within 1N of accuracy, but the ring land width is much harder to control.

Ring land width can vary between the upper land and the lower land in addition to across different circumferential locations. When calculating the TLOCR friction, the deterministic TLOCR model allows one oil control ring land width as the input. However, TLOCR land width variations are common in the current production engines. When using the deterministic TLOCR model to study the TLOCR friction in a production engine, a pre-determined land width error band should be used in calculation, and the friction boundaries should be provided.

In a case of a TLOCR with a 10N ring tension, after an extended period of operation, a land width error band of 0.06mm to 0.08mm corresponds to a unit pressure of 1.5MPa to 2MPa. Cases of oil temperatures at 120°C, 135°C and 150°C are considered.

Figure 69 shows the cycle friction coefficients at engine speeds from 700RPM to 6000RPM.

In the calculations, the multi-point correlation method is used for the liner surface input.

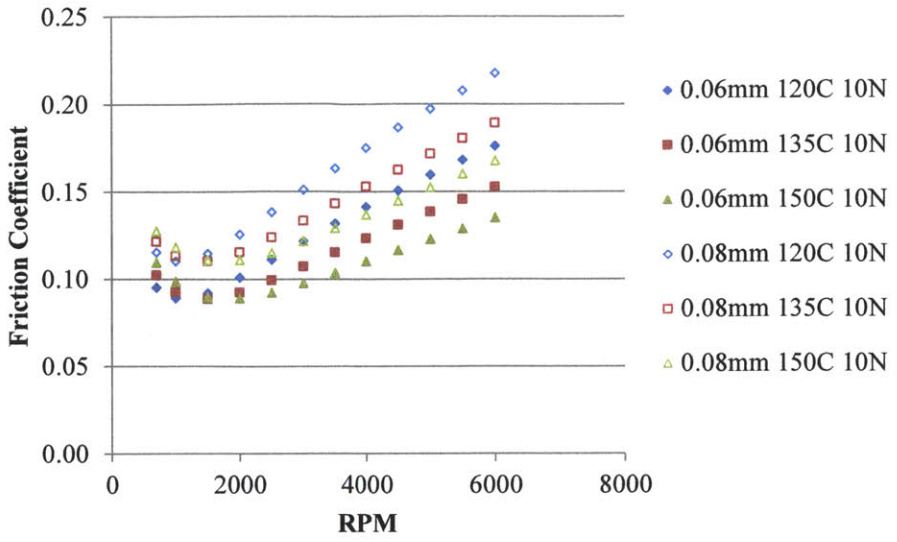

Figure 69: Ring land width effect on cycle mean friction coefficient using the multi-point correlation deterministic TLOCR model

For the scenarios considered, the results show that the TLOCR minimum cycle mean friction coefficients lie within the 1000~2000RPM range. Hydrodynamic shear stress becomes dominant at higher engine speeds and lower temperatures. A smaller TLOCR land width results in lower friction under the engine speeds covered in the calculation. The effects of land width variations on the TLOCR friction are significant.

5.3. Ring Tension Effect

Figure 70 shows the effects of the ring tension on FMEPs with both experimental and calculation results. With the same TLOCR land width, both results indicate that as the ring tension increases, the FMEPs of the TLOCR increase at all engine speeds. In addition, the increased unit pressure of the TLOCR shifts the minimum FMEP location towards the higher RPM region.

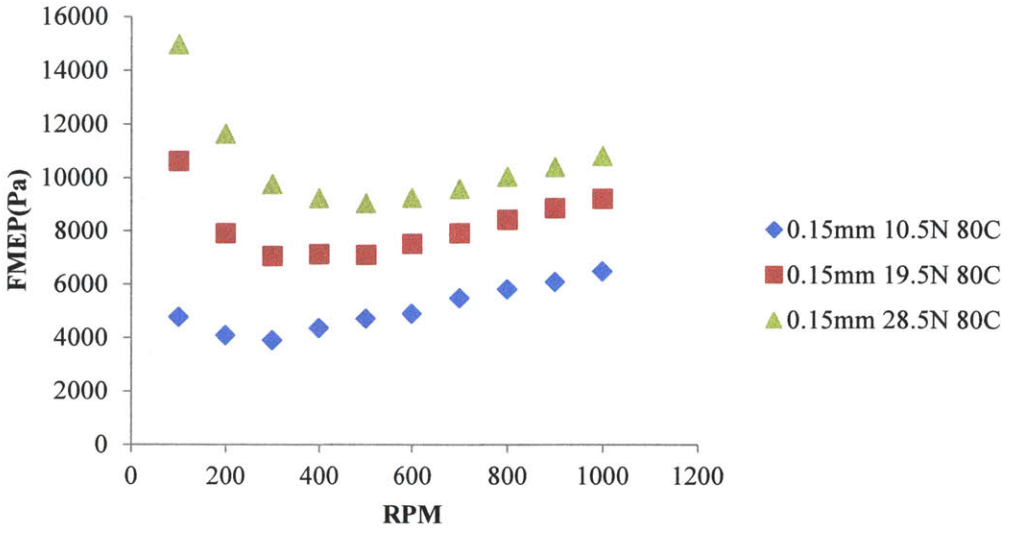

(a) Experimental results

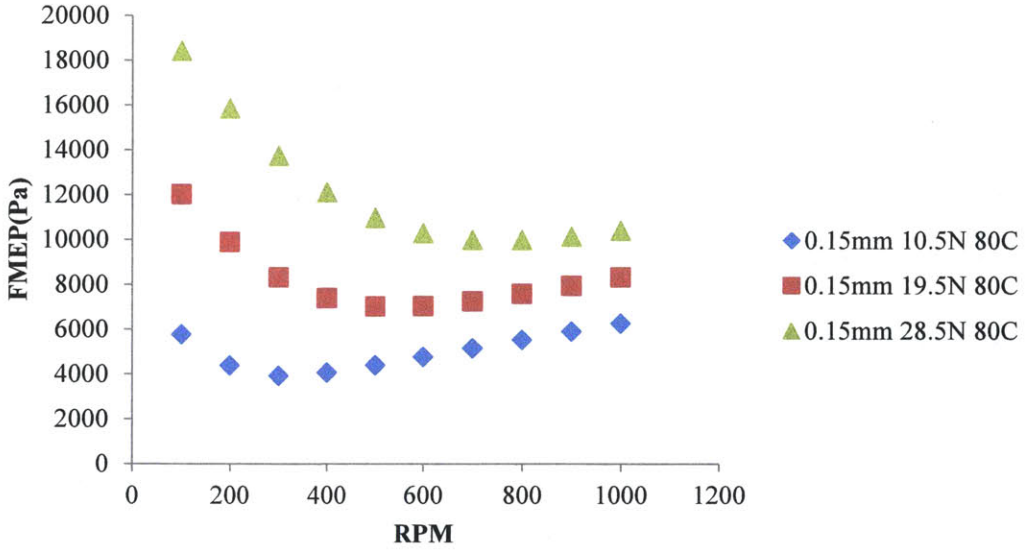

(b) Calculation results

Figure 70: FMEP trend of 0.15mm land width TLOCR at 80°C with 10.5N, 19.5N and 28.5N tension, (a) experimental results, (b) calculation results

5.4. Conclusion

In conclusion, in the hydrodynamic lubrication regime, with the same ring tension, a smaller ring land width reduces total ring friction due to less surface area exposed to viscous shear stress; the oil film thickness is also smaller. In the boundary contact-dominated lubrication regime, a larger

ring land width increases the oil film thickness between the ring and the liner, thus reducing contact. As a result, with the same ring tension, a large ring land width results in lower friction in the boundary lubrication regime. In addition, with the same ring land width, a higher ring tension results in higher friction across different lubrication regimes.

In addition, for a TLOCR with a tapered land design, the land width can increase with longer running time due to wear while the ring tension would have minimal changes. The results here indicate that, when the land width becomes larger and larger with wear, both oil film thickness and friction in the hydrodynamic regime would increase.

6. Cylinder Liner Roughness Effects

6.1. Break-in Effect

When predicting the ring friction using the deterministic TLOCR model, the surface input is a key element to the calculation. However, the newly manufactured liner surface undergoes rapid changes during the break-in period. In addition, it is the post break-in surface that will last for the majority of the life time of engines. Therefore, currently the liners need break-in before the measurement. If we can understand the effects of break-in on friction and model calculations, the save to the experimental side would be significant.

6.1.1. Liner Surface Selection

During the break-in period, contacts take place between the asperities on the liners and the piston rings. Cylinder liner surfaces undergo rapid changes that result in friction changes through the process. In order to study the break-in period, 6 different cylinder liners covering a wide range of surface roughness were tested.

Figure 71 shows the structure height and plateau characters of the 6 liners. On the plot, the surfaces become smoother towards the left; and the valley ratio becomes smaller towards the bottom. This thesis only focuses on the analysis of the break-in period of these liner finishes and the effects of the roughness from the FLE measurement side. Further study of the effects of these liner finishes on friction combining experiments and calculation will be presented in later works.

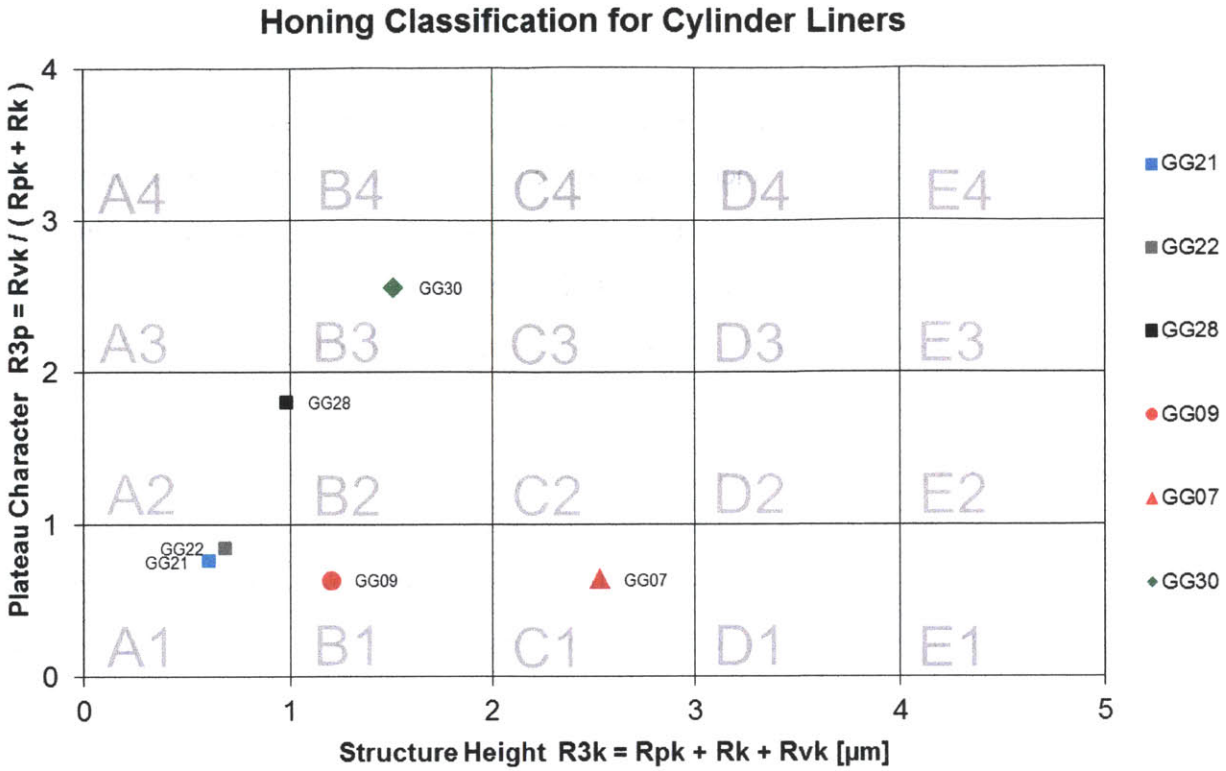

Figure 71: Surface structure information of the tested cylinder liners

6.1.2. Break-in Test and Calculation Setup

In the break-in tests, only the 0.15mm land width TLOCR was installed on the small piston. The piston has 100µm skirt clearance in diameter. Figure 17 shows the ring profile. The spring was replaced to give the TLOCR 19.5N tension. Open cylinder head motoring tests were used and the liner thrust side temperature was kept at 80°C.

At the very beginning of the break-in, when the liners were new, friction values were recorded from 100RPM to 1000RPM at 100RPM intervals. Thereafter, before each recording, the engine was operated at 400RPM for 30 minutes. The procedure of 30-minute engine operation followed by friction recording continued through the break-in process.

For the smoother liners, the break-in period usually lasted for 5 hours before the FMEP values stabilized. For the rougher liners, the break-in continued after the 5-hour period. Nonetheless, it is the surface changing process and the surface change effects on friction are of interest. Therefore, 5-hour tests providing 11 repeats of friction records are sufficient for the purpose.

The thin oil with HTHS of 1.4 mPa·s was used in the break-in tests. When calculating the instantaneous Stribeck curve from the experimental friction data, the oil viscosity needs to be included. When considering the shear-thinning property of the oil, the in-situ oil film thickness needs to be known. As a result, the liner surface structure needs to be accurately measured for model calculations. However, the liner surface undergoes rapid change during the break-in period. So in the calculations for this part, the oil viscosity under the high shear rate was used. Because other than the very short stroke distances close to the dead centers, oil usually operates under the high shear rate range.

Figure 72 shows the oil dynamic viscosity for two TLOCRs with different land widths at different engine speeds and temperatures. As the piston travels from the dead centers towards the mid-stroke, the increased piston linear speed results in higher shear rates and lower oil dynamic viscosity. The results in Figure 72 indicate that for most part of the stroke, the oil dynamic viscosity is closed to high shear rate values.

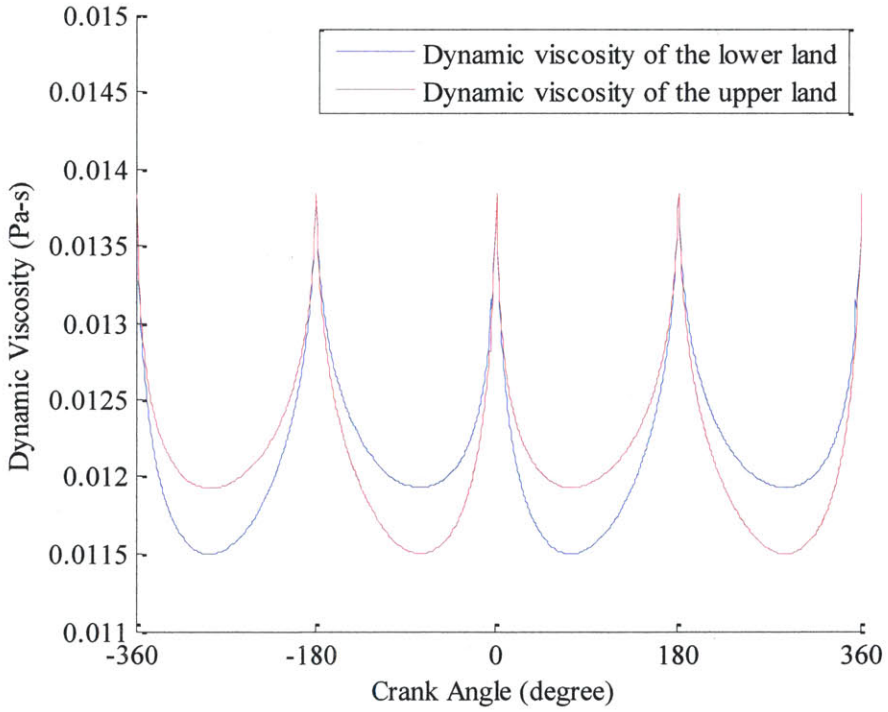

(a) a 10.5N 0.23mm TLOCR at 1500RPM, 40°C

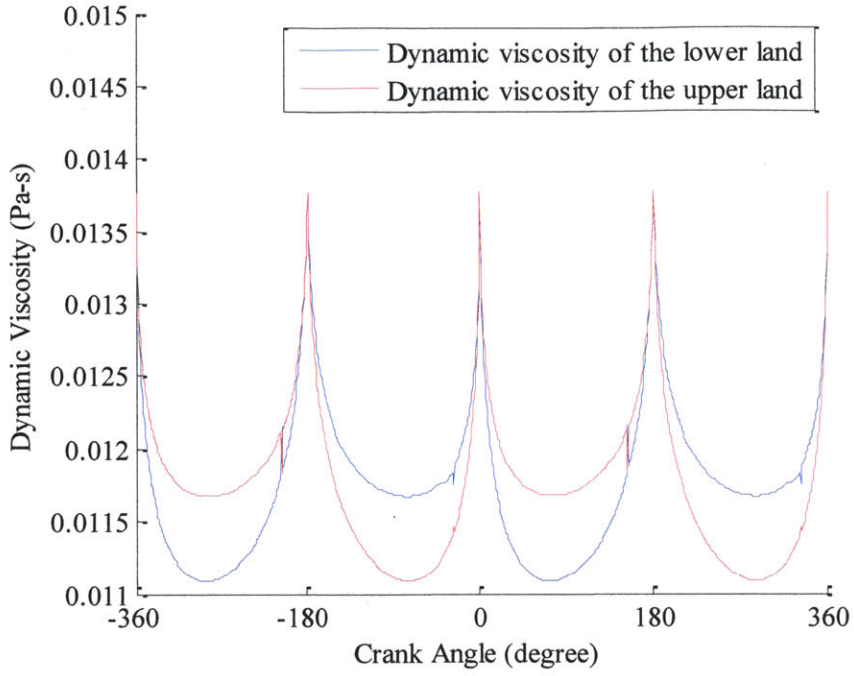

(b) a 10.5N 0.23mm TLOCR at 3000RPM, 40°C

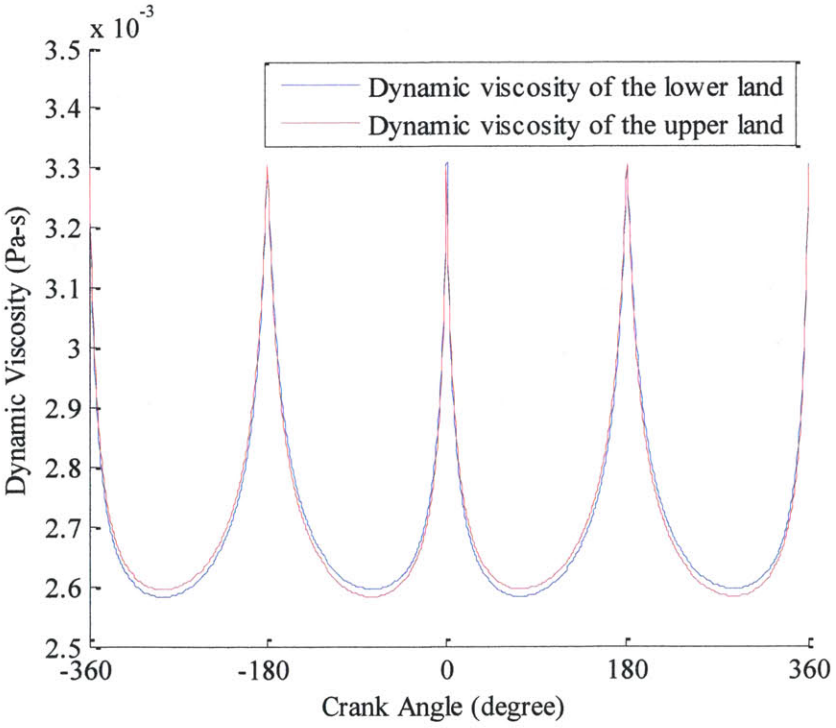

(c) a 10.5N 0.06mm TLOCR at 1000RPM, 100°C

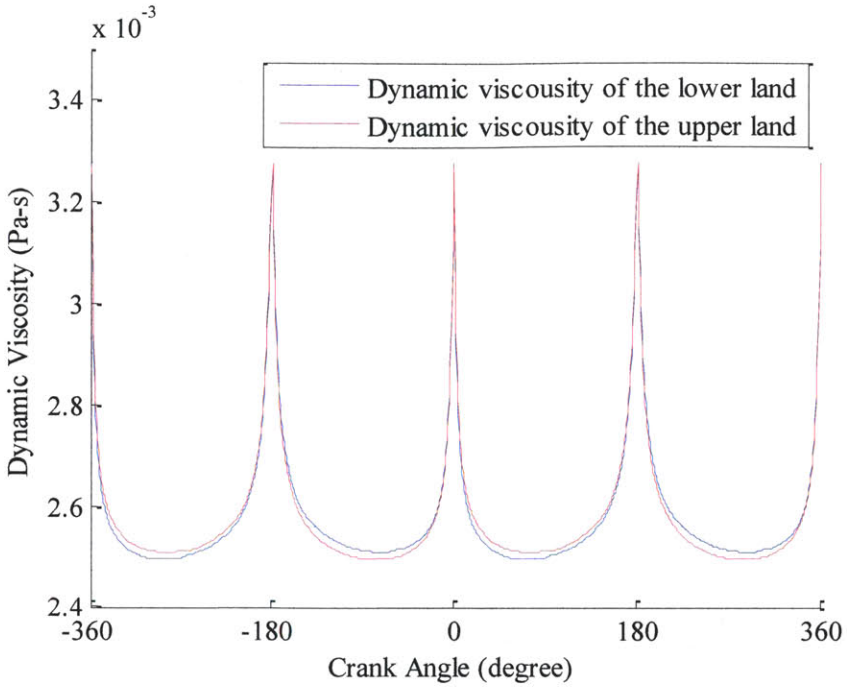

(d) a 10.5N 0.06mm TLOCR at 3000RPM, 100°C

Figure 72: Dynamic viscosity of the lower land and upper land, with the 1.4HTHS oil, for (a) a 10.5N 0.23mm TLOCR at 1500RPM, 40°C, (b) a 10.5N 0.23mm TLOCR at 3000RPM, 40°C, (c) a 10.5N 0.06mm TLOCR at 1000RPM, 100°C, and (d) a 10.5N 0.06mm TLOCR at 3000RPM, 100°C

Figure 73 shows the instantaneous Stribeck curve discrepancy results from using only the high shear rate oil viscosity.

In the calculations, the GG21 surface measurement was used as the input. The TLOCR land width was 0.23mm and the ring tension was 10.5N. The oil and the liner temperatures were both 40°C. The engine speeds were changed from 100RPM to 3000RPM at 100RPM intervals. The obtained instantaneous Stribeck curves cover the normal operating range of the TLOCR in the engines.

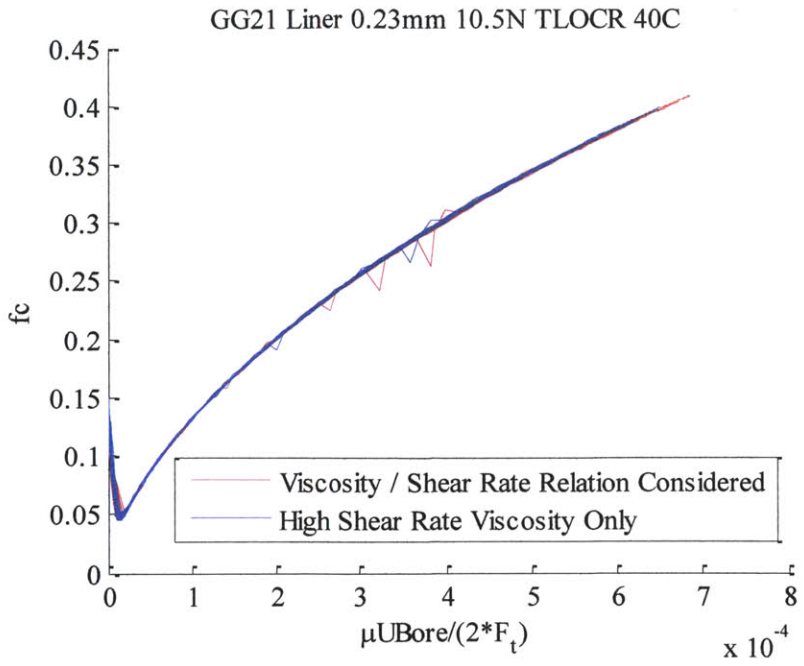

Figure 73: Instantaneous Stribeck curve calculated using oil viscosity under different shear rate assumptions

The difference between the two instantaneous Stribeck curves is minimal. In addition, friction traces and FMEPs obtained directly from measurement are not affected by the oil property assumptions.

6.1.3. GG07 Liner

Figure 74 and Table 7 provide the surface roughness information of the GG07 liner. The surface roughness was measured before break-in when the liner was new. All the other surfaces were also measured before break-in.

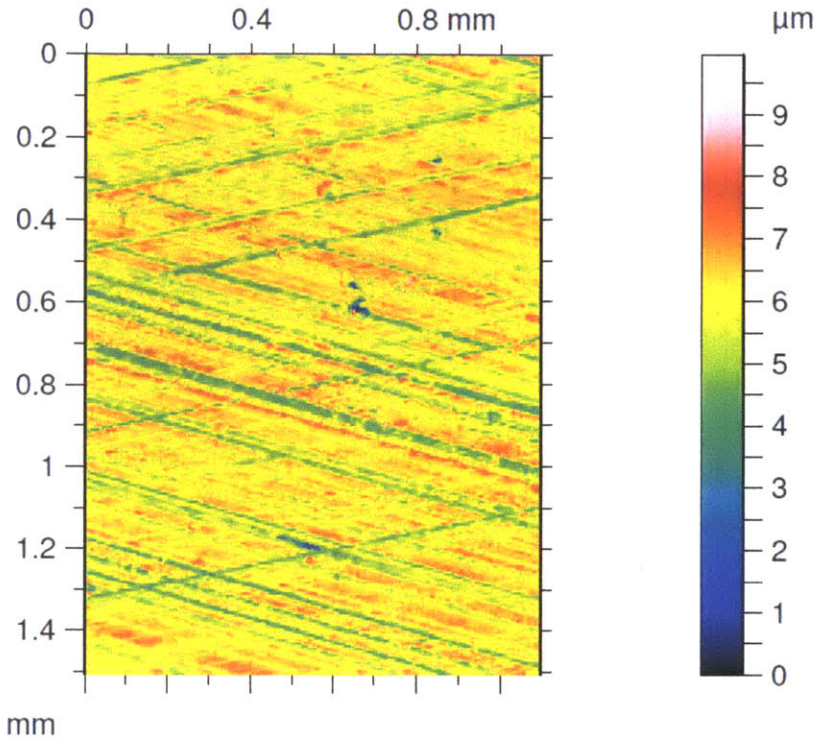

Figure 74: GG07 liner surface

Table 7: Surface roughness information of GG07 liner

	Rvk	Rk	Rpk
GG07	0.990	1.184	0.362

Eleven repeats of recordings from 100RPM to 1000RPM were taken at 30-minute intervals and the total operating time was about 5 hours. Figure 75 shows the FMEP change over the break-in period. Figure 75 suggests that the FMEP change of the rough GG07 liner at each RPM over the 5 hours period is little.

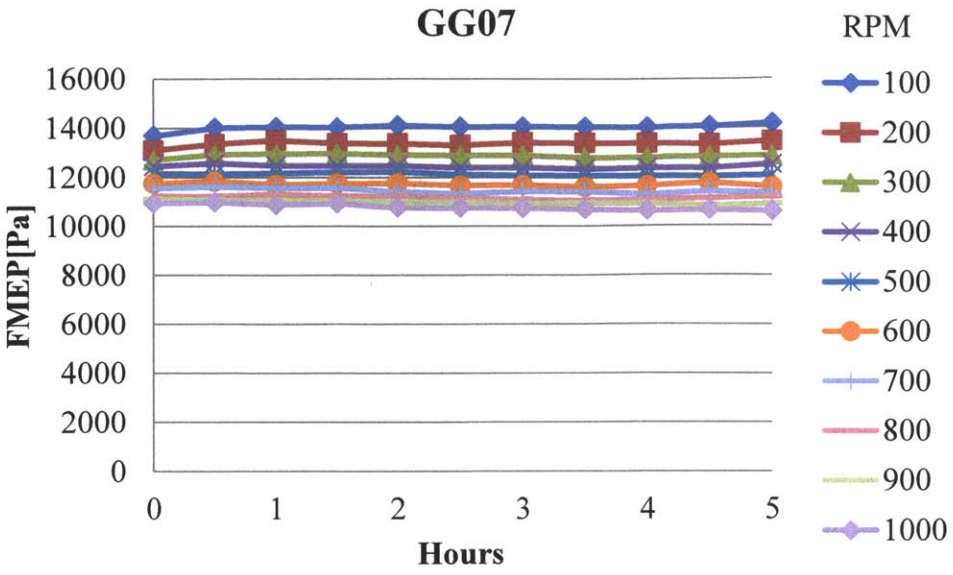

Figure 75: GG07 liner FMEP change over the break-in period

The friction traces shown in Figure 76 are the original measurement data including both the piston and the ring friction. Results of all the 11 repeats of tests are provided.

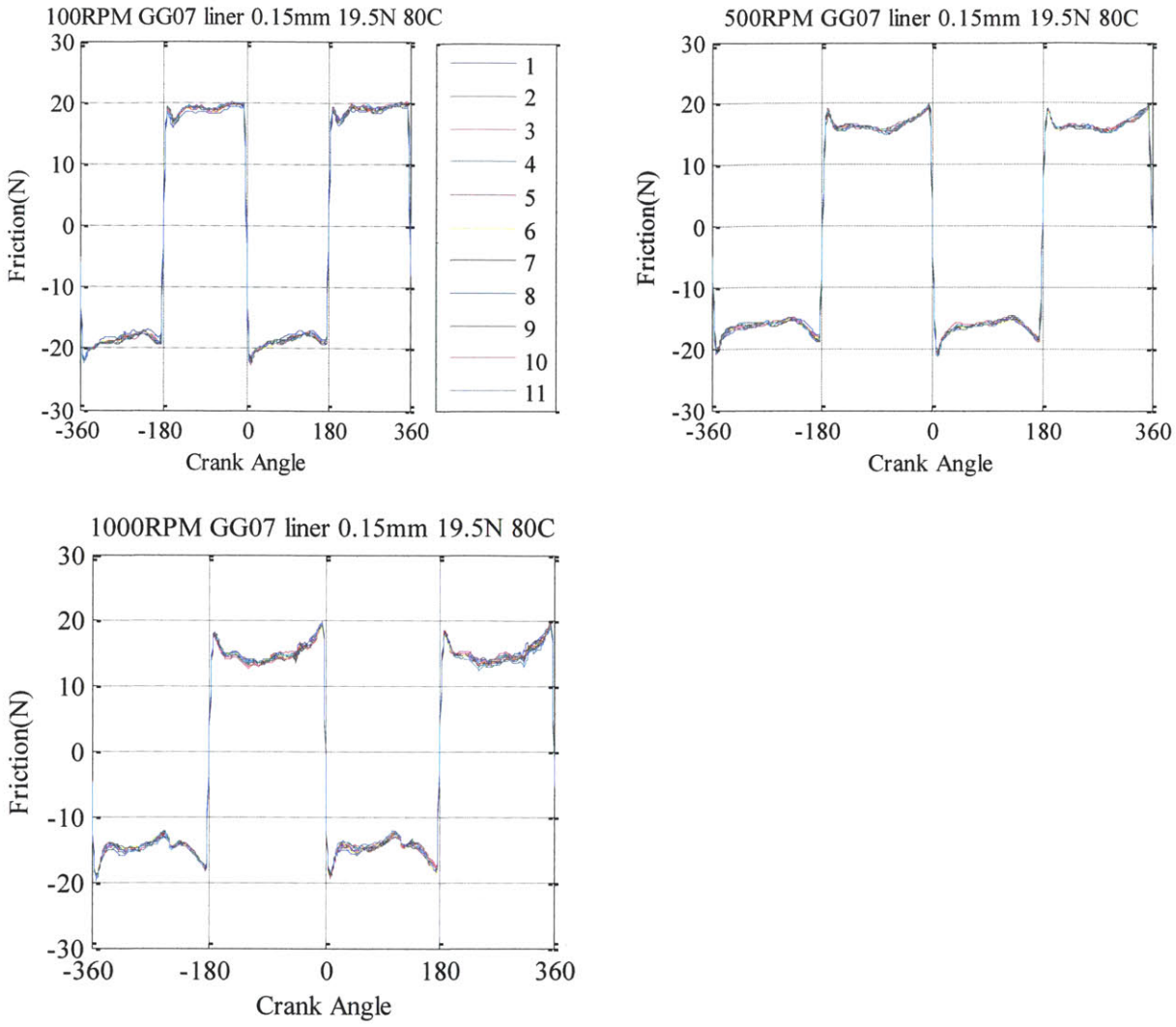

Figure 76: Friction traces of 0.15mm land width 19.5N tension TLOCR on GG07 liner over the break-in period, engine speeds of 100RPM, 500RPM and 1000RPM

GG07 is the liner with the highest surface roughness among all the liners tested. The 0.15mm land width 19.5N tension TLOCR mainly operates at a boundary to mixed lubrication regime at 80°C. At 1000RPM, the friction decreases as the piston speed increases towards the mid-stroke, indicating the TLOCR is transitioning towards the mixed lubrication regime from the boundary lubrication regime. Since the piston skirt friction due to shear stress is higher at the mid-stroke compared to the dead centers, the above observed trend will be preserved even after subtracting the piston friction.

Across the 11 sets of tests, or more than 5 hours of break-in, the TLOCR friction sees little change from 100RPM to 1000RPM.

Figure 77 shows the instantaneous Stribeck curve calculated using friction data from 100RPM to 1000RPM, at 40-45CAD, 90-95CAD and 165-170CAD from the TDC. The piston friction is subtracted. The instantaneous Stribeck curves from the 1st, 3rd, 5th, 7th, 9th and 11th measurement are shown to reveal the friction evolution trend at different parts of the liner surface. Due to piston speed change, the TLOCR operates at different lubrication regimes across different parts of the liner. With a low piston speed, boundary contact is most likely to take place near the dead centers, whereas the higher piston speed at the mid-stroke facilitates the hydro-pressure build-up. Each part of the liner may experience different surface evolution during the break-in period. The 40-45CAD data represent the upper part of the liner that is between the TDC and the mid-stroke. The 90-95CAD data represent the liner at the mid-stroke region. The 165-170CAD data represent the part of the liner that is close to the BDC.

For the current case, the instantaneous Stribeck curves from the three parts of the liner confirm the findings that 1) the TLOCR mainly operates at a boundary to mixed lubrication regime up till 1000RPM, and 2) during the 5-hour operation, the TLOCR friction at different parts of the liner has little change. The results imply that the surface still changes due to existence of asperity contact over the whole stroke. However, the change on the roughness is not substantial enough to result in noticeable friction change in the measured operational range. Compared with the results on smoother liners to be shown later, one can conclude that it takes much longer time than 5 hours to reach a stabilized ring friction.

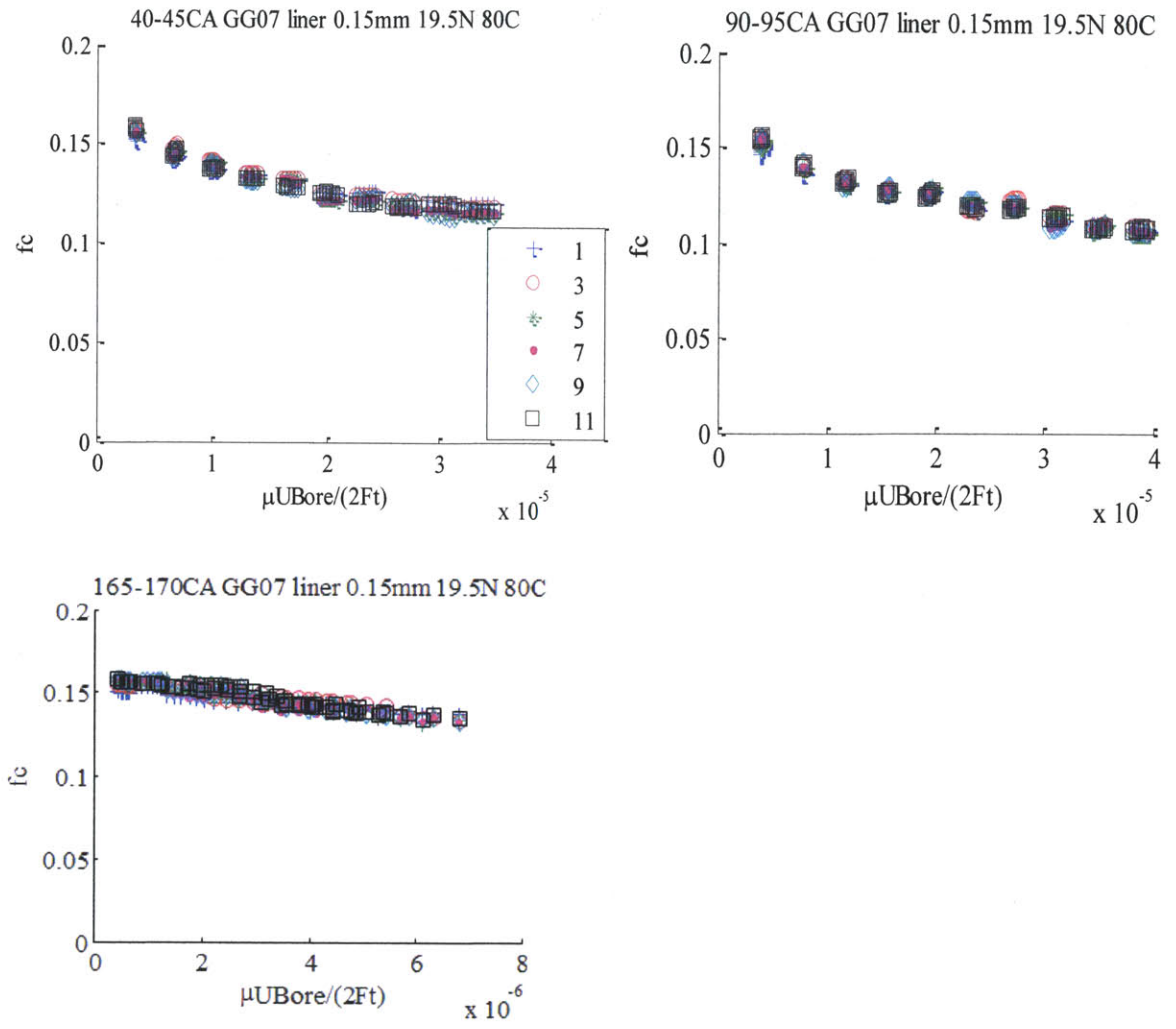

Figure 77: GG07 liner instantaneous Stribeck curve change over the break-in period, observed at upper part (40-45CAD), mid-stroke region (90-95CAD), and the area close to BDC (165-170CAD)

6.1.4. GG09 Liner

Figure 78 and Table 8 show the surface roughness information of the GG09 liner, measured before the experiment. The surface roughness of the GG09 liner is smaller than that of the GG07 liner.

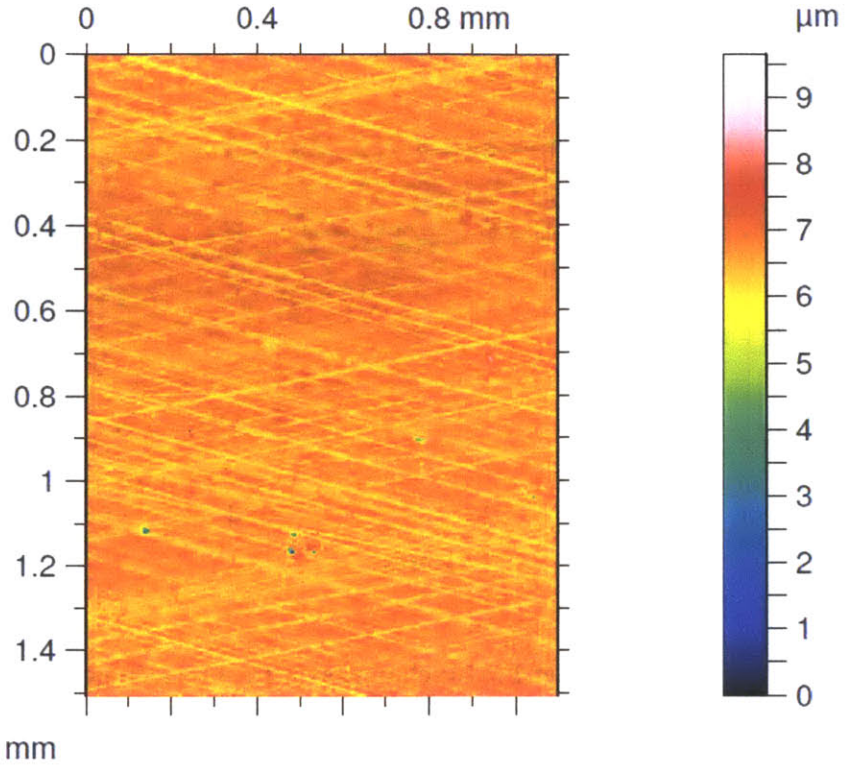

Figure 78: GG09 liner surface

Table 8: Surface roughness information of GG09 liner

	Rvk	**Rk**	**Rpk**
GG09	0.467	0.561	0.174

The break-in period lasted for about 5 hours and 11 sets of records were taken at 30-minute intervals. Figure 79 shows the FMEP change over the 5 hours.

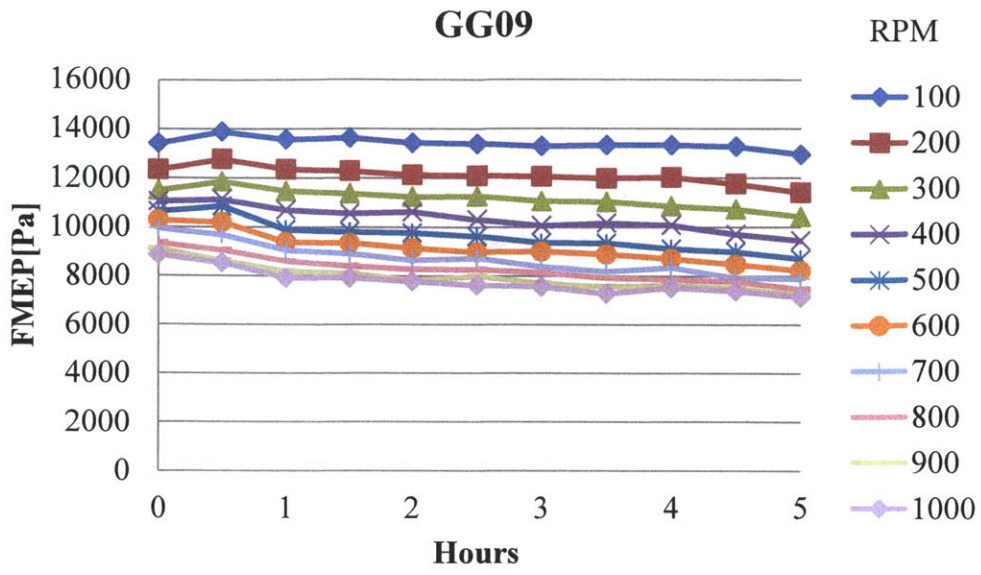

Figure 79: GG09 liner FMEP change over the break-in period

Figure 80 shows the 11 repeats of friction results at 100RPM, 500RPM and 1000RPM.

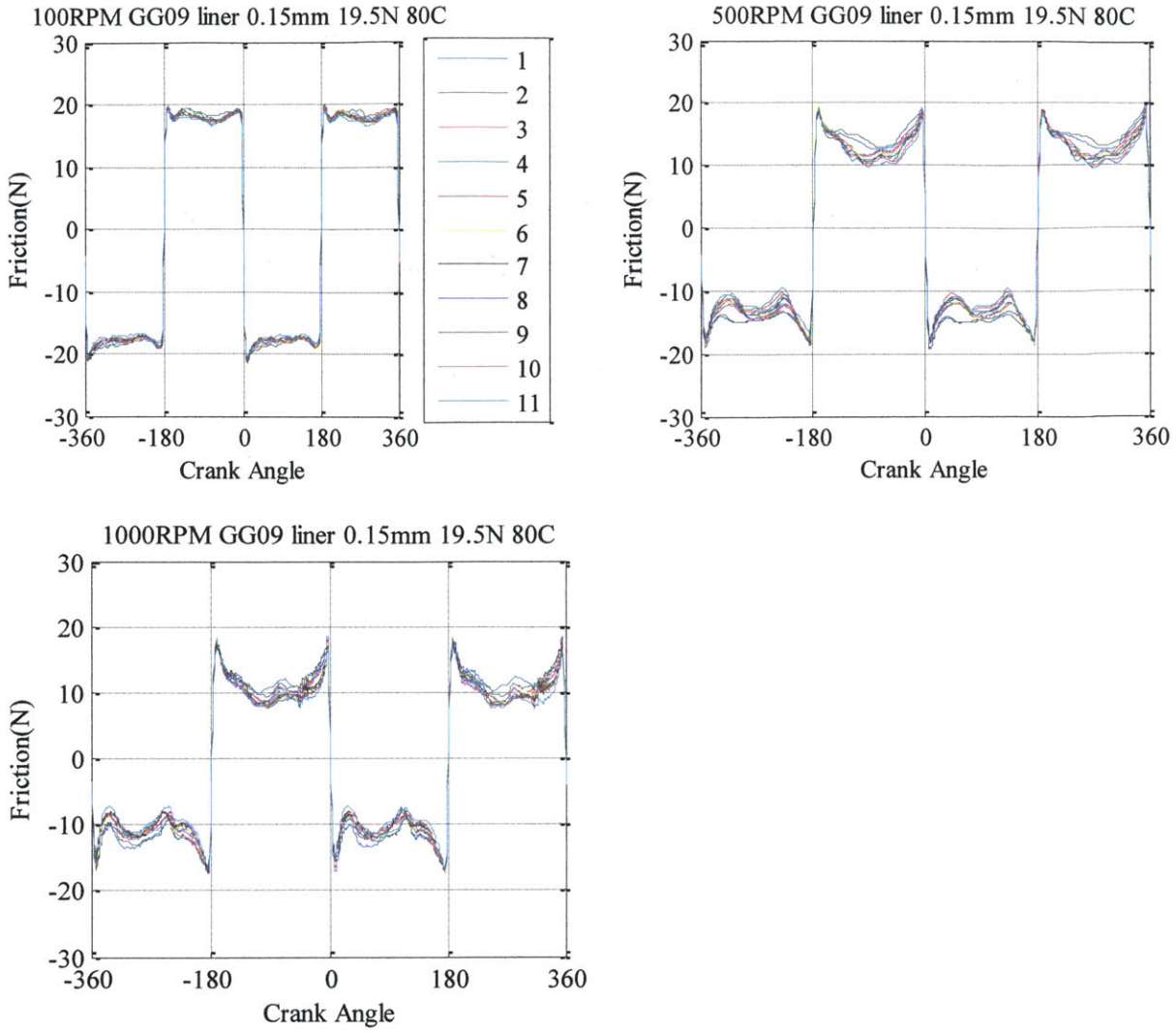

Figure 80: Friction traces of 0.15mm land width 19.5N tension TLOCR on GG09 liner over the break-in period, engine speeds of 100RPM, 500RPM and 1000RPM

At 100RPM, at the current surface roughness level, the low engine speed cannot bring the TLOCR out of the boundary contact-dominated regime. The friction has little change across different parts of the stroke. At higher engine speeds of 500RPM and 1000RPM, the TLOCR friction decreases as the piston speed increases when it travels towards the mid-stroke. A slight friction increase at the mid-stroke indicates the TLOCR has reached the minimum friction coefficient in the mixed lubrication regime.

In addition, at the mid-strokes of the 500RPM and 1000RPM friction traces, the friction decreases as the break-in progresses. The reduced boundary contact reduces the minimum friction that the TLOCR/liner mating pair can achieve. However, at 100RPM, due to the low

engine speed and large surface roughness, boundary contact dominates the entire stroke. As a result, there is little change in the friction through the 5-hour break-in period.

The instantaneous Stribeck curves of the GG09 liner shown in Figure 81 confirm the findings. The friction coefficient obtained from the 100RPM results (left-most points on each of the three graphs, clearly identifiable for 40-45CAD and 90-95CAD results) show little change across the 11 sets of tests. As moving rightwards on the instantaneous Stribeck curves, the ring / liner pair starts to enter the mixed lubrication regime, where the friction coefficient decreases as the break-in progresses.

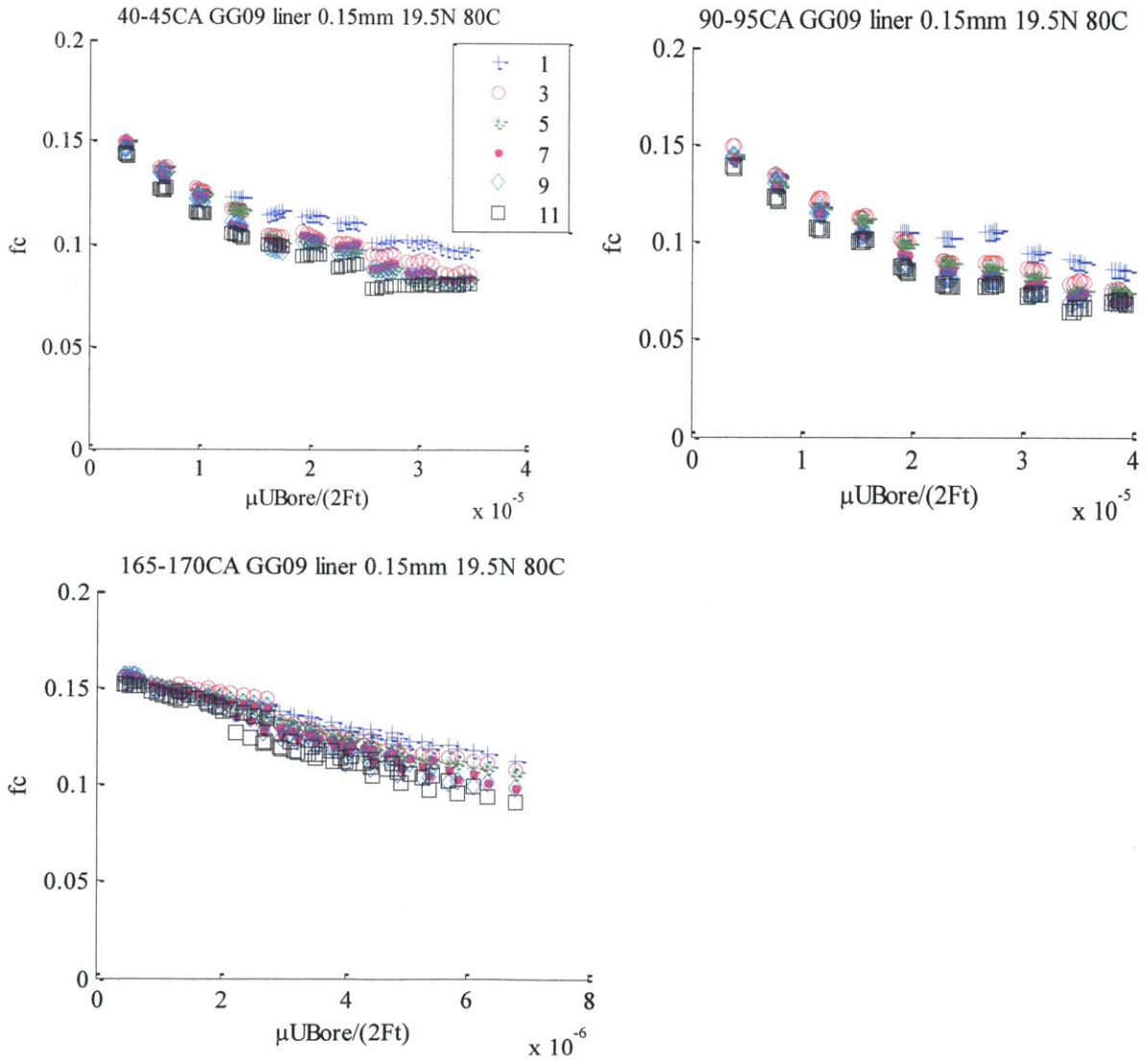

Figure 81: GG09 liner, instantaneous Stribeck curve change over the break-in period, observed at upper part (40-45CAD), mid-stroke region (90-95CAD), and the area close to BDC (165-170CAD)

6.1.5. GG21 Liner

Figure 82 and Table 9 shows the surface roughness information of the GG21 liner, measured before the experiment. The surface roughness of GG21 is the smallest among all the liners tested.

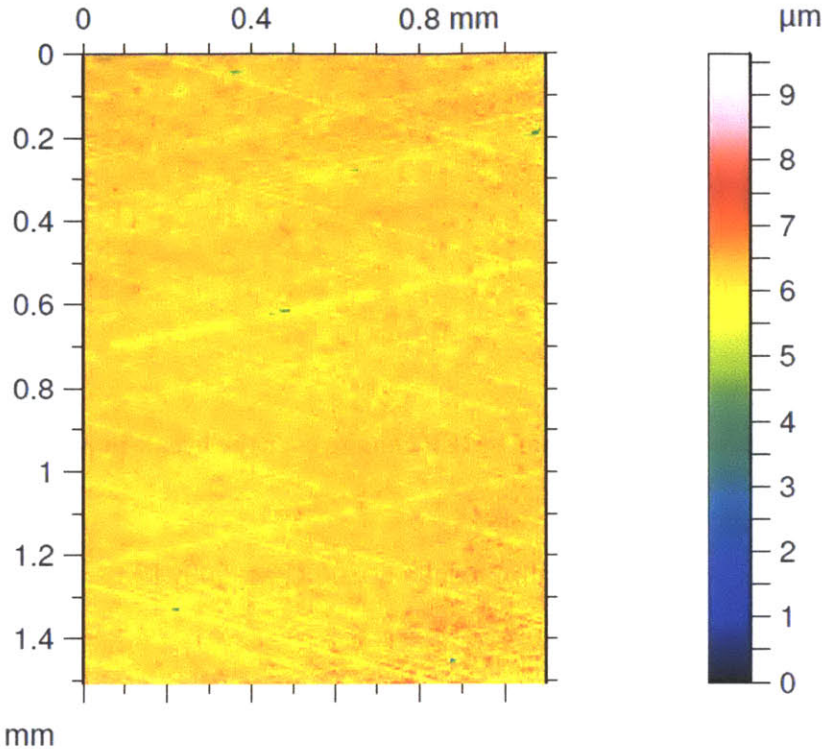

Figure 82: GG21 liner surface

Table 9: Surface roughness information of GG21 liner

	Rvk	Rk	Rpk
GG21	0.262	0.260	0.088

The break-in period lasted for about 5 hours and 11 sets of records were taken at 30-minute intervals. Figure 83 shows the FMEP change over the 5-hour period.

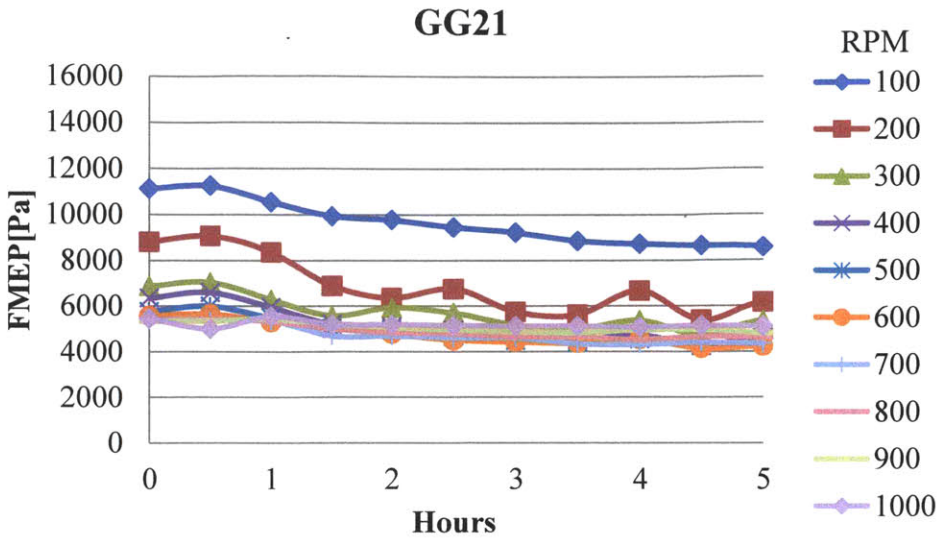

Figure 83: GG21 liner FMEP change over the break-in period

Figure 84 shows the 11 repeats of friction results at 100RPM, 500RPM and 1000RPM.

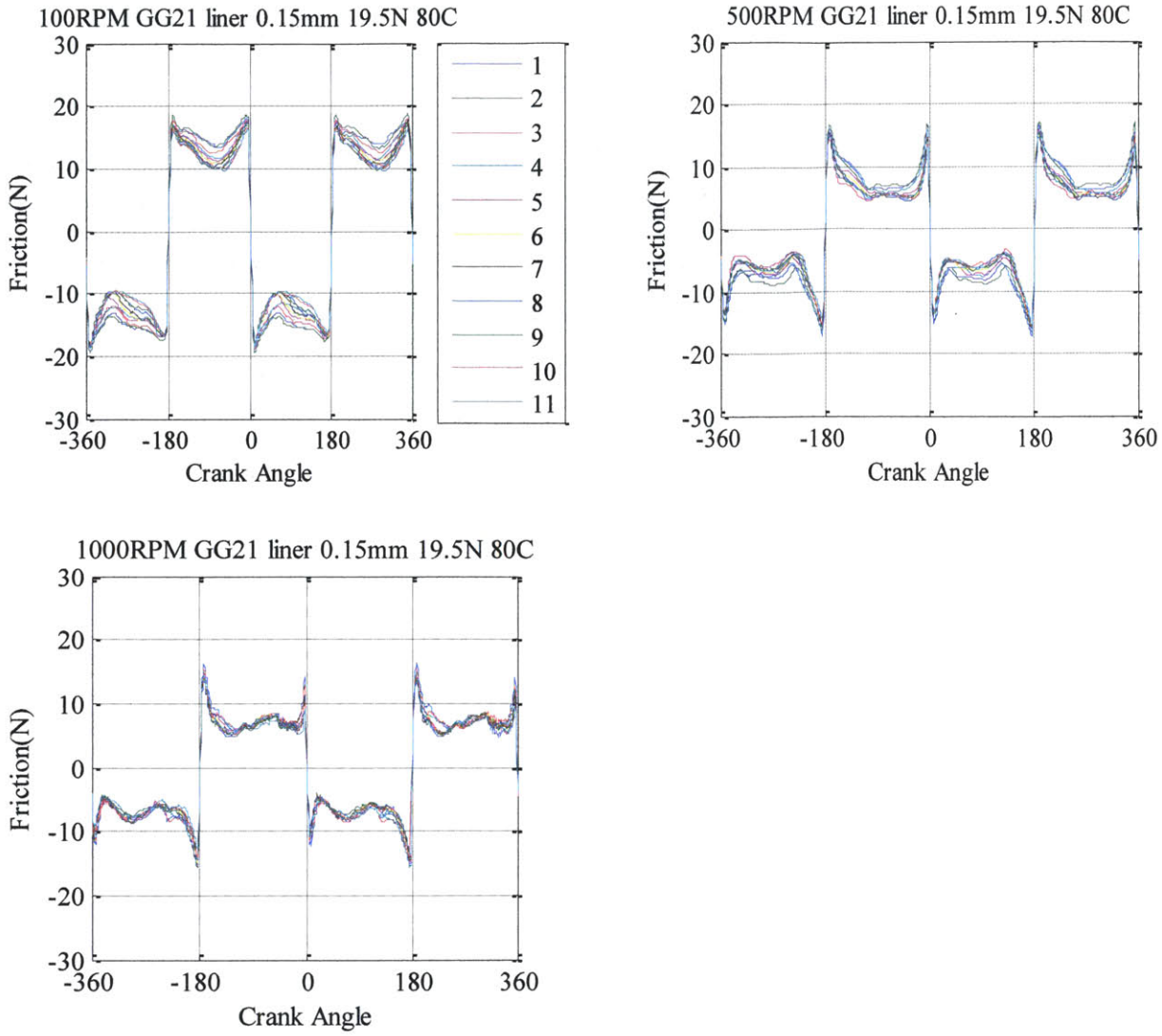

Figure 84: Friction traces of 0.15mm land width 19.5N tension TLOCR on GG21 liner over the break-in period, engine speeds of 100RPM, 500RPM and 1000RPM

For the smoother GG21 liner, the TLOCR leaves the boundary lubrication regime and enters the mixed lubrication regime at a lower engine speed. At 100RPM, the TLOCR friction decreases as it moves towards the mid-stroke. The ring obtains sufficient hydro-pressure support to reduce its boundary contact as piston speed increases. Similar trends are observed in 500RPM and 1000RPM. In addition, the slight friction increase at the mid-strokes at 500RPM and 1000RPM indicates the TLOCR has reached and passed the minimum friction coefficient location at the mixed lubrication regime.

In addition, the friction decrease as the liner break-in progresses is more obvious at the mid-strokes of 100RPM and 500RPM. In the boundary to mixed lubrication regime, the TLOCR

receives support from both asperity contact and hydro-pressure. The reduced asperity contact due to break-in sheds more support to hydro-pressure and reduces the overall friction.

The instantaneous Stribeck curves in Figure 85 confirm the effects of break-in at different lubrication regimes. The left-most points on the 165-170CAD plot correspond to the TLOCR operating at 100RPM close to BDC, where piston speed is low. Boundary contact always dominates and the friction coefficient has little change over the break-in period. The right-most points on the 40-45CAD and 90-95CAD plots correspond to the TLOCR operating at 1000RPM at the upper part or mid-stroke of the liner, where piston speed is relatively high. Hydrodynamic pressure mainly balances the TLOCR tension and the friction coefficient change over the break-in period is also little.

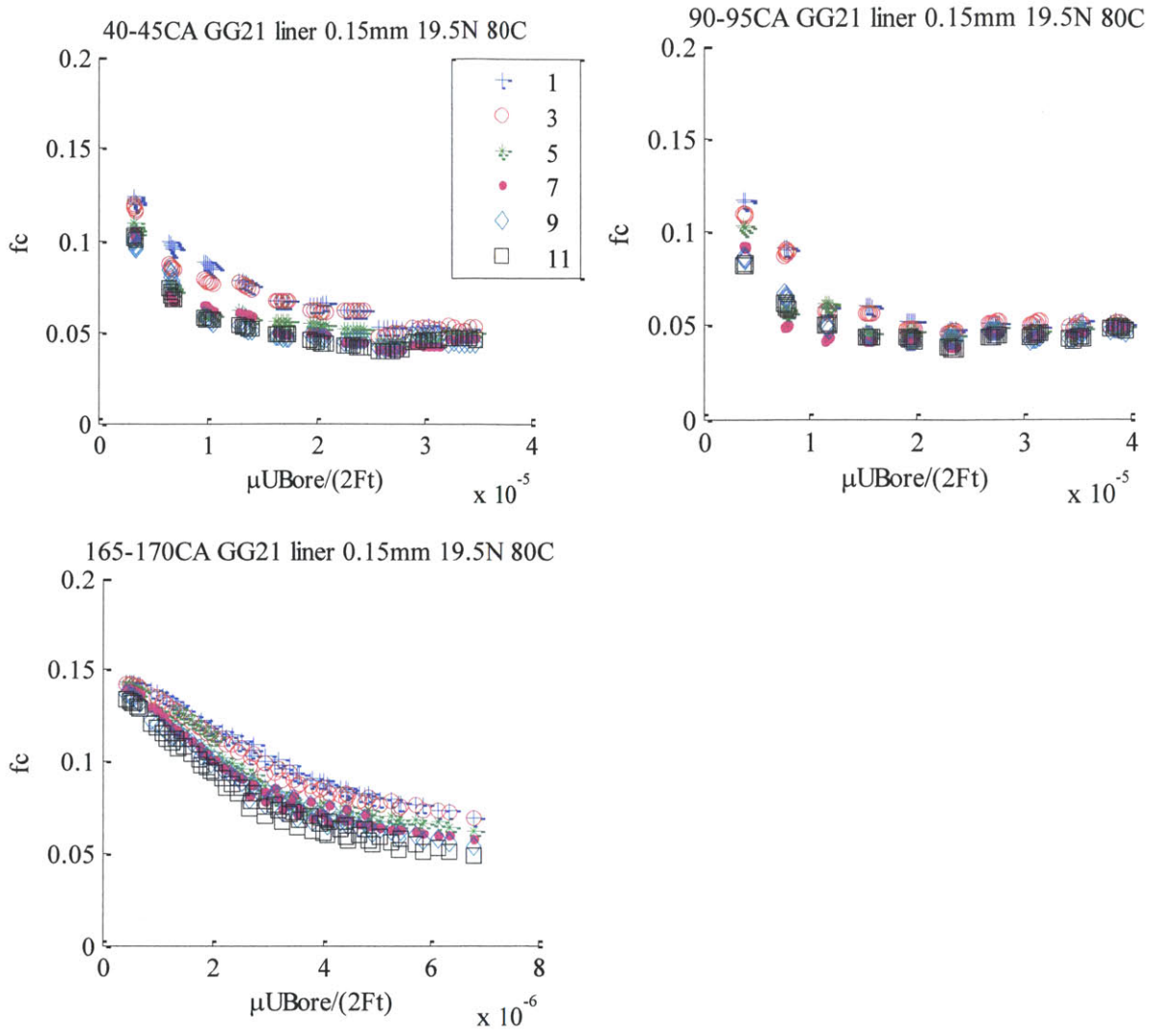

Figure 85: GG21 liner, instantaneous Stribeck curve change over the break-in period, observed at upper part (40-45CAD), mid-stroke region (90-95CAD), and the area close to BDC (165-170CAD)

6.1.6. GG22 Liner

Figure 86 and Table 10 show the surface roughness information of the GG22 liner, measured before the experiment. The surface roughness of GG22 is similar to that of the GG21 and belongs to the smoothest category A1.

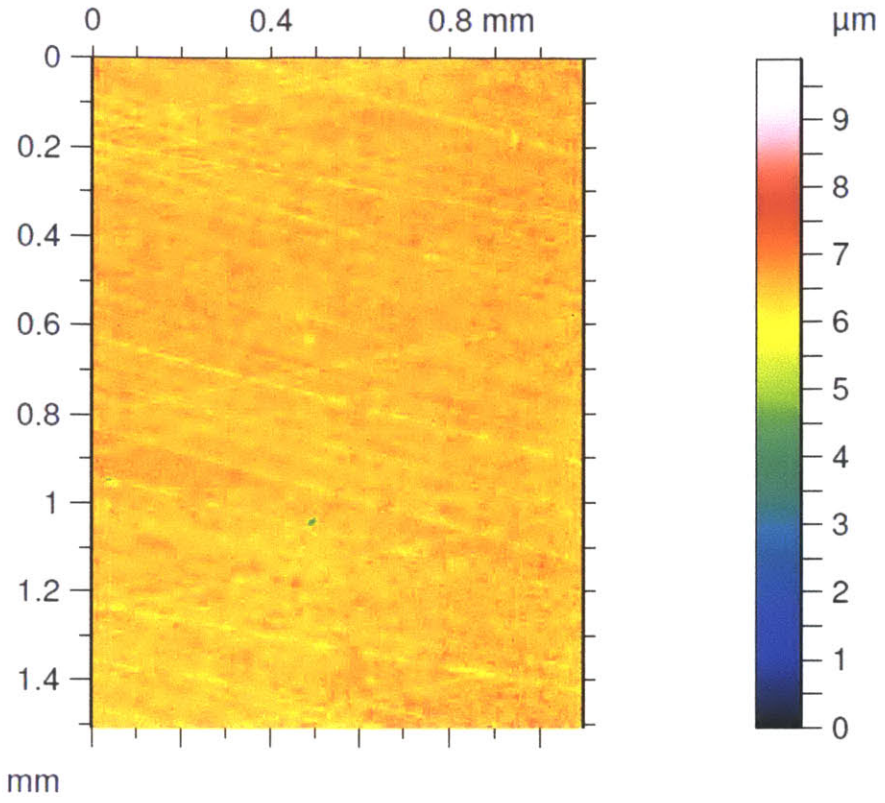

Figure 86: GG22 liner surface

Table 10: Surface roughness information of GG22 liner

	Rvk	**Rk**	**Rpk**
GG22	0.467	0.561	0.174

The break-in period of GG22 liner lasted for about 10 hours before the FMEPs stabilized. Figure 83 shows the FMEP change over the 10-hour period.

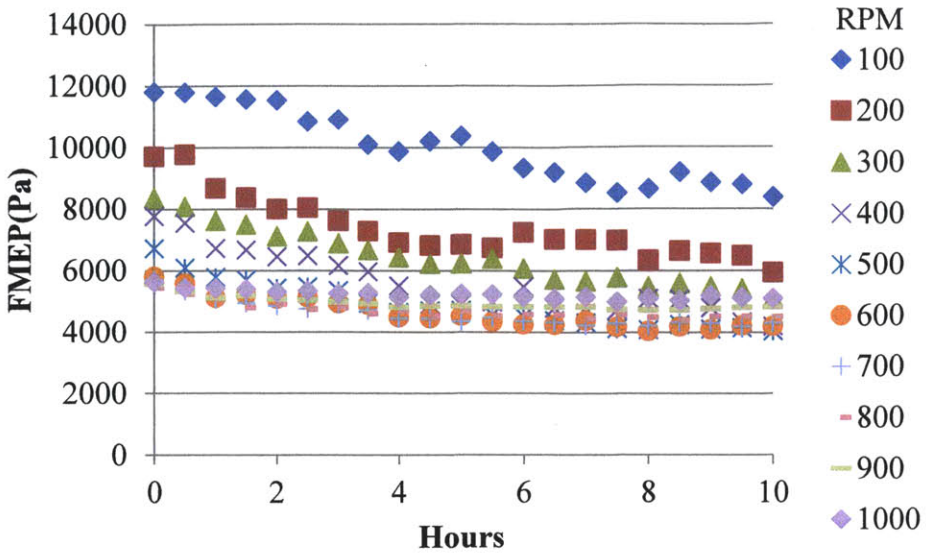

Figure 87: GG22 liner FMEP change over the break-in period

Friction from 100RPM to 1000RPM was recorded every 30 minutes for a total of 21 repeats. Figure 84 shows the 21 repeats of friction results at 100RPM, 500RPM and 1000RPM.

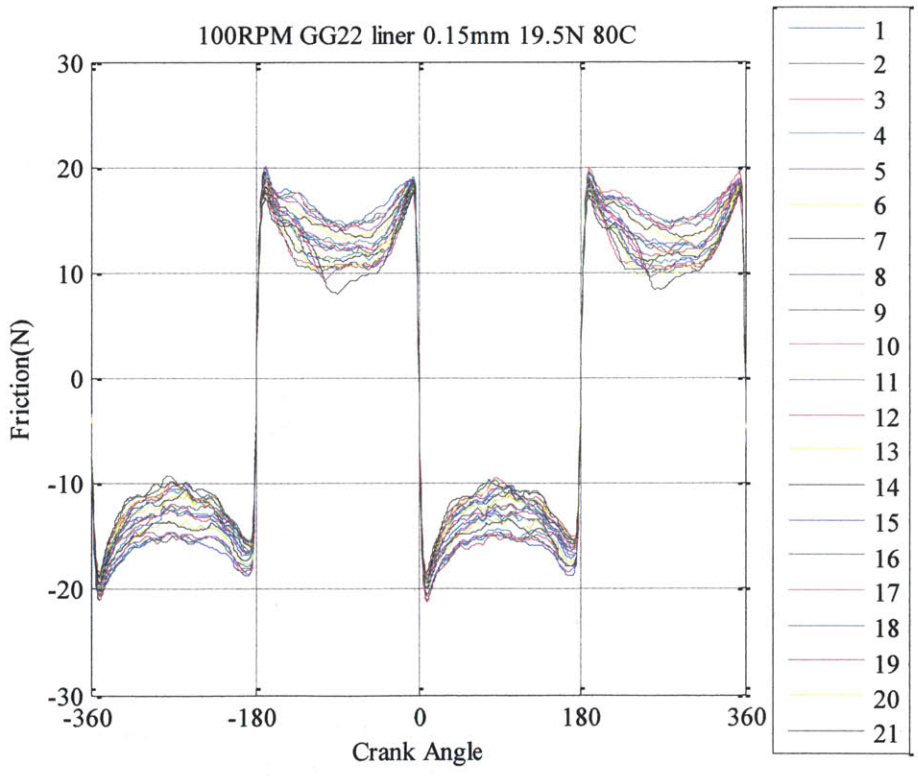

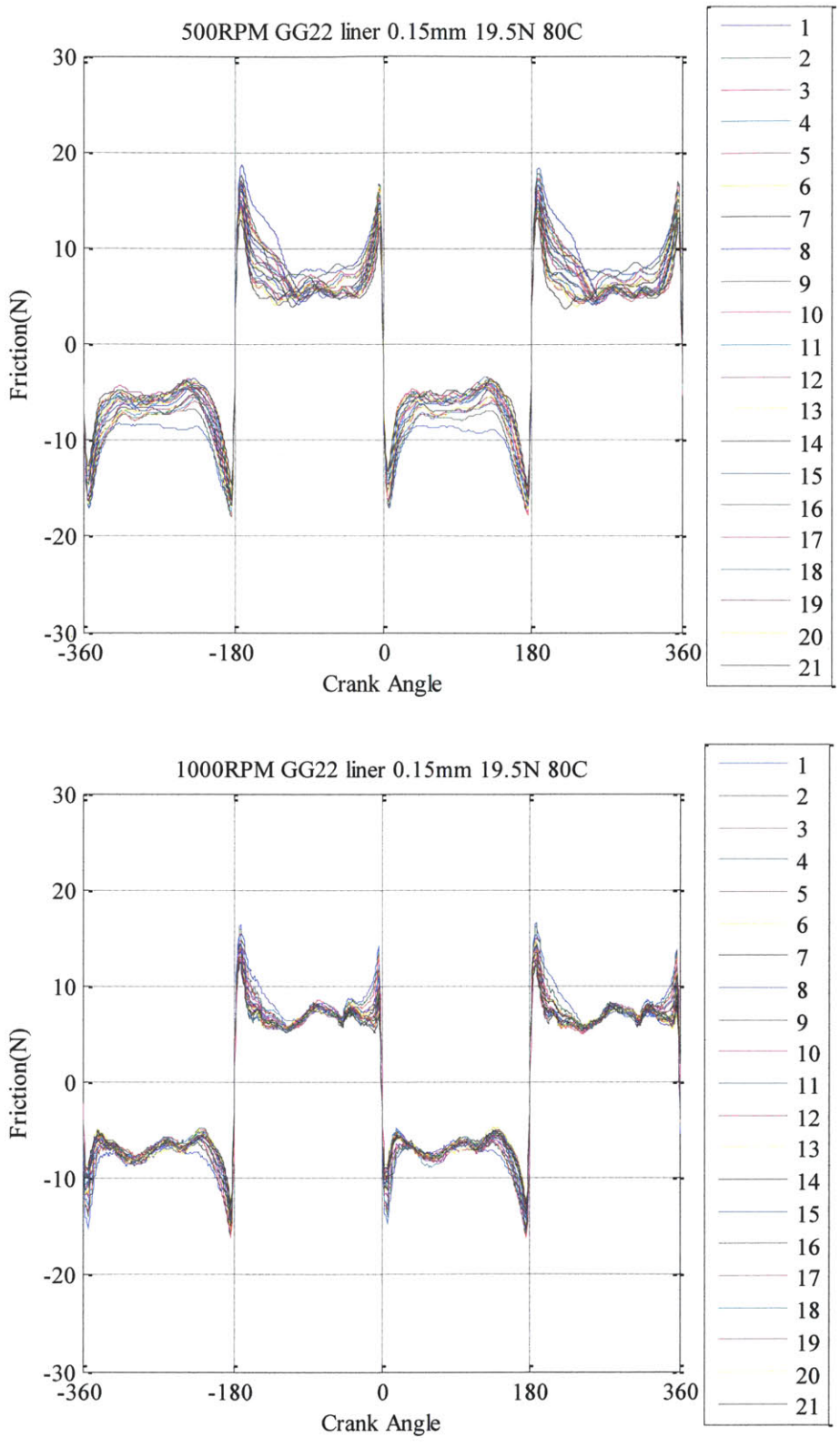

Figure 88: Friction traces of 0.15mm land width 19.5N tension TLOCR on GG22 liner over the break-in period, engine speeds of 100RPM, 500RPM and 1000RPM

Figure 89 indicates that the break-in effects on GG22 liner friction coefficients over different lubrication regimes are similar to that of the GG21 liner. The similar friction behavior from the two similar liners confirms the effects of surface roughness on ring/liner friction.

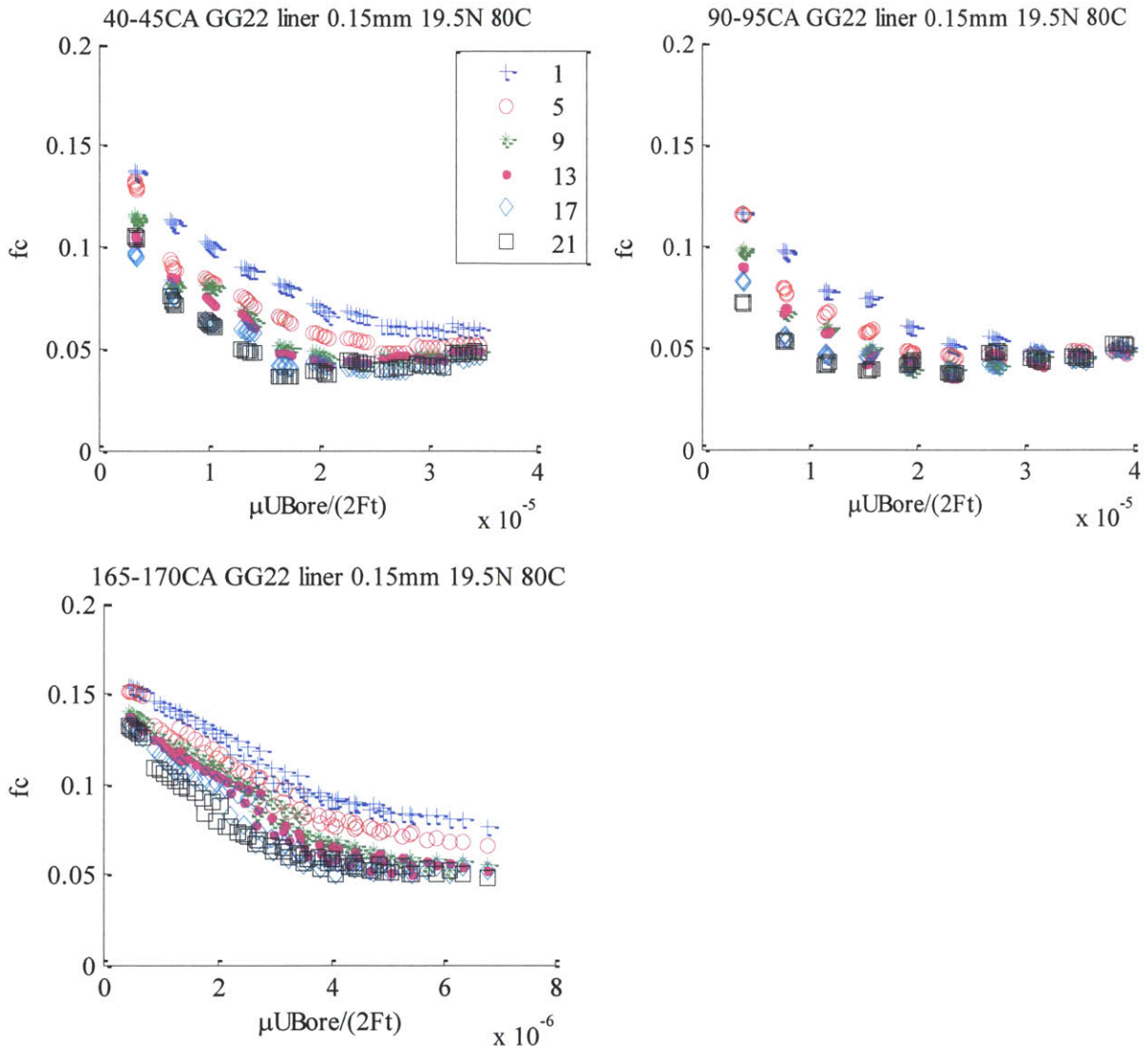

Figure 89: GG22 liner, instantaneous Stribeck curve change over the break-in period, observed at upper part (40-45CAD), mid-stroke region (90-95CAD), and the area close to BDC (165-170CAD)

6.1.7. GG28 Liner

Figure 90 and Table 11 show the surface roughness information of the GG28 liner, measured before the experiment. The GG28 liner has similar Rk and Rpk values with that of the GG21 liner but a larger valley ratio.

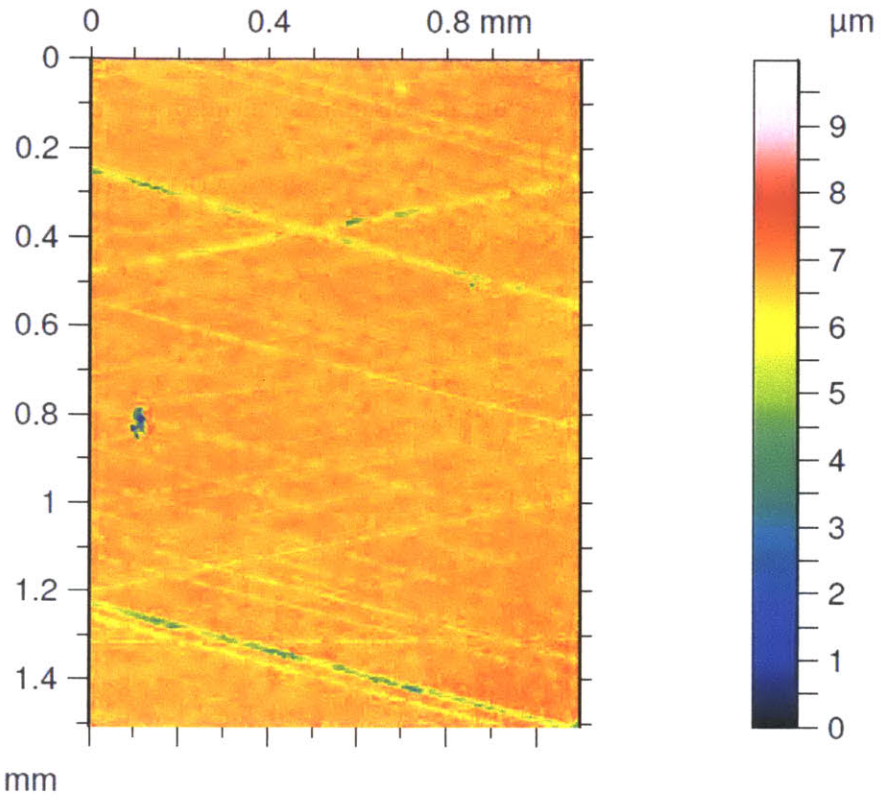

Figure 90: GG28 liner surface

Table 11: Surface roughness information of GG28 liner

	Rvk	**Rk**	**Rpk**
GG28	0.629	0.262	0.092

The break-in period of the GG28 liner lasted for about 5 hours. The FMEPs from 100RPM to 1000RPM were recorded at 30-minute intervals for 11 repeats. Figure 91 shows the FMEP evolution.

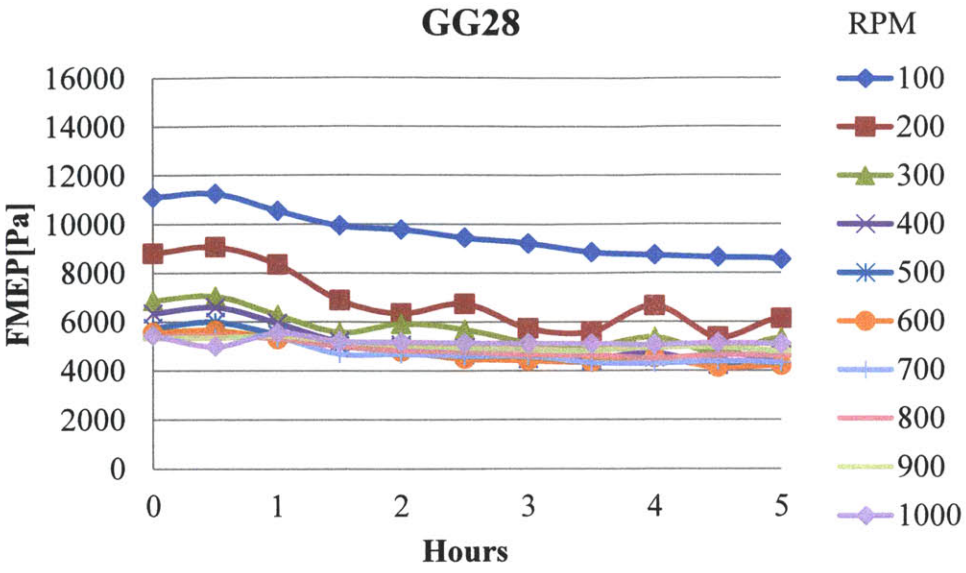

Figure 91: GG28 liner FMEP change over the break-in period

Figure 92 shows the friction traces of each repeat at 100RPM, 500RPM and 1000RPM.

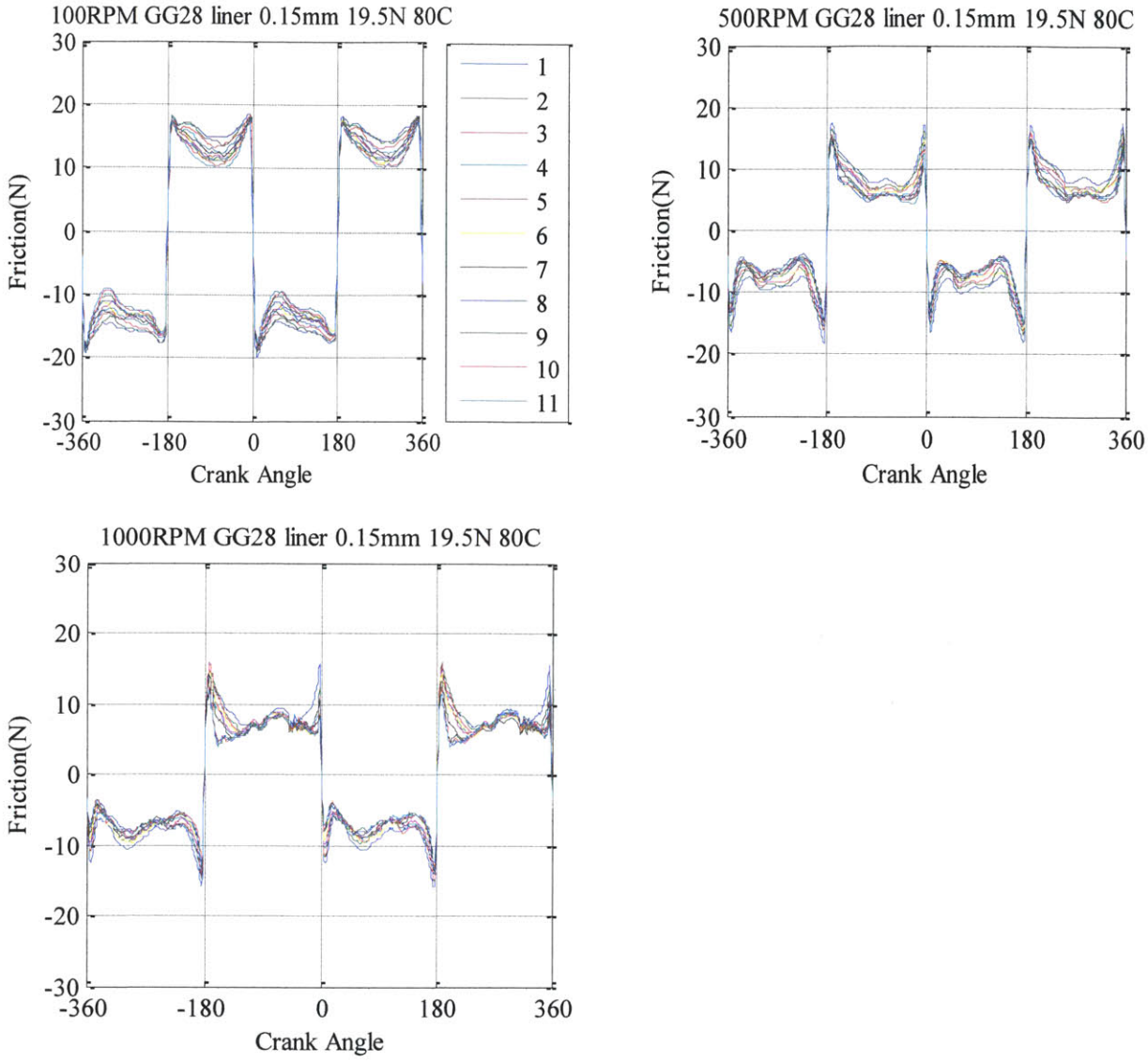

Figure 92: Friction traces of 0.15mm land width 19.5N tension TLOCR on GG28 liner over the break-in period, engine speeds of 100RPM, 500RPM and 1000RPM

When the TLOCR is operating in the mixed lubrication regime, such as at the mid-strokes of 100RPM and 500RPM, the friction reduces as break-in progresses. The friction change is less obvious at the dead centers on the 100RPM plot, where the TLOCR tension is mainly balanced by asperity contact. At the mid-strokes of 1000RPM, when hydrodynamic lubrication dominates, the reduction of friction over the break-in period is also not as significant.

The instantaneous Stribeck curves shown in Figure 93 confirm the previous findings. In addition, the 90-95CAD curve clearly shows that as break-in progresses, the minimum friction coefficient

reduces, and the minimum friction coefficient location on the instantaneous Stribeck curve moves leftwards.

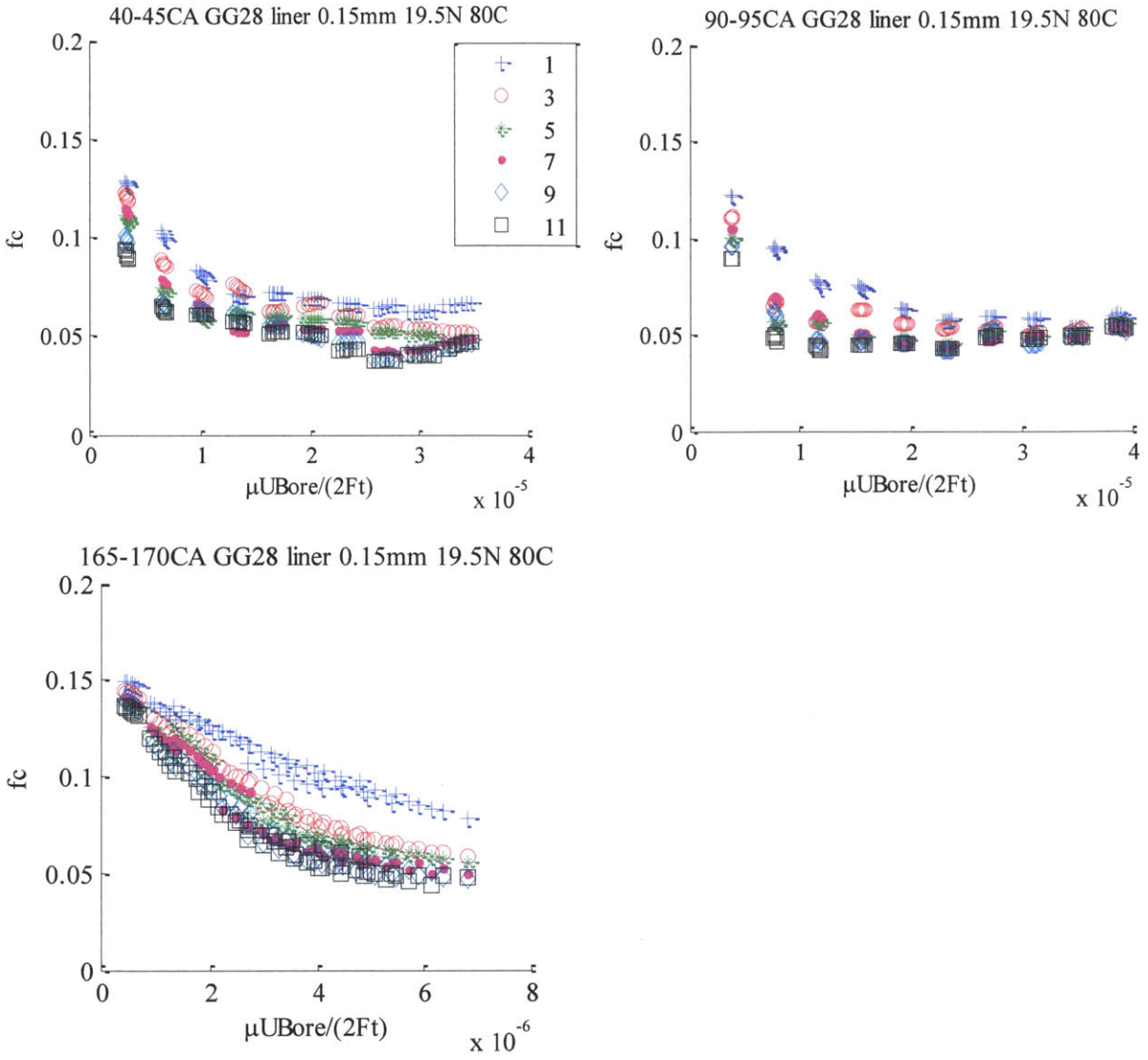

Figure 93: GG28 liner, instantaneous Stribeck curve change over the break-in period, observed at upper part (40-45CAD), mid-stroke region (90-95CAD), and the area close to BDC (165-170CAD)

6.1.8. GG30 Liner

Figure 94 and Table 12 shows the surface roughness information of the GG30 liner, measured before the experiment. The GG30 liner has the largest valley ratio among all the tested liners. The Rk and Rpk values of the GG30 liner are similar to that of the GG21 liner while the GG30 liner has a much larger Rvk.

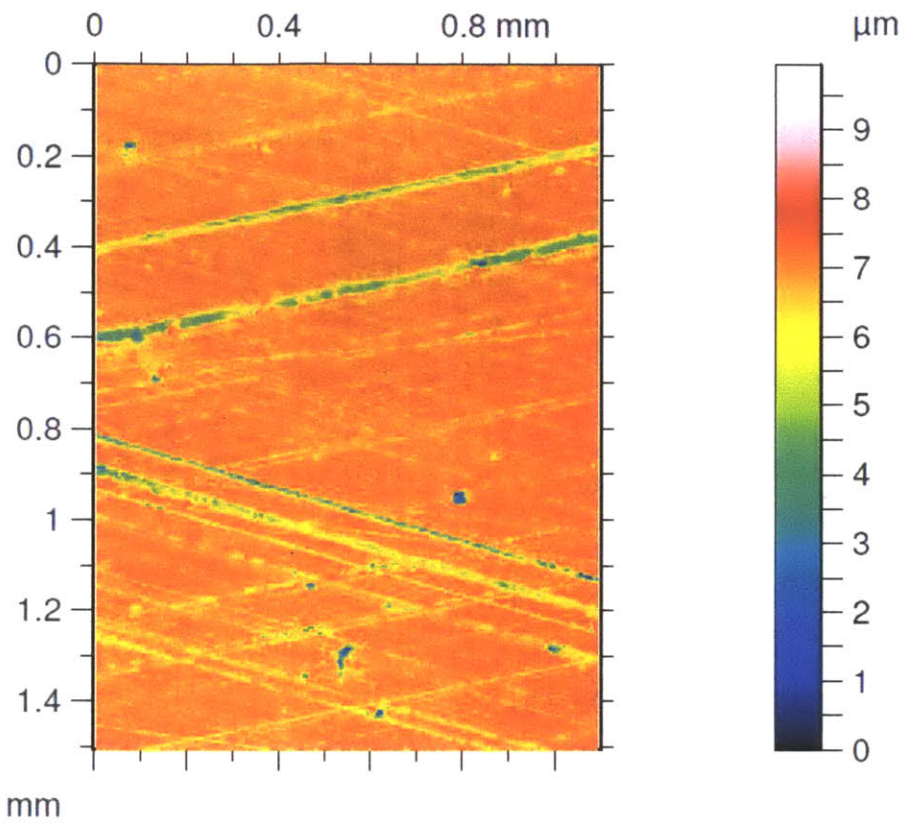

Figure 94: GG30 liner surface

Table 12: Surface roughness information of GG30 liner

	Rvk	**Rk**	**Rpk**
GG30	1.088	0.326	0.100

The break-in period of the GG30 liner lasted for about 5 hours. The friction from 100RPM to 1000RPM was recorded at 30-minute intervals for 11 repeats. Figure 95 shows the FMEP evolution.

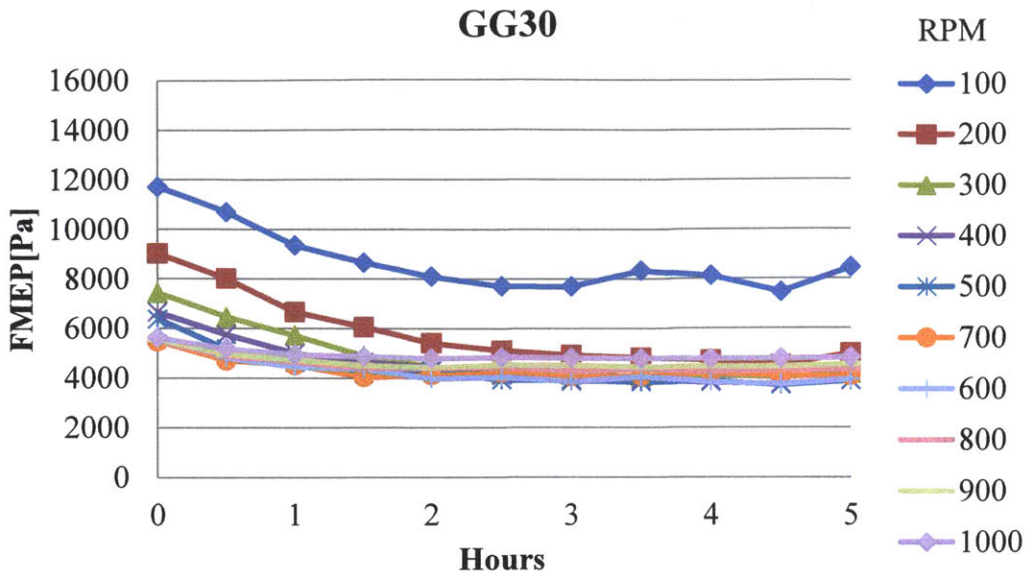

Figure 95: GG30 liner FMEP change over the break-in period

Figure 96 shows the friction traces of each repeat at 100RPM, 500RPM and 1000RPM.

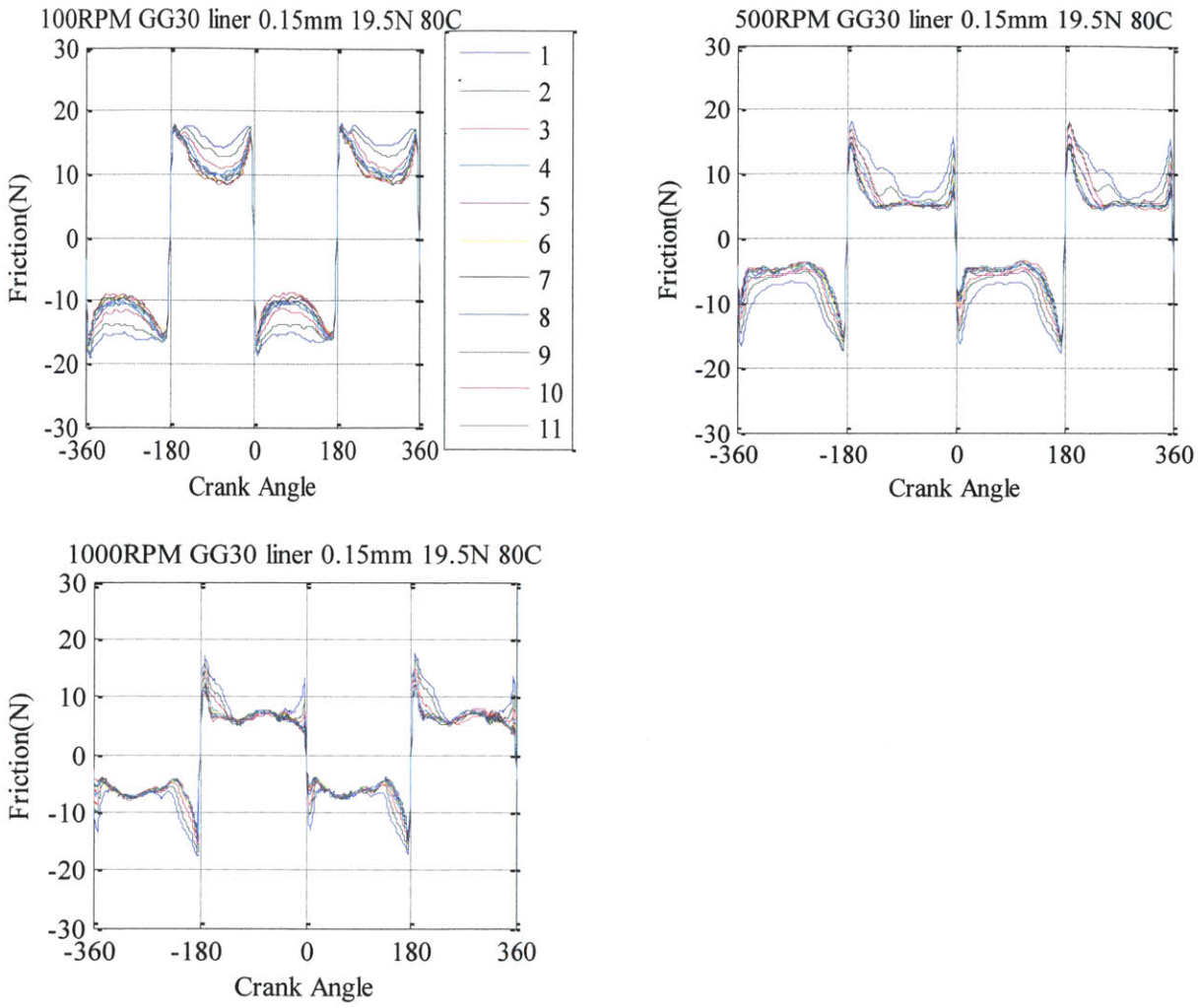

Figure 96: Friction traces of 0.15mm land width 19.5N tension TLOCR on GG30 liner over the break-in period, engine speeds of 100RPM, 500RPM and 1000RPM

Together with the instantaneous Stribeck curves from three liner locations shown in Figure 97, the results of GG30 liner confirm the previous findings: the break-in leads to clear friction reduction in the mixed lubrication regime, while the friction coefficient changes in the boundary contact-dominated and hydrodynamic-dominated lubrication regimes are little.

In addition, the surface change at different locations across the liner also varies. As a result, the instantaneous Stribeck curves obtained using friction results from different locations of the liner can have certain variations.

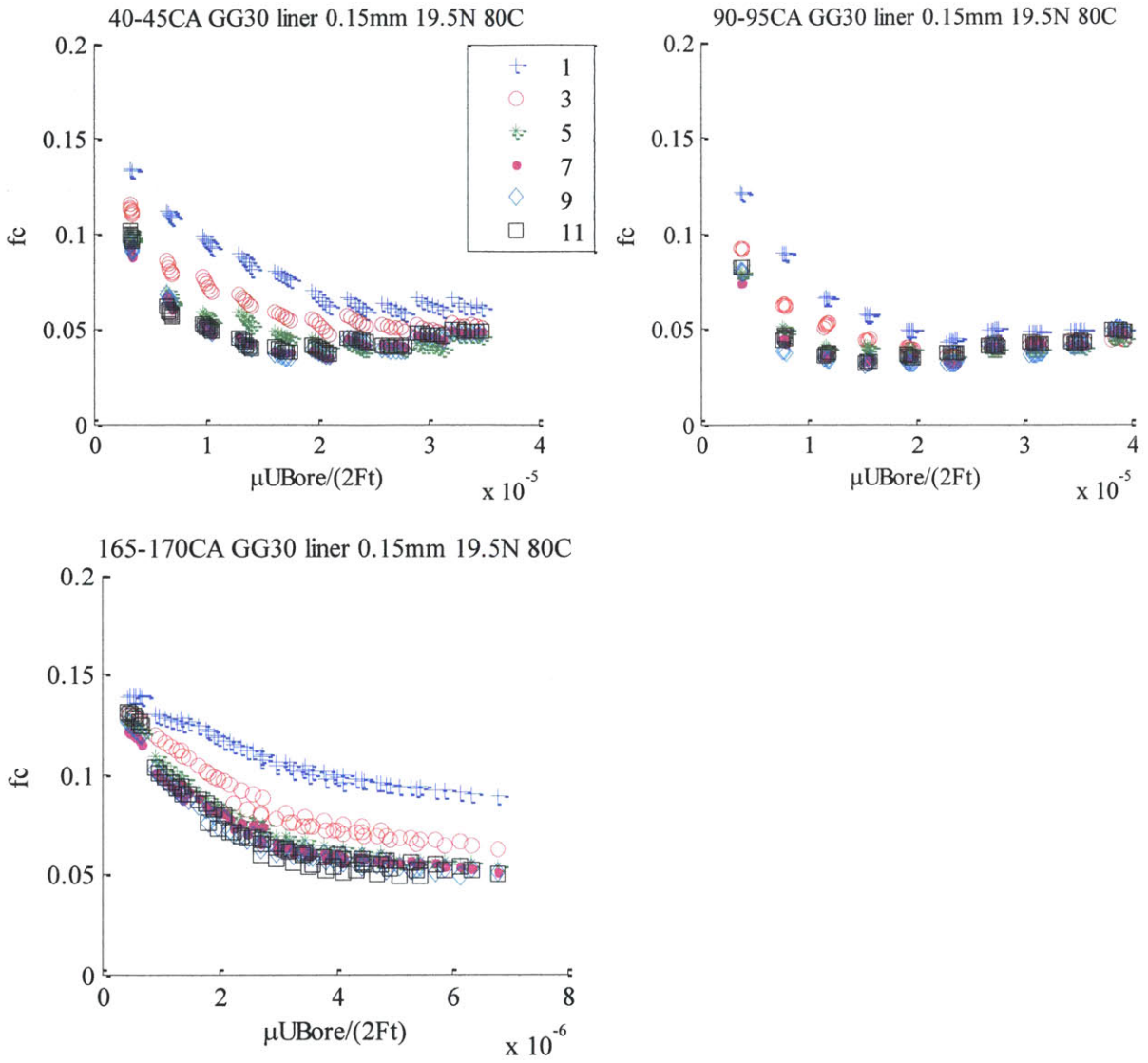

Figure 97: GG30 liner, instantaneous Stribeck curve change over the break-in period, observed at upper part (40-45CAD), mid-stroke region (90-95CAD), and the area close to BDC (165-170CAD)

6.1.9. Conclusion on the Break-in Tests

First, during the liner break-in period, the asperities are removed and the liner surface plateau roughness decreases. As a result, the hydro-pressure becomes effective at a lower engine speed and the minimum friction coefficient location moves leftwards on the instantaneous Stribeck curve. In addition, the value of the minimum friction coefficient also decreases. Such a trend can be clearly observed from a closer look at the minimum friction coefficient region on the instantaneous Stribeck curve shown in Figure 98. The GG21 liner friction results from 90-

91CAD and 135-136CAD, and 100RPM to 1000RPM are used to plot the instantaneous Stribeck curves. From the 1st repeat to the 11th repeat of the test, results from every 2 repeats of the tests are shown. It represents the instantaneous Stribeck curve change over the break-in period. Both curves see the minimum friction coefficient over the break-in period move leftward and downward.

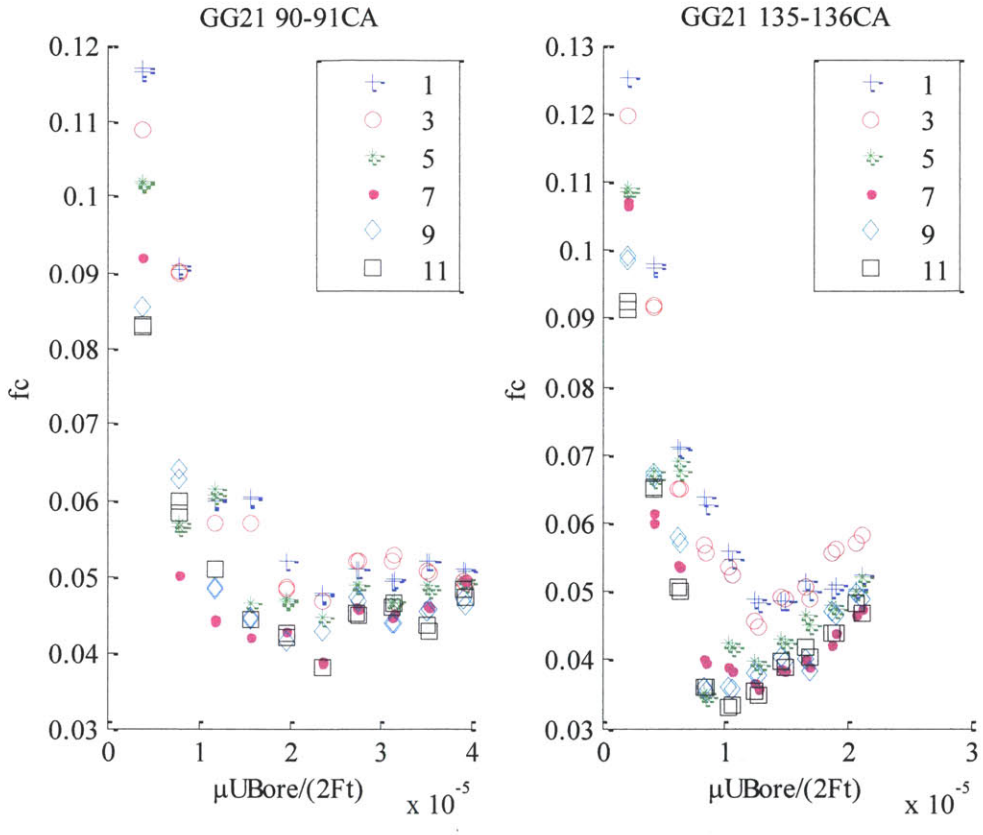

Figure 98: GG21, 90-91CAD and 135-136CAD instantaneous Stribeck curve change over the break-in period

Second, the reduction of friction is more obvious in the mixed lubrication regime while less obvious in the boundary contact or hydrodynamic lubrication-dominated lubrication regime. The instantaneous Stribeck curves shown in Figure 99 confirm the point. Figure 99 uses GG28 liner data from 75CA to 170CA, 1st, 3rd, 5th, 7th, 9th and 11th test. It starts from a boundary contact-dominated lubrication regime to a region that has passed the minimum friction coefficient point and where hydrodynamic lubrication starts gaining importance.

The boundary contact friction coefficient reflects the material property and should not change over the break-in period. The hydrodynamic lubrication friction coefficient reflects the hydro-pressure generation ability of the large liner structure. Over the break-in period, only individual asperities are removed. The large liner structure is preserved.

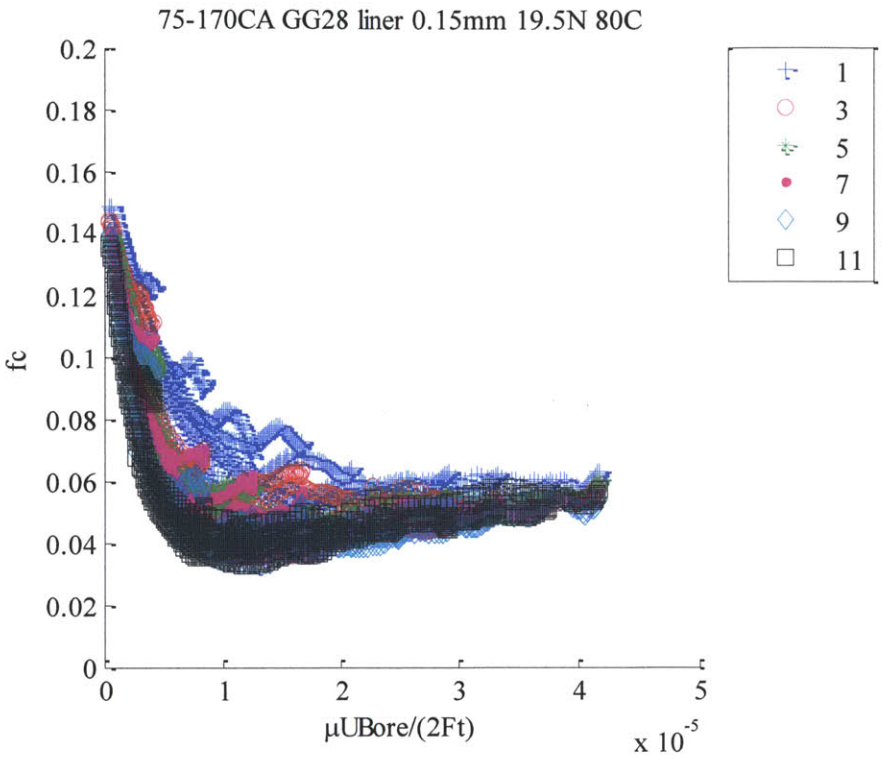

Figure 99: GG30 liner, instantaneous Stribeck curve change over the break-in period, using data from 75CAD to 170CAD

Third, the surface change at different locations of the liner varies. As a result, the instantaneous Stribeck curves calculated using friction data from different parts of the liner can be different.

6.1.10. Modeling the Break-in Period

From the experiment, during the break-in period, ring friction at mixed lubrication regime decreases while at hydrodynamic lubrication regime is preserved. Therefore, from the calculation side, the method introduced in Chapter 4 can be used to model the break-in period: keep the same pressure – ring/liner clearance (P-h) correlation while changing the plateau roughness (σ_p) to factor in surface roughness change.

A calculation sample is provided in Figure 100 using the break-in data of the GG21 liner. The calculation parameters are the same as that of the experiment. Calculation results of all crank angles from 100RPM to 1000RPM were used to generate the instantaneous Stribeck curves. Experimental results from 75-170CAD below TDC from 100RPM to 1000RPM were used to generate the instantaneous Stribeck curves.

From the calculation side, the P-h correlation was obtained from the surface measurement after the break-in period. The instantaneous Stribeck curve calculated from the original measurement is labeled 'CAL 1 SigmaP.' Since the plateau roughness reduces over the break-in period, σ_p was manually increased to 1.2 times the original value to represent the plateau roughness before break-in. The resulting instantaneous Stribeck curve is labeled 'CAL 1.2 SigmaP'. In addition, the instantaneous Stribeck curve obtained from the 1st set of tests and the 11th set of tests are also shown and labeled 'EXP 1st test' and 'EXP 11th test', respectively. The piston friction was subtracted before calculating the instantaneous Stribeck curve.

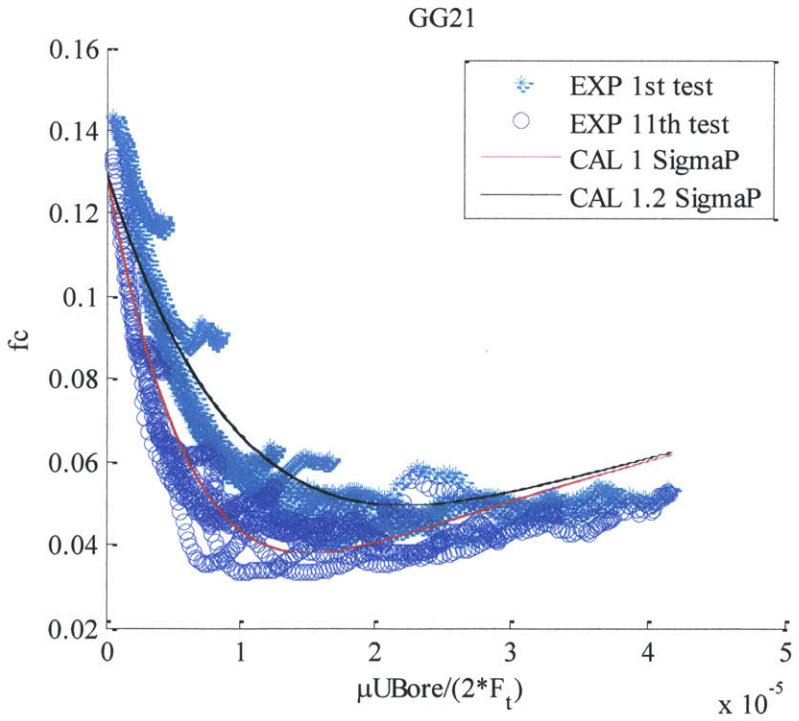

Figure 100: Model consideration of the break-in period, GG21, 19.5N tension 0.15mm land width TLOCR, 80°C, HTHS 1.4 oil

The comparison between the experimental and calculation results shown in Figure 100 indicates that the break-in period can be properly simulated by keeping the same P-h correlation and modifying σ_p in the deterministic TLOCR model.

6.2. Effects of Different Surface Finish on Friction

6.2.1. GG07, GG09, GG21 Liner with HTHS 1.4 Oil

Among the tested cylinder liners, GG07, GG09 and GG21 cover a large range of surface roughness. The three liners have similar valley ratios while GG07 is the roughest one and GG21 is the smoothest one. The friction results of the 0.15mm land width 10.5N tension TLOCR on the three liners were used for the study. The HTHS 1.4 thin oil was used and the measurements were taken after the initial break-in. Table 13 shows the initial surface roughness comparison of the three liners.

Table 13: Comparison of GG07, GG09 and GG21 surface roughness

	Rvk	Rk	Rpk
GG07	0.990	1.184	0.362
GG09	0.467	0.561	0.174
GG21	0.262	0.260	0.088

Figure 101 shows the FMEP results from the GG07, GG09 and GG21 liners at 40°C. It demonstrates that at lower engine speeds, when boundary lubrication dominates, a smoother surface leads to a lower cycle FMEP. However, as the engine speed increases, hydro-pressure accumulates and the benefit of a smoother liner becomes minimal. Overall, the minimum FMEP is lower on the smoother liners. In addition, the TLOCR enters the hydrodynamic lubrication regime at a lower engine speed on smoother liners.

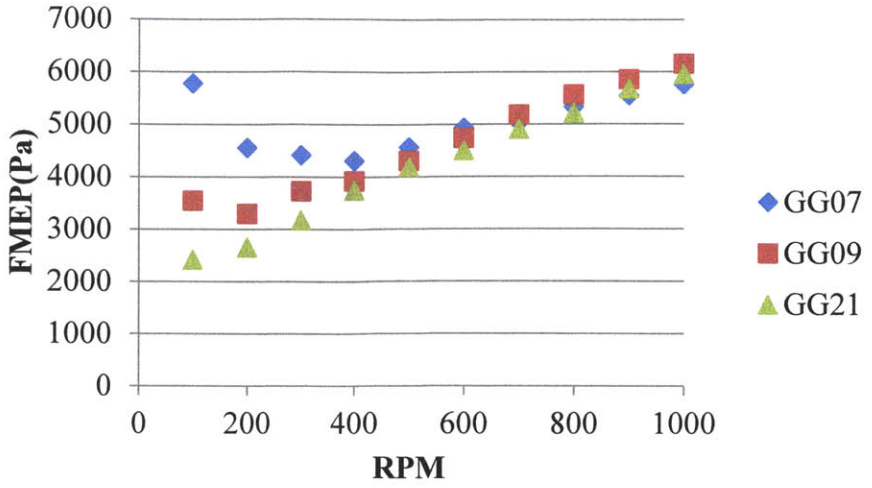

Figure 101: FMEP of 0.15mm land width 10.5N tension TLOCR on GG07, GG09 and GG21 liner at 40°C

Figure 102 shows the friction trace comparisons of the TLOCR on the GG07 and GG21 liner at 100RPM, 500RPM and 1000RPM. The TLOCR has much lower friction on the GG21 liner across the stroke at 100RPM when boundary contact is dominating. At 1000RPM, at the mid-stroke where the high piston speed moves the TLOCR into a hydrodynamic lubrication regime, the smoother GG21 liner results in higher friction than that of the GG07 liner.

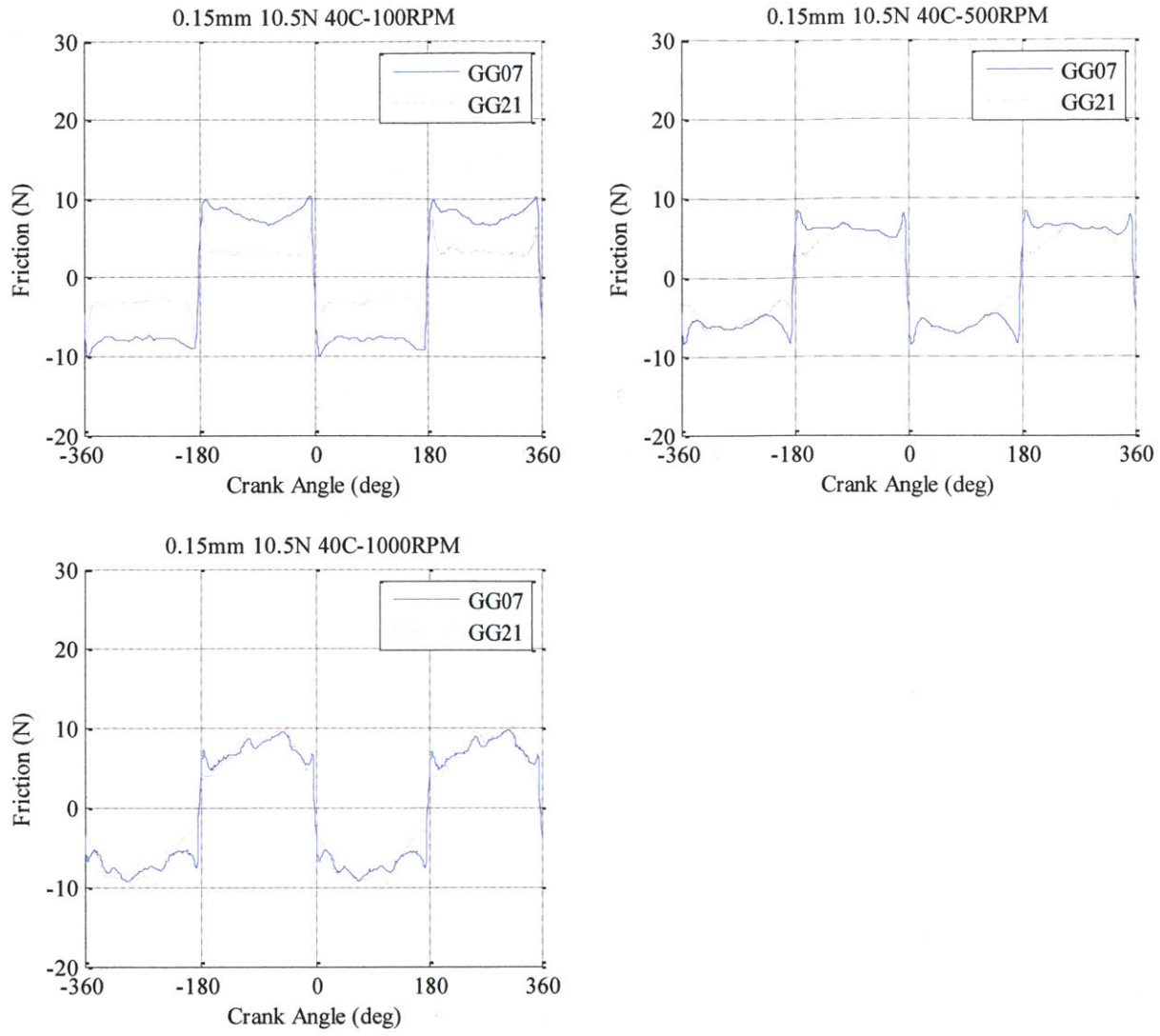

Figure 102: Friction traces comparison of 0.15mm land width 10.5N tension TLOCR on GG07 and GG21 liner, with HTHS 1.4 oil

6.2.2. GG08, GG22 Liner with HTHS 2.9 Oil

In the previous section, since the thin HTHS 1.4 oil was used in the experiments, the TLOCR was not operating well into the hydrodynamic lubrication regime at the lowest temperate 40°C and the highest engine speed of 1000RPM. To further demonstrate the effects of surface roughness in hydrodynamic lubrication regime, another set of experimental results using the thicker HTHS 2.9 oil are compared.

In the experiments, the GG08 liner and the GG22 liner were used. The GG08 liner is a rougher liner that is in the same category with the GG07 liner; the GG22 liner is a smoother liner that is

in the same category with the GG21 liner. The surface roughness information of the GG08 liner and the GG22 liner is provided in Table 14.

Table 14: Comparison of GG08 and GG22 surface roughness

	Rvk	Rk	Rpk
GG08	0.963	1.264	0.436
GG22	0.314	0.278	0.093

The 0.15mm land width 19.5N tension TLOCR was used for motoring tests. To observe the liner roughness effects in the hydrodynamic lubrication regime, the liner temperature was controlled to be at 40°C. Figure 103 shows the FMEPs of the GG08 liner and the GG22 liner.

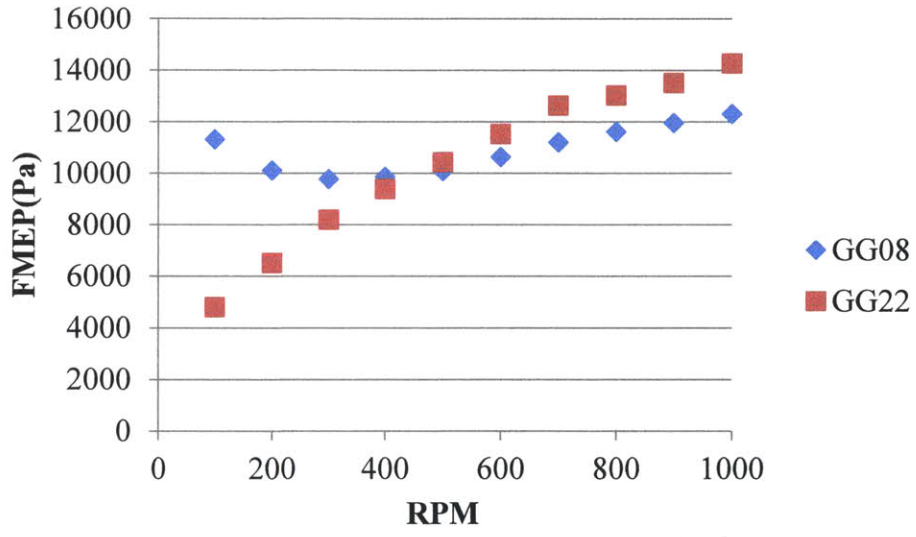

Figure 103: FMEP of 0.15mm land width 19.5N tension TLOCR on GG08, GG22 liner at 40°C

At lower engine speeds, the smoother GG22 liner results in lower TLOCR FMEPs than the rougher GG08 liner. But at 1000RPM when hydrodynamic lubrication is dominating, the TLOCR FMEPs of the GG22 liner is clearly higher than that of the GG08 liner. Once into the hydrodynamic lubrication regime, the FMEP increase slope of the GG22 liner is steeper than that of the GG08 liner, causing the FMEP overtaking trend from 100RPM to 1000RPM.

Figure 104 shows the friction trace comparisons of the GG08 liner and the GG22 liner at 100RPM, 500RPM and 1000RPM. The benefit of a smoother liner at the 100RPM is clear. However, at higher engine speeds of 500RPM and 1000RPM, the relationship reverses: although

the smoother GG22 liner still has lower friction near the TDC and BDC, at the mid-stroke where the hydrodynamic lubrication dominates, the smoother liner results in higher shear stress. As the cycle FMEP is more affected by the mid-stroke friction, the overall FMEPs of the smoother liners are higher at higher engine speeds.

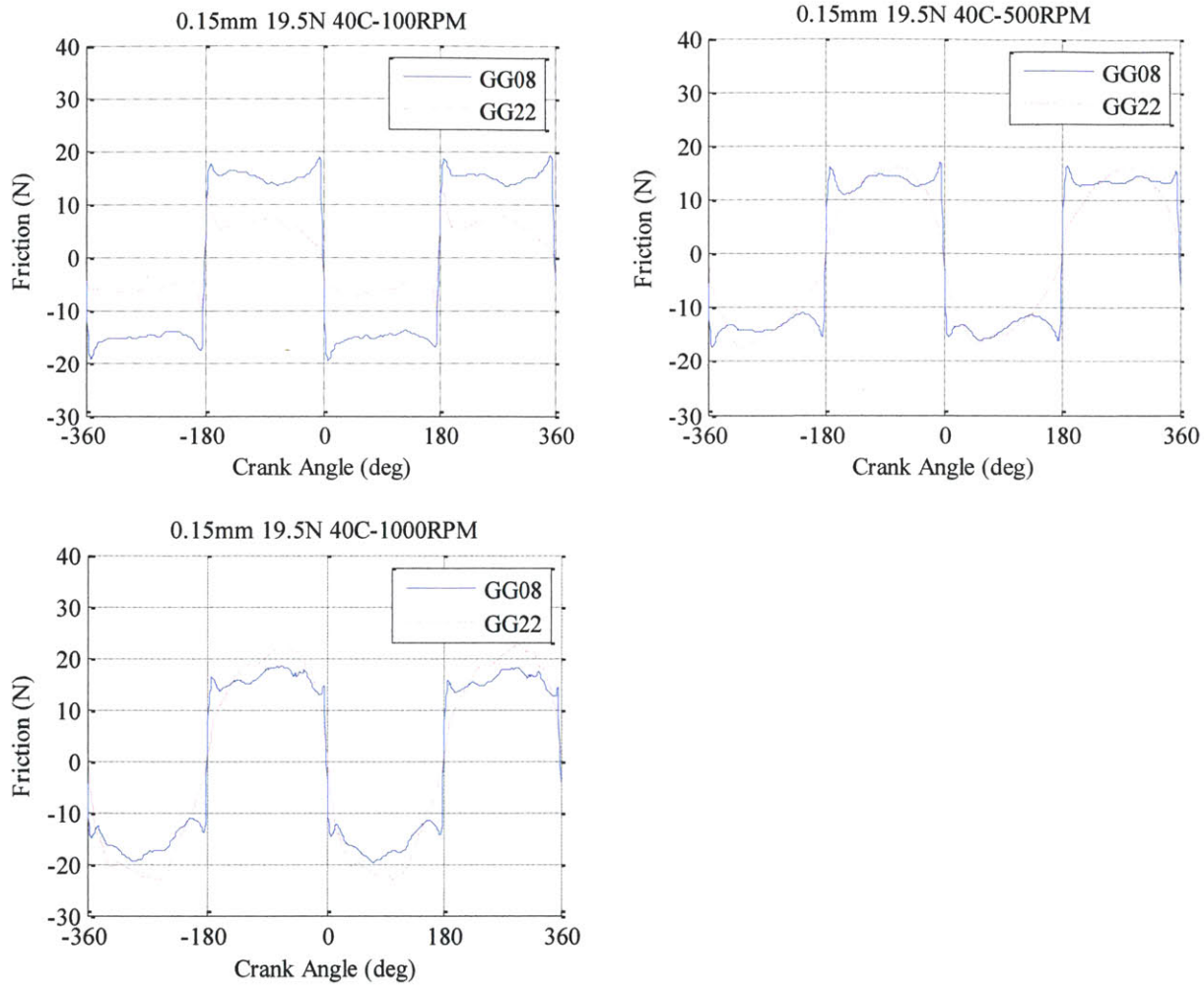

Figure 104: Friction traces comparison of 0.15mm land width 19.5N tension TLOCR on GG08 and GG22 liner, with HTHS 2.9 oil

6.2.3. Conclusion on Surface Finish Effect on Friction

All other factors being the same, a smoother liner can result in lower friction in boundary to mixed lubrication regime. However, in the hydrodynamic lubrication regime, a well-designed rougher liner usually facilitates hydro-pressure build-up, resulting in a higher oil film thickness and lower friction. In addition, the minimum friction coefficient is smaller for smoother liners.

The smoother liners also reach the minimum friction coefficient point on the instantaneous Stribeck curve at a lower engine speed.

7. TLOCR Friction Improvement Case Study

For the friction optimization of the TLOCR, the major constraint is the minimum oil film thickness (MOFT) between the ring and the liner. MOFT is a good representation of the oil that can pass the TLOCR. Once passes the TLOCR, the oil can potentially transport upwards towards the combustion chamber and burn. Keeping the same oil control capability, changing other parameters to reach a minimum TLOCR friction is the target.

In the study, a baseline case was set up based on the current industry ring/liner system design norm. From the knowledge developed in this work and the available parts, the ring land width, ring tension and liner surface finish were changed to reach an improved design. Both experimental and calculation results were used for the study.

The baseline case used a large structure plateau honing liner. The ring land width was 0.15mm and the ring tension was 19.5N. The experimental and calculation results in the previous chapters show: 1) a smoother liner tends to result in a smaller oil film thickness; 2) with the same ring tension, a smaller ring land width leads to a lower ring friction in the hydrodynamic lubrication regime; and 3) a lower ring tension results in lower friction and a higher oil film thickness. As a result, for the improved design case, a smoother liner, GG21, a smaller land width, 0.06mm and a lower ring tension, 10.5N were selected. For both cases, the HTHS 2.9 oil was used.

Table 15 and Table 16 show the summary of the ring and liner selection for the baseline and the improved case.

Table 15: TLOCR selection for baseline and the improved case

	TLOCR land width	TLOCR tension
Baseline	0.15mm	19.5N
Improved case	0.06mm	10.5N

Table 16: Liner characteristics for the baseline and improved case

	Baseline liner	Improved case liner
Rpk (μm)	0.223	0.075
Rk (μm)	0.264	0.230
Rvk (μm)	1.449	0.261
Mr1(%)	5.595	4.618
Mr2 (%)	73.293	81.875
Ra (μm)	0.341	0.089
Rq(μm)	0.527	0.125

Figure 105 and Figure 106 show the experimental results of the FMEP comparison between the baseline and the improved case at 100°C and 40°C, respectively. Compared to the 100°C results, the FMEP results of 40°C extend further into the hydrodynamic lubrication regime. For both cases, significant improvement of the FMEPs is observed by changing from the baseline to the improved case.

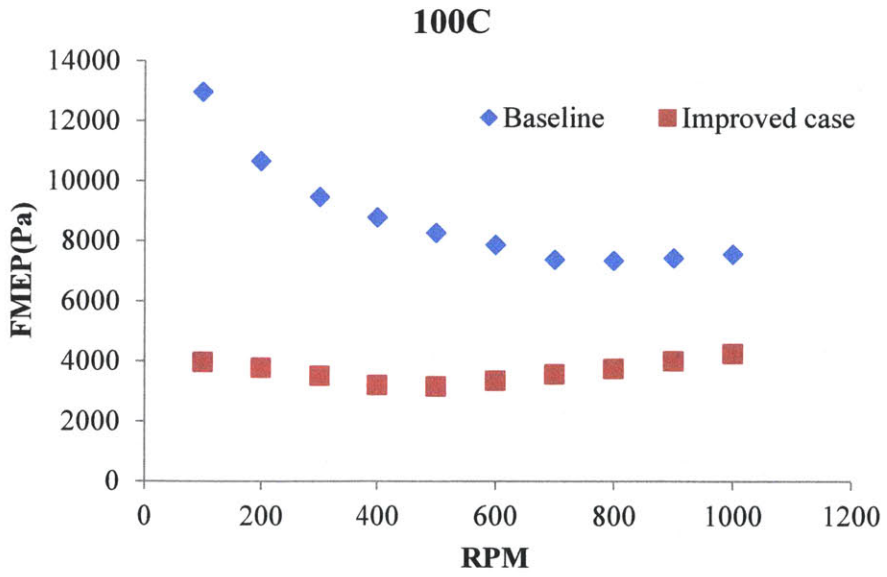

Figure 105: Comparison of the experimental FMEP from baseline setup and improved case at 100°C

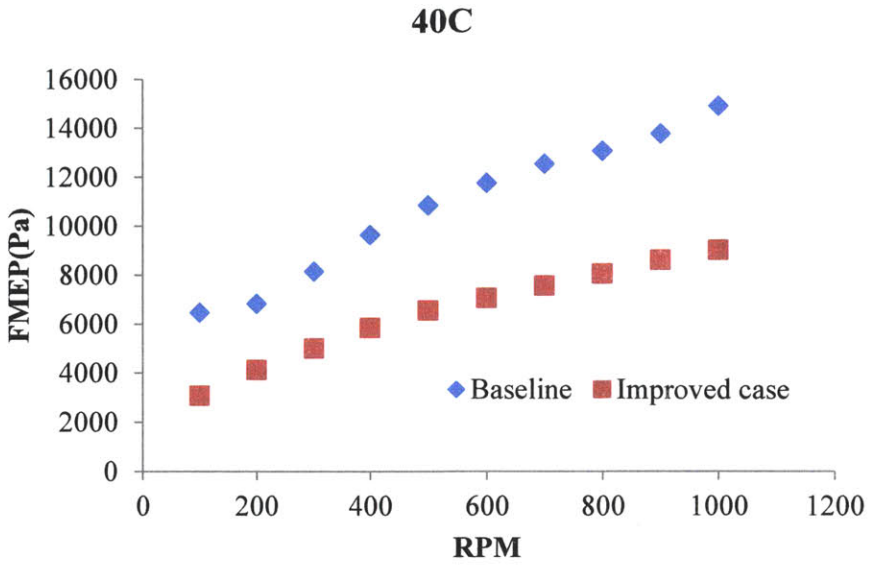

Figure 106: Comparison of the experimental FMEP from baseline setup and improved case at 40°C

Figure 107 and Figure 108 show the instantaneous Stribeck curve comparisons between the experimental and the calculation results. For both the baseline and the improved case, experimental and calculation results reach good agreement across different lubrication regimes. The calculation results can be used to provide more insight into the trends observed from the experiments.

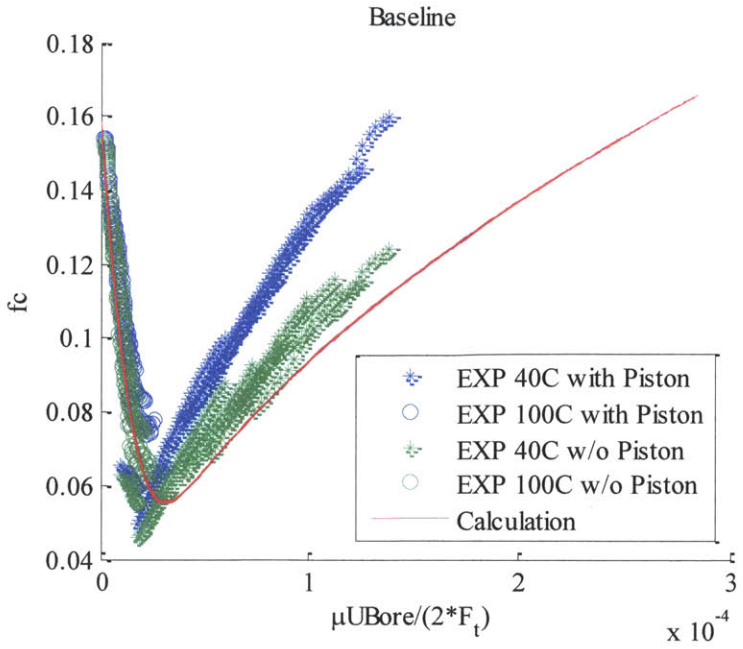

Figure 107: Instantaneous Stribeck curve comparison between the experimental and calculation results of the baseline

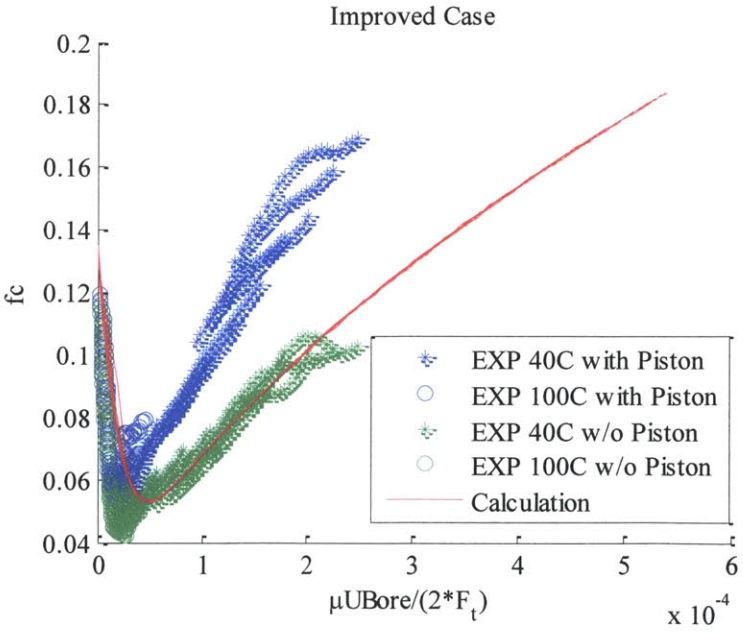

Figure 108: Instantaneous Stribeck curve comparison between the experimental and calculation results of the improved case

Figure 109 and Figure 110 show the calculcated minimum oil film thickness comparison between the baseline and the improved case. Calculation results from 40°C and 100°C at

1000RPM are used. At 40°C, the TLOCR is operating in the hydrodynamic lubrication regime and has a higher MOFT than the MOFT at 100°C. In addition, under both temperatures, the improved case has lower MOFTs than the baseline. Therefore, the experimental and calculation results show that the improved case achieve lower friction loss and better oil control than the baseline.

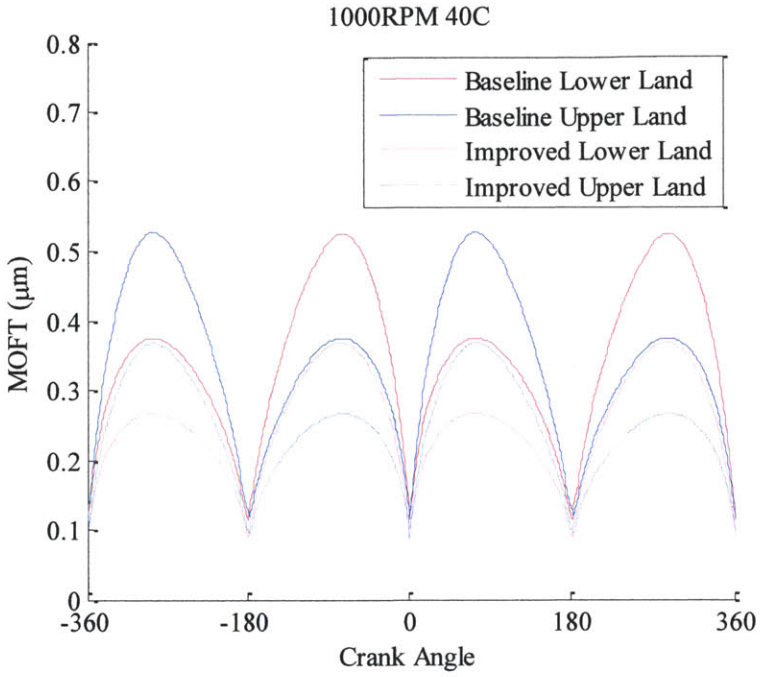

Figure 109: Minimum oil film thickness comparison between the baseline and improved case at 1000RPM, 40°C

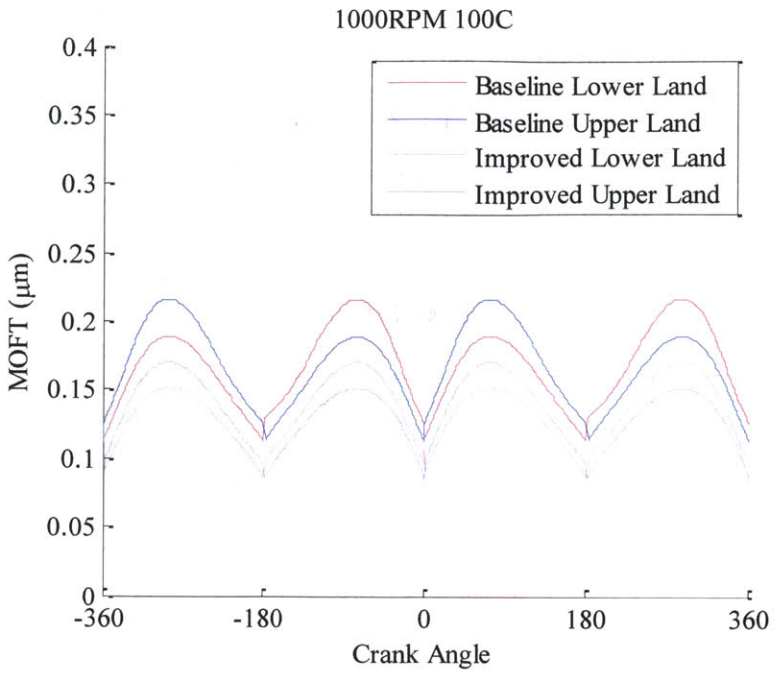

Figure 110: Minimum oil film thickness comparison between the baseline and improved case at 1000RPM, 100°C

Furthermore, the deterministic TLOCR model can be used to explore the ring FMEPs across the entire engine operating ranges, where reliable experimental results are hard to obtain.

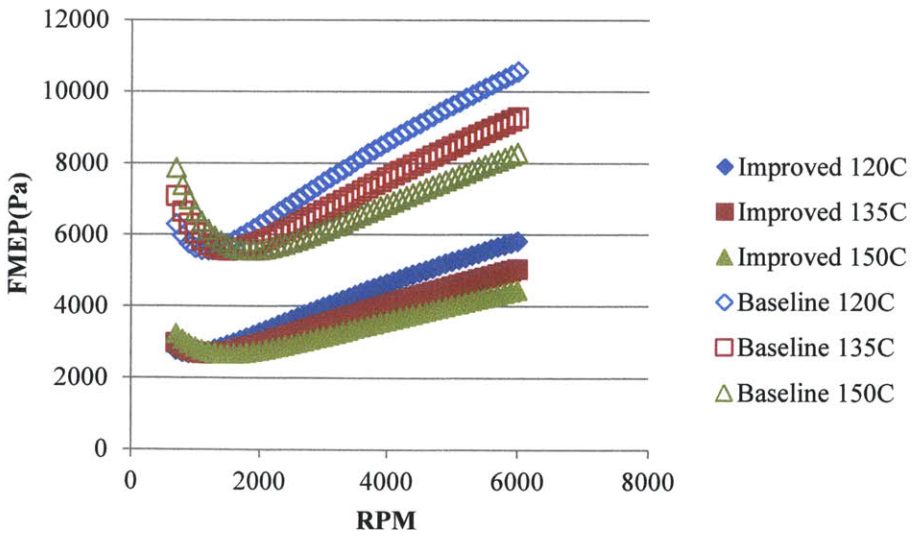

Figure 111: FMEP calculation results of baseline and improved case at 120°C, 135°C and 150°C, from 700RPM to 6000RPM at 100RPM intervals

Figure 111 shows that from 700RPM to 6000RPM, at 120°C, 135°C and 150°C, the improved case always has significantly lower FMEPs than that of the baseline. In addition, Figure 112 shows that under different operating conditions, the improved case achieve better oil control than that of the baseline.

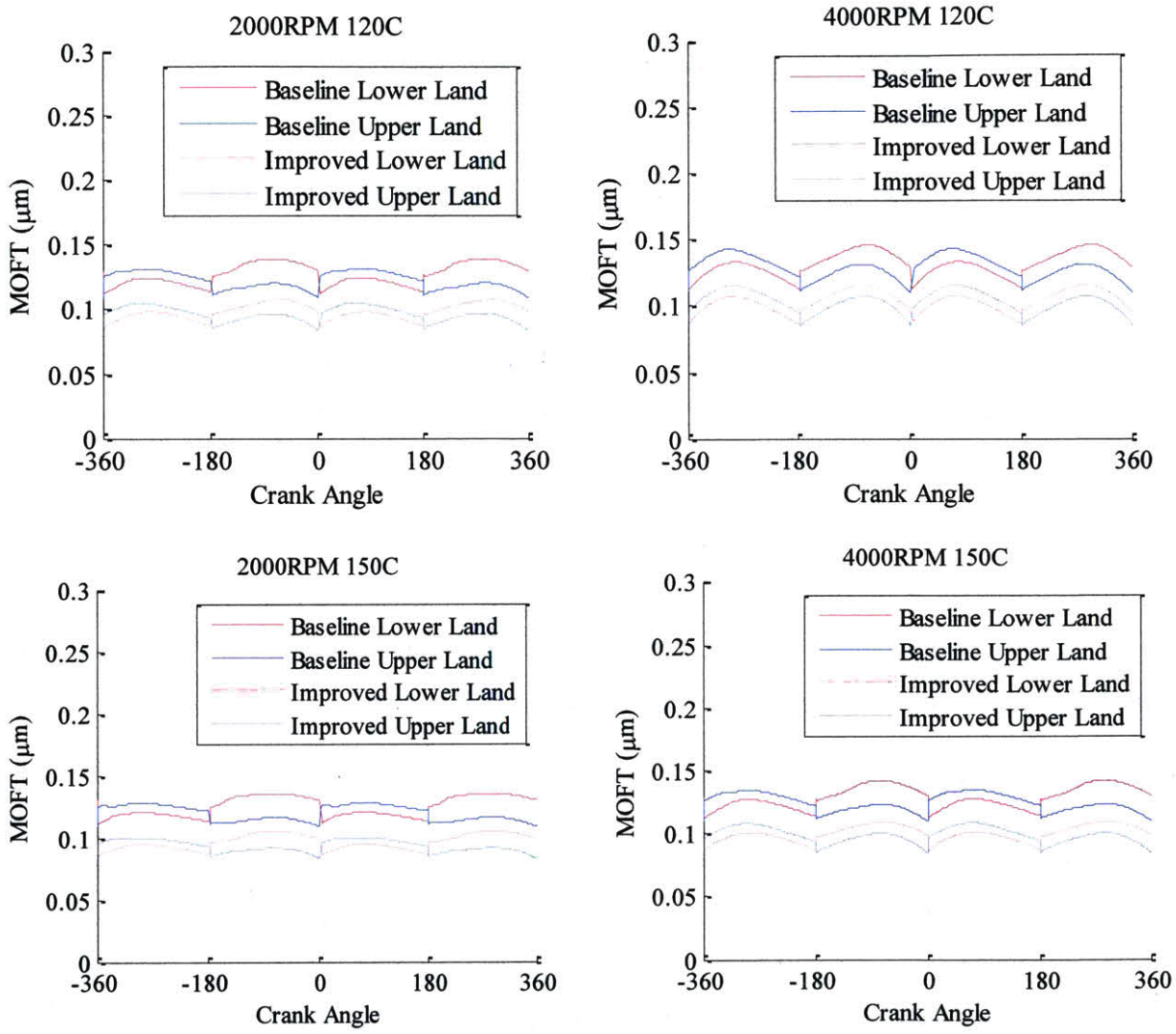

Figure 112: Calculation results of MOFT of baseline and improved case at 2000RPM and 4000RPM, 120°C and 150°C.

Therefore, after building up confidence in the TLOCR model through experiment-model comparison, the deterministic TLOCR model can be used to optimize the ring/liner system design. For the current case, an improved design can achieve lower TLOCR FMEPs and better oil control across engine operating conditions.

8. Conclusion

8.1. Summary

This thesis combined efforts from both experimentation and calculation to study the factors affecting piston ring friction.

A FLE system was modified to study the oil control ring friction. The modified FLE system showed good repeatability and self-consistency.

The deterministic TLOCR model results were compared with the experiment. Proper methods to prepare inputs for the model, including that of the ring, liner and lubricant were discussed. Uncertainties from the experiment, mainly the piston secondary motion and the lateral stoppers, and from the calculation, mainly the surface variations across the liner and ring land width variations were addressed. Considering all the uncertainties, reasonable agreement between experimental and calculation results was observed.

The effects from the ring land width and the ring tension on the TLOCR friction were discussed. The break-in of liners with a large range of surface structure sizes and roughness were studied. After the liner surfaces reached the steady state, the surface structure effects on both the friction and the oil film thickness between the ring and liner were discussed.

8.2. General Conclusions

The friction of the TLOCR is determined by a complex interaction among the ring, liner, and lubricants. Minimizing friction needs to optimize the combined effect of the ring, liner, and lubricant. In general, designs with less ring tension combined with smaller land width, thinner lubricants, and smoother and well-structured liner can lead to less and less friction from the TLOCR. However, design changes of the three components have to be directed in a coordinated manner to achieve desired results. To do it effectively, necessary knowledge and tools are needed and this work represents a major step toward this direction.

The study in this thesis leads to several general conclusions:

1. In the hydrodynamic lubrication regime, with the same ring tension, a smaller ring land width leads to lower friction and smaller minimum oil film thickness (MOFT) between the ring and liner.
2. During the liner break-in period when individual asperities on the plateau are removed, in the mixed lubrication regime, the ring friction reduces; the minimum friction coefficient reduces and its location moves leftwards on the instantaneous Stribeck curve.
3. During the liner break-in period, in the hydrodynamic lubrication regime, the hydro-pressure generation ability is mainly decided by the large surface structure and the friction change is limited.
4. In the deterministic TLOCR model, the liner break-in period can be described by maintaining a constant pressure-clearance (P-h) correlation while changing the plateau roughness (σ_p). This method lays a foundation for predicting the ring-liner friction evolution given a new liner measurement.
5. At steady state, a well-designed rougher liner can lead to a larger oil film thickness in the hydrodynamic lubrication regime. As a result, the hydrodynamic shear stress can be lower than that of a smoother liner. However, the friction benefit is at the cost of worse oil control, as the oil film thickness is large on rougher liners.
6. When optimizing the oil control ring/liner friction, the minimum oil film thickness (MOFT) between the ring and liner usually acts as the main constraint, representing the oil control functionality of the ring/liner. A smaller MOFT indicates better oil control. Compared to the current industry norm, a smaller ring land width, a lower ring tension accompanied by a smoother liner seems to lead to a lower ring FMEP and a smaller MOFT at the same time.
7. The temperature change in the experiments seems to only affect the ring friction by the corresponding viscosity change. Boundary lubrication friction seems to be not affected.

8.3. Future Work

One major direction of future work is to better understand the uncertainties from FLE measurement due to piston secondary motion. It can be seen from the current measurement, when piston speed is high, abnormal friction traces appear. Other FLE designs can be compared with the current system.

Another direction of future work is the effects of lubricant additives on friction. The current thesis covers the effects of lubricant viscosity. Friction modifiers and antiwear additives all have the potential to change friction coefficient in the boundary to mixed lubrication regime. Current measurement does not see significant reduction in boundary friction coefficient due to friction modifier. It is possible that the antiwear additives and friction modifiers are acting in the opposite directions on boundary friction coefficient. However, no explicit evidence shows the antiwear additive will function under a low contact pressure environment as in the ring / liner interface. The current model does not explicitly consider the effects from friction modifier or antiwear additives.

In addition, in the current deterministic TLOCR model, the contact module does not deterministically calculate the boundary contact pressure or friction. Uncertainties still exist on the calculation of contact pressure of surfaces with different surface structure and roughness. An improvement on the contact model will be much beneficial to the deterministic TLOCR model and the further study on the topic of ring friction.

References

[1] McGeehan, J. A., 1978, "Literature Review of the Effects of Piston Ring Friction and Lubricating Oil Viscosity on Fuel Economy," SAE Paper, 780673.

[2] Heywood, J. B., 1988, "Internal Combustion Engine Fundamentals," McGraw-Hill Book Company, pp725-730

[3] Richardson, D. E., 2000 "Review of Power Cylinder Friction for Diesel Engines", ASME Journal of Engineering for Gas Turbines and Power, Vol. 122, pp 506-519.

[4] Chen, H., 2011, "Modeling the Lubrication of the Piston Ring Pack in Internal Combustion Engines Using the Deterministic Method," PhD Thesis, Massachusetts Institute of Technology

[5] Tian, T., 1997, "Modeling the Performance of the Piston Ring-Pack in Internal Combustion Engines," PhD Thesis, Massachusetts Institute of Technology

[6] Drury, C., and Withehouse, S., 1994 "The effect of Lubricant Phosphorus Level on Exhaust Emissions in a Field Trial of Gasoline Engine Vehicles", SAE paper 940233.

[7] Ueda, F., Sugiyama, S., Arimura, K., Hamaguchi, S., and Akiyama, K., 1994 "Engine Additive Effects on Deactivation of Monolithic Three-Way Catalysts and Oxygen Sensors", SAE paper 940746.

[8] Federal Mogul, "Piston Ring Handbook".

[9] Chen, H., Li, Y. and Tian, T., 2008 "A novel approach to model the lubrication and friction between the twin-land oil control ring and liner with consideration of micro structure of the liner surface finish in internal combustion engines", SAE International Powertrains, Fuels and Lubricants Congress, SAE2008-01-1613.

[10] Tian T., Chen H., Senzer, E., 2010, "Elements for Friction Reduction in the Engine Power Cylinder System," Györer Tribologie Tagung, Györ, H; 09-13-2010; in: "1. GyŐrer Tribologie Tagung", UNIVERSITAS-GYŐR Nonprofit Kft., (2010), ISBN: 978-963-9819-57-3, 49-62

[11] Liao, K., Liu, Y., Kim, D., Urzua, P., Tian, T., 2012 "Practical challenges in determining piston ring friction," Proceedings of the Institution of Mechanical Engineers, Part J: Journal of Engineering Tribology, Nov., 2012

[12] Pawlus, P., 1994, "A study on the functional properties of honed cylinders surface during running-in," Wear 176 (1994) 247-254

[13] Pawlus, P., Cieslakb, T., Mathia, T., 2009, "The study of cylinder liner plateau honing process," Journal of Materials Processing Technology 209 (2009) 6078–6086

[14] Noorman, M., 2000, "Overview of Techniques for Measuring Friction Using Bench Tests and Fired Engines," SAE Paper, 2000-01-1780.

[15] Benzing, R., M. Peterson, et.al, "Friction and Wear Devices," ASLE Publication, Park Ridge, Illinois, 1976.

[16] ASTM G99 Standard: Test Method for Ultra Testing with a Pin-On-Disk Apparatus, ASTM, PA, 1990.

[17] ASTM G77 Standard: Test Method for Ranking Materials to Sliding Wear Using Block-On-Ring Wear Tester, ASTM, PA, 1983.

[18] Patterson, D., Hill, S., and S. Tung, 1991, "Bench Wear Testing of Engine Power Cylinder Components," Presented at the ASME Fall Technical Conference, Muskegon, Michigan.

[19] Tung, S., et al, 2004, "Engine Oil Effects on Friction and Wear Using 2.2L Direct Injection Diesel Engine Components for Bench Testing Part 2- Tribology Bench Test Results and Surface Analyses," SAE Technical Paper, 2004-01-2005

[20] Hartfield-Wunsch, S., Tung, S. and C. Rivard, 1993, "Development of a Bench Test for the Evaluation of Engine Cylinder Components and the Correlation with Engine Test Results," SAE 1993 Transactions, Section 3, P. 1131-1138, Paper No. 932693.

[21] Hartfield-Wunsch, S. and S. Tung, 1994, "The Effect of Microstructures on the Wear Behavior of Thermal Sprayed Coatings," Reprint from the 1994 7th Thermal Spray Conference Proceedings, Boston, Massachusetts.

[22] Takiguchi, M., Ando, H., Takimoto, T., Uratsuka, A., 1996, "Characteristics of friction and lubrication of two-ring piston," JSAE Review, 17 (1996) 11-16

[23] Madden D. et al., "Part 1: Piston Friction and Noise Study of Three Different Piston Architectures for an Automotive Gasoline Engine," SAE Paper 2006-01-0427, 2006

[24] Kim, K., Godward, T., Takiguchi, M., and Aoki, S., 2007, "Part 2: The Effects of Lubricating Oil Film Thickness Distribution on Gasoline Engine Piston Friction," 2007-01-1247

[25] Kim, K., et al., 2009, "Part 3: A Study of Friction and Lubrication Behavior for Gasoline Piston Skirt Profile Concepts," SAE International, 09PFL-1163

[26] Wakabayashi, R., et al., 2007, "The Effects of Piston Rings and Liner Break-in on Lubricating Condition," SAE Paper. 2007-01-1250

[27] Furuhama, S. and M. Takiguchi, 1979, "Measurement of Piston Frictional Force in Actual Operating Diesel Engine," SAE Paper No. 790855.

[28] Furuhama, S. et al. , 1981, "Effect of Piston and Piston Ring Designs on the Piston Friction Force in Diesel Engines," SAE Paper No. 810977.

[29] Sherrington, I and E. H. Smith, 1988, "The Measurement of Piston-Ring Friction by the 'Floating-Liner' Method," SAE Paper No. 884707.

[30] Tung, S. C., and Tseregounis, S. I., 2000, "An Investigation of Tribological Characteristics of Energy-Conserving Engine Oils Using a Reciprocating Bench Test," SAE Technical Paper 2000-01-1781.

[31] Hartfield-Wunsch, S., et al., 1993, "Development if a Bench Wear Test for the Evaluation of Engine Cylinder Components and the Correlation with Engine Test Results," SAE Technical Paper, 932693

[32] Takiguchi, M., Aoki, S., 2007, "Friction Analysis of a Piston for Gasoline Engines," JSAE Technical Paper No. 20075101

[33] Cho, S., et al, 2000, "Frictional Modes of Barrel Shaped Piston Rings Under Flooded Lubrication," Tribology International, 33 (2000) 545–551

[34] Shayler, P. J., Leong, D. K. W., Pegg, I. G., and Murphy, M., 2008, "Investigations of Piston Ring Pack and Skirt Contributions to Motored Engine Friction," SAE International, 2008-01-1046

[35] Tian T. and Wong, V.W., 1998, "Modeling the Lubrication, Dynamics, and Effects of Piston Dynamic Tilt of Twin-Land Oil Control Rings in IC Engines," 1998 Fall ASME ICE Technical Conference, September 1998, Clymer, NY. ASME Transaction, Journal of Engineering for Gas Turbines and Power, Vol. 122, pp 119-129, January 2000.

[36] Li, Y., Chen, H. and Tian, T., 2008, "A deterministic model for lubricant transport within complex geometry under sliding contact and its application in the interaction between the oil control ring and rough liner in internal combustion engines", SAE International Powertrains, Fuels and Lubricants Congress, SAE2008-01-1615.

[37] Li, Y., 2011, "Multiphase Oil Transport at Complex Micro Geometry", PhD Thesis, the Department of Mechanical Engineering, Massachusetts Institute of Technology, Cambridge, USA.

[38] Greenwood, J. A. and Tripp, J. H., 1971, "The contact of two nominally flat surfaces". Proc. Inst. Mech. Engrs, 1971, 185, 625-633.

[39] Hu, Y., Cheng, H. S., Arai, T., Kobayashi, Y. and Aoyama, S., 1994, "Numerical simulation of piston ring in mixed lubrication – a nonaxisymmetrical analysis". Trans. ASME, J. Tribology, 1994, 116, 470-478.

[40] R. Stribeck, Die wesentlichen Eigenschaften der Gleit- und Rollenlager (The basic properties of sliding and rolling bearings), Zeitschrift des Vereins Deutscher Ingenieure, 2002, Nr. 36, Band 46, p. 1341-1348, p. 1432-1438 and 1463-1470

[41] Kim, D., Yoshiga, Y., Sofwan, M., Takiguchi, M., 2006, "The state of piston lubrication on supercharged small bore diesel engine", Transaction of the Society of Automotive Engineering of Japan, 37(6), 85-90, 2006-11-25

[42] Liao, K., Chen, H., and Tian, T., 2012, "The Study of Friction between Piston Ring and Different Cylinder Liners using Floating Liner Engine - Part 1," SAE Technical Paper 2012-01-1334, doi:10.4271/2012-01-1334.